ISSN: 2220-9506 (Print)
ISSN: 2414-0473 (Online)

ПРИБОРЫ И МЕТОДЫ ИЗМЕРЕНИЙ

DEVICES AND METHODS OF MEASUREMENTS

Том 13 № 2 Vol. 13

2022

ПРИБОРЫ И МЕТОДЫ ИЗМЕРЕНИЙ

Научно-технический журнал

Основан в 2010 г.

Учредитель
Белорусский национальный технический университет

Выходит 4 раза в год

Журнал включен в базы данных:
Web of Science Core Collection (ESCI),
EBSCO, DOAJ, WorldCat, OpenAIRE, Google Scholar, РИНЦ,
ЭБС «Лань», НЭБ «КиберЛенинка», Соционет

Том 13 № 2 2022

Издание зарегистрировано в Министерстве информации Республики Беларусь 25 июня 2010 г.
Регистрационный номер 1372

В соответствии с решением ВАК от 8 июля 2011 г. №13/1 журнал включен в Перечень научных изданий для опубликования результатов диссертационных исследований; научное направление: «Средства и методы измерений, контроля, диагностики и оценки качества объектов и процессов» (технические и физико-математические науки)
ISSN 2220-9506

Подписка осуществляется через почтовые отделения связи по «Каталогу газет и журналов Республики Беларусь».
Подписные индексы – 74835; 748352.

Ответственный секретарь редакции: Шахлевич Л.Н.
Редактор: Чабарова О.Л.
Набор и верстка выполнены в редакции журнала «Приборы и методы измерений».
Подписано в печать 29.06.2022. Формат бумаги 60×84 1/8. Бумага мелованная.
Гарнитура Times New Roman. Печать цифровая. Усл. печ. л. 9,30. Уч.-изд. л. 3,64. Тираж 100 экз.
Дата выхода в свет 05.07.2022. Заказ № 421.
Отпечатано в Белорусском национальном техническом университете. ЛП № 02330/74 от 03.03.2014. Пр-т Независимости, 65, 220013, г. Минск

АДРЕС РЕДАКЦИИ:
Белорусский национальный технический университет
пр-т Независимости, 65, 220013, г. Минск, Республика Беларусь,
тел.: +375 (17) 293 96 67, факс: +375 (17) 292 67 94
e-mail: pimi@bntu.by
http://pimi.bntu.by

DEVICES AND METHODS OF MEASUREMENTS

Scientific and Engineering Journal

Founded in 2010

Founder
Belarusian National Technical University

Issued four times a year

The Journal is included in the following databases:
Web of Science Core Collection (ESCI),
EBSCO, DOAJ, WorldCat, OpenAIRE, Google Scholar,
RISC, Lan, CyberLeninka, Socionet

Volume 13 **№ 2** **2022**

ADDRESS:
Belarusian National Technical University
Nezavisimosty Ave., 65, Minsk 220013, Belarus
Tel.: +375 (17) 293 96 67, fax: +375 (17) 292 67 94
e-mail: pimi@bntu.by
http://pimi.bntu.by

СОДЕРЖАНИЕ

Средства измерений

Методы измерений, контроля, диагностики

CONTENTS

Prediction of Dynamic Characteristics of Thermocouples with Thin-Wire Sensing Elements

I.A. Safina, S.A. Artemyeva

*A.N. Tupolev Kazan National Research Technical University,
K. Marx str., 10, Kazan 420111, Russia*

Received 29.03.2022
Accepted for publication 23.05.2022

Abstract

Thermocouples dynamic characteristics' prediction is one of the relevant directions in the field of dynamic measurements of non-stationary temperatures of liquid and gaseous media. Thermocouples dynamic characteristics' prediction makes it possible to provide effective continuous correction in automatic control systems for non-stationary temperatures. The purpose of this paper was to develop a theoretically justified relation linking the current or expected time constant of fine-wire thermocouples with the known time constant established at known parameters of liquid and gaseous media.

A formula linking the time constant of fine-wire thermocouples with the conditions of heat exchange with the measured medium and the thermophysical characteristics of the thermocouple sensing elements has been deducted. An approximate formula is also given for calculating the internal resistance of wire sensing elements of thermocouples, which must be considered when calculating the time constant of a thermocouple. In consideration of the obtained formulas, a multi-parameter relation linking the current or expected time constant of fine-wire thermocouples with the known time constant set at the known parameters of the measured media has been formed.

It is suggested to simplify the formed multi-parameter relation and make it dependent, for example, on the "expected velocity of the measured medium×expected density of the measured medium" complex ($V_{m2}\rho_{m2}$). Simplified relations in the form of hyperbolic functions with constant parameters and argument in the form of $V_{m2}\rho_{m2}$ complex were obtained for airflowat different temperatures, pressures, and velocities.

On the example of airflow, it is shown that the complex multi-parametric relation linking the expected and known time constants of thermocouples can be simplified to a hyperbolic dependence, where the argument can be the $V_{m2}\rho_{m2}$ complex. Moreover, the degree of approximation of hyperbolic dependencies to the exact values of the multi-parametric relation can reach the *R*-square = 0.9592 criterion.

A multi-parametric relation has been proposed. That relates the known time constant of a thermocouple to the expected or current time constant of the same thermocouple at other parameters of the measured medium from the point of view of the heat exchange and thermal conduction theory. The proposed relation can be used in automatic control systems of non-stationary temperature of various liquid or gaseous media to provide continuous correction of thermocouples dynamic characteristics. Depending on the number of measured medium parameters, the suggested multi-parameter relation can be replaced by simplified relations with other complexes containing, for example, density, velocity, flow rate and pressure of the measured medium.

Keywords: thermocouple, dynamic characteristics, transmission function.

DOI: 10.21122/2220-9506-2022-13-2-83-92

Адрес для переписки:
Сафина И.А.
Казанский национальный исследовательский технический университет имени А.Н. Туполева – КАИ,
ул. К. Маркса, 10, г. Казань 420111, Россия
e-mail: Sab-ilnata@mail.ru

Address for correspondence:
Safina I.A.
A.N. Tupolev Kazan National Research Technical University,
K. Marx str., 10, Kazan 420111, Tatarstan, Russia
e-mail: Sab-ilnata@mail.ru

Для цитирования:
I.A. Safina, S.A. Artemyeva.
Prediction of Dynamic Characteristics of Thermocouples with Thin-Wire Sensing Elements.
Приборы и методы измерений.
2022. – Т. 13, № 2. – С. 83–92.
DOI: 10.21122/2220-9506-2022-13-2-83-92

For citation:
I.A. Safina, S.A. Artemyeva.
Prediction of Dynamic Characteristics of Thermocouples with Thin-Wire Sensing Elements.
Devices and Methods of Measurements.
2022, vol. 13, no. 2, pp. 83–92.
DOI: 10.21122/2220-9506-2022-13-2-83-92

Прогнозирование динамических характеристик термопар с тонкопроволочными чувствительными элементами

И.А. Сафина, С.А. Артемьева

Казанский национальный исследовательский технический университет имени А.Н. Туполева – КАИ,
ул. К. Маркса, 10, г. Казань 420111, Россия

Поступила 29.03.2022
Принята к печати 23.05.2022

Прогнозирование динамических характеристик термопар является одним из актуальных направлений в области динамических измерений нестационарных температур жидких и газообразных сред. Прогнозирование динамических характеристик термопар позволяет обеспечить эффективную непрерывную коррекцию в системах автоматического управления нестационарной температурой. Целью данной работы являлась разработка теоретически обоснованного соотношения, связывающего текущую или ожидаемую постоянную времени тонкопроволочных термопар, с известной постоянной времени, установленной при известных параметрах жидких и газообразных сред.

Выведено выражение, связывающее постоянную времени тонкопроволочных термопар с условиями теплообмена с измеряемой средой и теплофизическими характеристиками чувствительных элементов термопар. Получена также приближённая формула для расчёта внутреннего сопротивления проволочных чувствительных элементов термопар, которое необходимо учитывать при вычислении постоянной времени термопары. С учётом полученных выражений сформировано многопараметрическое соотношение, связывающее текущую или ожидаемую постоянную времени тонкопроволочных термопар, с известной постоянной времени, установленной при известных параметрах измеряемых сред.

Сформированное многопараметрическое соотношение предложено упростить и сделать зависимым, например, от комплекса «ожидаемая скорость измеряемой среды×ожидаемая плотность измеряемой среды» ($V_{m2}\rho_{m2}$). Для воздушного потока при различных температурах, давлении и скорости получены упрощённые соотношения в виде гиперболических функций с постоянными параметрами и аргументом в форме комплекса $V_{m2}\rho_{m2}$.

На примере воздушного потока показано, что сложное многопараметрическое соотношение, связывающее ожидаемую и известную постоянные времени термопар, можно упростить до гиперболической зависимости, где аргументом может выступить комплекс $V_{m2}\rho_{m2}$. Причём степень приближения гиперболических зависимостей к точным значениям многопараметрического соотношения может достигать по критерию R-square = 0.9592.

Предложено точное с точки зрения теории теплообмена и теплопроводности многопараметрическое соотношение, связывающее известную постоянную времени термопары с ожидаемой или текущей постоянной времени этой же термопары при иных параметрах измеряемой среды. Предложенное соотношение может быть использовано в системах автоматического управления нестационарной температурой различных жидких или газообразных сред для обеспечения непрерывной коррекции динамических характеристик термопар. В зависимости от числа измеряемых параметров среды предложенное многопараметрическое соотношение может быть заменено упрощёнными соотношениями с другими комплексами, содержащими, например, плотность, скорость, расход и давление измеряемой среды.

Ключевые слова: термопара, динамические характеристики, передаточная функция.

DOI: 10.21122/2220-9506-2022-13-2-83-92

Адрес для переписки:
Сафина И.А.
Казанский национальный исследовательский технический университет имени А.Н. Туполева – КАИ,
ул. К. Маркса, 10, г. Казань 420111, Россия
e-mail: Sab-ilnata@mail.ru

Address for correspondence:
Safina I.A.
A.N. Tupolev Kazan National Research Technical University,
K. Marx str., 10, Kazan 420111, Tatarstan, Russia
e-mail: Sab-ilnata@mail.ru

Для цитирования:
I.A. Safina, S.A. Artemyeva.
Prediction of Dynamic Characteristics of Thermocouples with Thin-Wire Sensing Elements.
Приборы и методы измерений.
2022. – Т. 13, № 2. – С. 83–92.
DOI: 10.21122/2220-9506-2022-13-2-83-92

For citation:
I.A. Safina, S.A. Artemyeva.
Prediction of Dynamic Characteristics of Thermocouples with Thin-Wire Sensing Elements.
Devices and Methods of Measurements.
2022, vol. 13, no. 2, pp. 83–92.
DOI: 10.21122/2220-9506-2022-13-2-83-92

Introduction

Thermocouples with sensing thin-wire elements of various diameters are widely used to measure the temperature of air and gas flows in aviation gas turbine engines (GTE). In accordance with GOST 1790-2016 "Wire made of chromel *T*, alumel, copel and constantan alloys for thermoelectrodes of thermoelectric converters" thermoelectrode wires for thermocouples are made with a diameter from 0.2 to 5.0 mm.

When thermocouples are used as parts of automatic control systems (ACS) by temperature of gas-air flows there is a need for continuous correction of their dynamic characteristics with changing modes of operation of the GTE. Some design and research issues of various corrective devices and correction methods in the ACS of GTE and in other subjects where measurement of non-stationary temperatures is needed were explained in the works [1–9].

For optimal and continuous correction of dynamic characteristics of thermocouples in the ACS, it is necessary to set the structure and parameters of transfer functions of thermocouples with required accuracy. Meanwhile, changes of functions in changing operating modes of the GTE must also be taken into account. Works [10–17] are devoted to identification of dynamic characteristics of various temperature sensors and other measuring instruments.

In works [1–17] compensation of inertia of thermocouples is produced by using a dynamic first order model. This transfer function is:

$$W(p) = \frac{k}{Tp+1}, \tag{1}$$

where k is the static conversion coefficient of a thermocouple, mV/°C; T is the time constant or an indicator of thermal inertia which depends on gas-air flows influencing parameters, s; p is the Laplace variable, 1/s.

There are several different ratios for accounting changes in the time constant T because of influencing parameters of gas-air flows in (1).

In the TGM 1594-79 "Measurement of non-stationary air flow temperature during bench tests of the GTE. Thermometers" the following ratio is given:

$$\varepsilon_1 = \varepsilon_0 \left(\frac{V_0\, p_{0\,st}}{V_1\, p_{1\,st}} \right)^n, \tag{2}$$

where ε_0 is the indicator of thermal inertia of the thermometer at velocity V_0 and static pressure p_{0st}; ε_1 is the indicator of thermal inertia of the thermometer at velocity V_1 and static pressure $p_{1\,st}$; $n = 0.488$ is the empirical coefficient for an open transversely streamlined sensing element of a thermometer.

There are relations in works [4, 9]:

$$T_{tc} = T_{tc\,c} \left(\frac{G_{g\,c}}{G_g} \right)^{0.5}, \tag{3}$$

where T_{TCC} is the calculated time constant of the thermocouple at the estimated flow rate G_{gc} of the gas flowing around it; Ttc is current (expected) time constant of the thermocouple at the current (expected) consumption G_g of the gas flowing around it.

There is also a relation[1]:

$$\tau = \tau_0 \left(\frac{\rho_0 V_0}{\rho_i V_i} \right)^n \frac{A(\rho_i V_i)^n + 1}{A(\rho_0 V_0)^n + 1}, \tag{4}$$

where τ is the current (expected) time constant of the thermocouple; ρ and V are air density and velocity that is blowing over the thermocouple; indexes 0 and i are related to the conditions of the experiment and flight; $n = 0.6–0.85$; $A = 0–0.05$ are constants determined by the design features of the thermocouple.

The theoretical justification of the relations (2)–(4) and the accuracy of calculating current or expected time constants of thermocouples based on them (indicators of thermal inertia), as well as their application areas had not been found. Analysis of (2)–(4) relationships also showed that time constants or indicators of thermal inertia established experimentally on certified installations at known speeds, air flow pressures and temperatures [18] are used as the initial data for the calculation.

Theoretical justification of the dependence of the time constant of the thermocouple on the expected operating conditions are given in the works [19–21]. This dependence has the following form:

$$T(\alpha) = \frac{1}{\alpha \Psi_T} + T_\infty, \tag{5}$$

where α is the heat transfer coefficient of the sensing element of the thermocouple with the measured medium, W/(m²·K); Ψ_T is the criterion that

[1] Sinyakov, A.N. Automatic control systems for aircraft and their power plants / A.N. Sinyakov, F.A. Shaymardanov. – M.: Mechanical engineering, 1991.

characterizes the uneven distribution of temperatures in a thermocouple and depends on the geometrical and physical features of the thermocouple and the conditions of its heat exchange; T_∞ is the value of the time constant with $\alpha \to \infty$.

The purpose of this work was to develop theoretically justified ratio, linking the current or expected time constant of thermocouples, described by a dynamic model (1), with a time constant established experimentally on air installations certified for these purposes.

The main part

Time constant of thermocouples with wire sensing elements depends on the heat exchange with the measured medium (by air or gas flow), dimensions of sensing elements and their thermophysical characteristics.

Figure 1 shows the scheme of a transversely streamlined continuous cylinder of infinite length. The scheme is used for theoretical justification heat exchange of wire sensing elements of thermocouples with the measured medium.

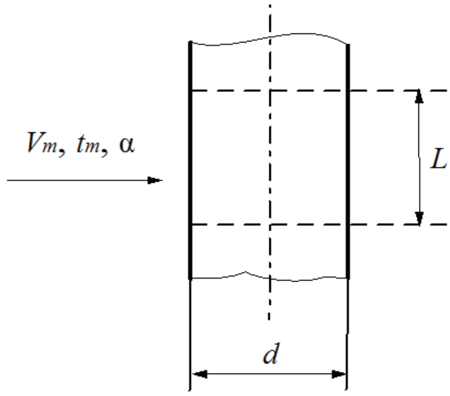

Figure 1 – Diagram of a transversely streamlined infinite cylinder: V_m – the velocity of the medium; t_m – the temperature of the medium; α – the average heat transfer coefficient on the cylinder surface; d – the diameter of the cylinder; L – the length of the elementary section of the cylinder

The following expression defines time constant during heating or cooling of the cylinder illustrated on Figure 1:

$$T = \left(R_\alpha + R_T\right)C_T = R_\alpha C_T + R_T C_T = R_\alpha C_T + T_\infty, \qquad (6)$$

where R_α is the thermal resistance on the cylinder surface at length L; R_T is the internal thermal resistance of the solid homogeneous cylinder; C_T is the thermal capacity of the elementary section of the cylinder; $T_\infty = R_T C_T$ is the time constant with $\alpha \to \infty$.

Thermal resistance R_α on the surface of the cylinder at length L is determined by the following known hyperbolic dependence on the heat transfer coefficient α:

$$R_\alpha = \frac{1}{\alpha S} = \frac{1}{\alpha \pi d L}\ [\text{K/W}].$$

The thermal capacity of the elementary section of the cylinder is equal to:

$$C_T = c\rho U = c\rho \frac{\pi d^2}{4} L\ [\text{J/K}], \qquad (7)$$

where c is the specific heat capacity coefficient of the cylinder material, J/(kg·K); ρ is the cylinder material density, kg/m^3; U is the volume of the elementary section of the cylinder, m^3.

There is no exact formula for the calculation of the internal thermal resistance R_T of solid homogeneous cylinder. An approximate formula with a high degree of approximation can be obtained as follows.

There are precise calculation formulas for temperatures coaxial section and the average temperature of the cross-section of a cylinder of infinite length in the theory of thermal conductivity of solid bodies in non-stationary modes. The thermal EMF developed by thermocouples is determined by the average cross-section temperature of the $\overline{\Theta}(\tau)$ of the sensing elements. Therefore the following known dependence is used to derive the calculation formula of the internal thermal resistance:

$$\overline{\Theta}(\tau) = \left(\Theta_m - \Theta_0\right)\cdot\left[1 - \sum_{n=1}^{\infty} \frac{4}{\mu_n^2} \exp\left(-\mu_n^2 \,\mathrm{Fo}\right)\right], \qquad (8)$$

where Θ_0 is the initial temperature of the solid cylinder; μ_n are the roots of the Bessel function of the first kind of zero order; Fo is Fourier number.

For a solid cylinder Fourier number defined by the following expression:

$$\mathrm{Fo} = \frac{\lambda}{c\rho R^2}\tau,$$

where λ is the coefficient of thermal conductivity of the solid cylinder material, W/(m·K); $R = d/2$ is the radius of a solid cylinder, m; τ is the time of the transition process of heating or cooling, s.

The following expression for the reduced average temperature over the cross section of the solid cylinder will be obtained if in (8) ratio was accepted that $\Theta_0 = 0$ and $\Theta_m = 1$:

$$\overline{\Theta}(\tau) = 1 - \sum_{n=1}^{\infty} \frac{4}{\mu_n^2} \exp\left(-\mu_n^2 \,\mathrm{Fo}\right). \quad (9)$$

Figure 2 illustrates a graph of the dependence of the average cross-section temperature $\overline{\Theta}(\tau)$ from the Fo number.

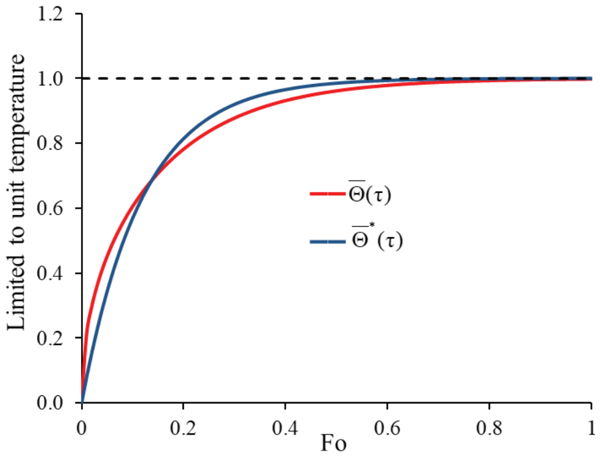

Figure 2 – Dependences of temperatures reduced to unity on the Fourier number

The average cross-section temperature $\overline{\Theta}(\tau)$ is formed from the sum of an infinite number of exponents with different bases and weight coefficients, as can be seen from (9). We propose to replace this dependency with a single exponent, the basis of which provides the best approximation to its dependence (9). The following regression function was obtained $\overline{\Theta}^*(\tau)$ with the use of regression analysis:

$$\overline{\Theta}^*(\tau) = 1 - \exp(-8.422 \cdot \mathrm{Fo}). \quad (10)$$

Figure 2 illustrates a graph of the installed function $\overline{\Theta}^*(\tau)$, which provides an approximation to the function $\overline{\Theta}(\tau)$ at least 95.8 % on the interval Fo from 0 to 1.0.

The base of the exponent in (10) is transformed as follows:

$$-8.422 \cdot \mathrm{Fo} = -8.422 \frac{\lambda}{c\rho R^2}\tau = -\frac{\tau}{\left(\frac{c\rho R^2}{8.422 \cdot \lambda}\right)} = -\tau / \left(R_T C_T\right) = -\tau / T_\infty. \quad (11)$$

The following approximate expression for the internal thermal resistance of a solid cylinder was obtained from (11) with (7) taken into account:

$$R_T = \frac{0.1187}{\pi \lambda L} \,[\mathrm{K/W}].$$

At the same time, the time constant T_∞ with $\alpha \to \infty$ will be equal to:

$$T_\infty = \frac{0.029675 \, c\rho d^2}{\lambda} \,[\mathrm{s}].$$

There is a main formula for calculating the average coefficient of convective heat transfer on any cylindrical surface of the examined body in the case of transverse air (gas) flow for practical calculations:

$$\alpha = \lambda_m \frac{C \,\mathrm{Re}^n \,\mathrm{Pr}^m}{d} = \lambda_c \frac{C\left(\frac{V_m d \rho_m}{\eta_m}\right)^n \left(\frac{\eta_m c_p}{\lambda_m}\right)^m}{d}, \quad (12)$$

where $C = 0.5$, $n = 0.5$, $m = 0.38$ with Re is from 5 to 10^3; $C = 0.25$, $n = 0.6$, $m = 0.48$ with Re is from 10^3 to $2 \cdot 10^5$; $C = 0.023$, $n = 0.8$, $m = 0.37$ with Re is from $2 \cdot 10^5$ to $2 \cdot 10^9$; λ_m is the coefficient of thermal conductivity of the medium, W/(m·K); η_m is the coefficient of dynamic viscosity of the medium, Pa·s; c_p is the heat capacity of the medium at constant pressure, J/(kg·K); $\mathrm{Re} = V_m d / \nu_m$ is Reynolds number; Rr is Prandtl number.

Formula (12) is valid for thermocouples with open transversely streamlined wire sensing elements.

If the wire sensing elements of thermocouples are placed in the braking chambers, then it is necessary to use the speed in the braking chamber V_{kt} instead of the speed of V_m in formula (12). This isis proposed to be calculated by the following expression in the work [20]:

$$V_{kt} = V_m \sqrt{\frac{1 - \xi_{tc}}{1 - \xi_{se}}},$$

where ξ_{tc} is the recovery coefficient of a thermocouple with a braking chamber; ξ_{se} is therecovery coefficient of the thermocouple sensor; V_m is the velocity of the measured medium flowing around the thermocouple.

The values of ξ_{tc} and ξ_{se} of specific types of thermocouples are established experimentally on certified installations [18].

Approach to solving the problem

Let's consider the expression (6) for two different heat exchange conditions corresponding to the heat exchange coefficients α_1 and α_2:

$$T_1(\alpha_1) = \frac{0.25 c\rho d}{\alpha_1} + \frac{0.029675 \, c\rho d^2}{\lambda} \,[\mathrm{s}];$$

$$T_2(\alpha_2)=\frac{0.25c\rho d}{\alpha_2}+\frac{0.029675\,c\rho d^2}{\lambda}\ \text{[s]},$$

where $T_1(\alpha_1)$ is the time constant of a thermocouple with a wire sensing element with a heat transfer coefficient α_1; $T_2(\alpha_2)$ is the time constant of the same thermocouple with the heat transfer coefficient α_2.

It can be seen that the time constants $T_1(\alpha_1)$ and $T_2(\alpha_2)$ agree well with the dependency (5).

Take the relation $T_2(\alpha_2)$ to $T_1(\alpha_1)$ taking into account the heat transfer coefficients according to (12):

$$\frac{T_2(\alpha_2)}{T_1(\alpha_1)}=\frac{\dfrac{0.25c\rho d}{\alpha_2}+T_\infty}{\dfrac{0.25c\rho d}{\alpha_1}+T_\infty}=\frac{\alpha_1\left(0.25c\rho d+\alpha_2 T_\infty\right)}{\alpha_2\left(0.25c\rho d+\alpha_1 T_\infty\right)}=$$

$$=\left(\frac{V_{m1}}{V_{m2}}\right)^n\left(\frac{\rho_{m1}\,\eta_{m2}}{\rho_{m2}\,\eta_{m1}}\right)^n\left(\frac{c_{m1}\eta_{m1}\,\lambda_{m2}}{c_{m2}\eta_{m2}\,\lambda_{m1}}\right)^m\left(\frac{\lambda_{m1}}{\lambda_{m2}}\right)\left[\frac{c\rho d^2+4C\lambda_{m2}T_\infty\left(\dfrac{c_{m2}\eta_{m2}}{\lambda_{m2}}\right)^m\left(\dfrac{V_{m2}\,d\,\rho_{m2}}{\eta_{m2}}\right)^n}{c\rho d^2+4C\lambda_{m1}T_\infty\left(\dfrac{c_{m1}\eta_{m1}}{\lambda_{m1}}\right)^m\left(\dfrac{V_{m1}\,d\,\rho_{m1}}{\eta_{m1}}\right)^n}\right].$$

If we assume that the time constant $T_1(\alpha_1)$ of the thermocouple is determined by the experimental transient characteristic obtained on a certified installation with known parameters of the air flow, then the expected time constant $T_2(\alpha_2)$ with the expected parameters of the air flow can be calculated by the following ratio, similar in appearance to the ratios (2)–(4):

$$T_2(\alpha_2)=T_1(\alpha_1)\cdot\Psi, \tag{13}$$

where

$$\Psi=\left(\frac{V_{m1}}{V_{m2}}\right)^n\left(\frac{\rho_{m1}\,\eta_{m2}}{\rho_{m2}\,\eta_{m1}}\right)^n\left(\frac{c_{m1}\eta_{m1}\,\lambda_{m2}}{c_{m2}\eta_{m2}\,\lambda_{m1}}\right)^m\left(\frac{\lambda_{m1}}{\lambda_{m2}}\right)\left[\frac{c\rho d^2+4C\lambda_{m2}T_\infty\left(\dfrac{c_{m2}\eta_{m2}}{\lambda_{m2}}\right)^m\left(\dfrac{V_{m2}\,d\,\rho_{m2}}{\eta_{m2}}\right)^n}{c\rho d^2+4C\lambda_{m1}T_\infty\left(\dfrac{c_{m1}\eta_{m1}}{\lambda_{m1}}\right)^m\left(\dfrac{V_{m1}\,d\,\rho_{m1}}{\eta_{m1}}\right)^n}\right].$$

The ratio (13) is an accurate from the point of view of the theory of heat transfer and thermal conductivity within the accuracy of calculating the internal thermal resistance of wire sensing elements of thermocouples. It is also can be used for gaseous media in which the thermophysical characteristics are known.

Research methodology

Relation (13) is a complex multiparametric expression. It is wise to simplify it without significant loss of accuracy for easier practical use.

If we use the ratio (13) to track the change in the time constant of the thermocouple with continuous correction of its dynamic characteristic in the ACS GTD, then it is desirable to simplify it to two measured parameters. For example, to the current velocity V_{m2} and the current density ρ_{m2}. One of the options of this simplification might involve establishing the parameters of some regression function F where the argument is a $V_{m2}\,\rho_{m2}$ complex.

Let's consider a particular case when the measured medium is an air flow with a speed ranged from 100 to 250 m/s, with a pressure ranged from 0.1 to 2 MPa and a temperature ranged from 20 to 727 °C.

As the object of research thermocouples with wire thermoelectrodes of chromel-alumel calibration with diameters of 0.2 and 1.2 mm were selected.

It was assumed that the time constants $T_1(\alpha_1)$ of thermocouples were determined by experimental transient characteristics obtained on a certified installation with known parameters of the air flow, specifically when $V_{m1}=100$ m/s, $p_{m1}=0.1$ MPa, $t_{m1}=20$ °C and $\rho_{m1}=1.205$ kg/m^3.

In our studies the number of Re was in the range from 10^3 to $15\cdot10^3$, which in (13) corresponded to $C=0.25$, $n=0.6$ and $m=0.48$.

The results of calculating the function Ψ of the complex $V_{m2}\,\rho_{m2}$ at $d=0.2$ mm and $T_1(\alpha_1)=0.092$ s are given in Table 1.

Table 1

The results of calculating the function Ψ of the complex $V_{m2}\,\rho_{m2}$ at d = 0.2 mm and $T_1(\alpha_1)$ = 0.092 s

V_{m2}, m/s	p_{m2} = 0.1 MPa t_{m2} = 20 °C		p_{m2} = 0.1 MPa t_{m2} = 227 °C		p_{m2} = 1 MPa t_{m2} = 227 °C		p_{m2} = 0.1 MPa t_{m2} = 727 °C		p_{m2} = 2 MPa t_{m2} = 627 °C	
	Ψ	$V_{m2}\rho_{m2}$, kg/(m²s)	Ψ	$V_{m2}\rho_{m2}$, kg/(m²s)	Ψ	$V_{m2}\rho_{m2}$, kg/(m²s)	Ψ	$V_{m2}\rho_{m2}$, kg/(m²s)	Ψ	$V_{m2}\rho_{m2}$, kg/(m²s)
100	1.0000	120.5	1.1634	70.0	0.2946	694.0	0.3357	347.0	0.2186	769.0
150	0.7846	180.8	0.9128	105.0	0.2316	1041.0	0.2638	520.5	0.1720	1153.5
200	0.6607	241.0	0.7685	140.0	0.1953	1388.0	0.2224	694.0	0.1452	1538.0
250	0.5782	301.3	0.6725	175.0	0.1712	1735.0	0.1949	867.5	0.1273	1922.5

The results of calculating the function Ψ of the complex $V_{m2}\rho_{m2}$ at d = 1.2 mm and $T_1(\alpha_1)$ = 1.130 s are given in Table 2.

Table 2

The results of calculating the function Ψ of the complex $V_{m2}\,\rho_{m2}$ at d = 1.2 mm and $T_1(\alpha_1)$ = 1.130 s

V_{m2}, m/s	p_{m2} = 0.1 MPa t_{m2} = 20 °C		p_{m2} = 0.1 MPa t_{m2} = 227 °C		p_{m2} = 1 MPa t_{m2} = 227 °C		p_{m2} = 0.1 MPa t_{m2} = 727 °C		p_{m2} = 2 MPa t_{m2} = 627 °C	
	Ψ	$V_{m2}\rho_{m2}$, kg/(m²s)	Ψ	$V_{m2}\rho_{m2}$, kg/(m²s)	Ψ	$V_{m2}\rho_{m2}$, kg/(m²s)	Ψ	$V_{m2}\rho_{m2}$, kg/(m²s)	Ψ	$V_{m2}\rho_{m2}$, kg/(m²s)
100	1.0000	120.5	1.1625	70.0	0.2983	694.0	0.3392	347.0	0.2228	769.0
150	0.7858	180.8	0.9132	105.0	0.2356	1041.0	0.2677	520.5	0.1764	1153.5
200	0.6625	241.0	0.7697	140.0	0.1995	1388.0	0.2265	694.0	0.1497	1538.0
250	0.5805	301.3	0.6743	175.0	0.1755	1735.0	0.1991	867.5	0.1319	1922.5

Figure 3 shows the results of calculating the function Ψ as a function of the complex $V_{m2}\rho_{m2}$ in the form of point values according to the data from Tables 1 and 2.

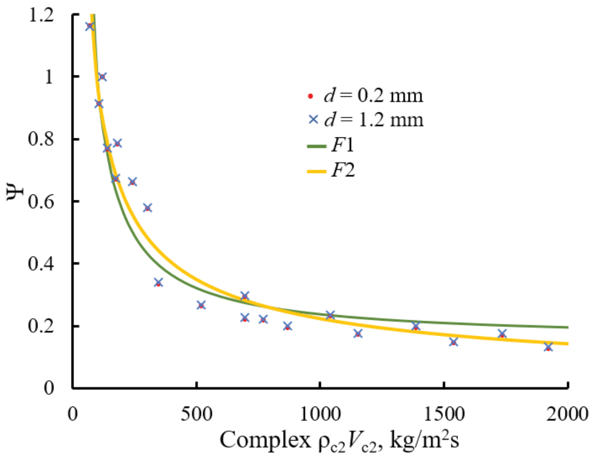

Figure 3 – Dependence of the function Ψ on the complex $V_{m2}\rho_{m2}$ at d = 0.2 mm and d = 1.2 mm

As it can be seen from Figure 3 and Tables 1 and 2, the results of calculating the function Ψ for the same values of the complexes $V_{m2}\rho_{m2}$ almost do not depend on the selected diameters of the wire thermoelectrodes of the thermocouples.

In addition, there is a hyperbolic law of dependence of the function Ψ on complexes $V_{m2}\rho_{m2}$ that may be the basis for choosing a regression function.

The following two functions are selected as a regression functions:

$$F1 = \frac{A}{\rho_{m2}V_{m2}} + B \quad \text{and} \quad F2 = \frac{A}{\left(\rho_{m2}V_{m2}\right)^{l}} + B.$$

The following parameters of the selected regression functions were determined with an accuracy estimate based on the R-square criterion with the use of the regression analysis:

$$F1 = \frac{84.05}{\rho_{m2}V_{m2}} + 0.1529 \quad \text{with } R\text{-square} = 0.9184;$$

$$F2 = \frac{19.22}{\left(\rho_{m2} V_{m2}\right)^{0.6445}} \quad \text{with } R\text{-square} = 0.9592.$$

Graphs of functions $F1$ and $F2$ are also shown in Figure 3.

If the regression function $F2$ is chosen as the most accurately describing function Ψ, then the relation (13) will take the following simplified form:

$$T_2(\alpha_2) = T_1(\alpha_1) \cdot \frac{19.22}{\left(\rho_{m2} V_{m2}\right)^{0.6445}}.$$

According to (13) the accuracy of determining the time constant $T_2(\alpha_2)$ also depends on the accuracy of establishing $T_1(\alpha_1)$ according to experimental transient characteristics obtained on installations certified for these purposes.

As is known, experimental transient characteristics always contain interference of various levels and spectra, which reduce the accuracy of determining time constants.

A spectral method for determining the time constants of various dynamic models of thermocouples based on experimental transient characteristics containing high-level interference lying outside the information part of the amplitude spectrum of the signal $s(\tau)$ and formed according to the established rules from the transient characteristic is proposed in work [22].

For transfer functions of thermocouples of the (1) type in [22], the following relation is proposed to determine the time constant T under known test conditions:

$$S(j\omega) = \frac{U_m \cdot T}{\sqrt{1 + \omega^2 T^2}}, \tag{14}$$

where $S(j\omega)$ is the signal amplitude spectrum $s(\tau)$; ω is the frequency, rad/s; U_m is the amplitude of the $s(\tau)$ signal with $\tau = 0$; T is the time constant, s.

In cases where the experimental transient characteristics contain harmonic interference of any level and frequency the work [23] proposes a spectral method insensitive to harmonic interference for determining time constants of different dynamic models of thermocouples.

The following relation is proposed for transfer functions of thermocouples of the (1) type in [23] to determine the time constant T under known test conditions:

$$\mathrm{Im}(\omega) = \frac{U_m T}{1 + \omega^2 T^2}, \tag{15}$$

where $\mathrm{Im}(\omega)$ is the imaginary part of the amplitude spectrum $S(j\omega)$; ω is the frequency, rad/s; T is the time constant, s.

The determination of time constants T in (14) and (15) in [22, 23] is proposed to calculate with the use of regression analysis on the calculated amplitude spectrum and its imaginary part.

According to the methods proposed in [22, 23] the established time constants of the experimental transient characteristics can be used as time constants $T_1(\alpha_1)$ in (13) to increase the accuracy of forecasting the expected time constants.

Conclusion

Ratio linking the known time constant of a thermocouple obtained during tests on certified installations with known thermophysical characteristics, velocity and pressure of the gas flow with the expected or current time constant of the same thermocouple with other thermophysical characteristics, velocities and pressures of the gas flow has been developed.

This relation was developed according to the theory of the heat transfer theory and the thermal conductivity in the external flow of cylindrical bodies.

As opposed to the known equivalent ratios this developed ratio takes into account the entire complex of gas flow parameters, thermophysical characteristics and the diameter of the sensor element of the thermocouple that determines values of the time constants of the thermocouple.

Simplified relations linking the known time constant of a thermocouple obtained during tests on certified installations at a known speed and pressure of the gas flow with the expected or current time constant of the same thermocouple at different speeds and pressures of the gas flow are proposed. Simplified ratios describe the initial ratio with an accuracy no worse than R-square = 0.9184. It was shown with the use of changing the temperature of the air flow by a thermocouple with wire thermoelectrodes of chromel-alumel calibration with diameters 0.2 and 1.2 mm as example.

Further research in this field can be aimed at establishing simplified dependencies of the function Ψ for gas flows that are products of combustion of various fuels in atmospheric air and at replacing simplified ratios that contain pressure, flow rate, velocity and density of gas flows.

Acknowledgments

The assistance of associate Professor of the Department of Electronic Instrumentation and Quality Management of KNITU-KAI A.F. Sabitov as a great help in discussing the content of the article and preparing it for publication is gratefully acknowledged.

References

1. Wittenmark B., Middleton R.H., Goodwin G.C. Adaptive Decoupling of Multivariable Systems. *International Journal of Control*, 1987, vol. 46, no. 6, pp. 1992–2009. **DOI:** 10.1080/00207178708934029

2. Lutz W.J., Hakimi S.L. Design of Multi-Input Multi-Output Systems with Minimum Sensitivity. *IEEE Transaction on circuits and systems*, 1988, vol. 35, no. 9, pp. 1114–1122. **DOI:** 10.1109/31.7571

3. Kaizuka H. Multivariable servo system design method using structural features of controlled systems. *International Journal of Control*, 1989, vol. 49, no. 4, pp. 1409–1419. **DOI:** 10.1080/00207178908559712

4. Petunin V.I. [GTE gas temperature determination with the use of indirect measurements]. *Izvestiya vuzov. Aviacionnaya tekhnika* [News of universities. Aviation equipment], 2008, no. 1, pp. 51–55 (in Russian).

5. Zimmerschied R., Isermann R. Nonlinear time constant estimation and dynamic compensation of temperature sensors. *Contr. Eng. Pract.*, 2010, vol. 18, no. 3, pp. 300–310.
DOI: 10.1016/j.conengrac.2009.11.008

6. Petunin V.I., Sibagatullin R.R., Frid A.I. [Development of requirements for the accuracy of compensation of the inertia of the thermocouple in the gas temperature control loop]. *Izvestiya vuzov. Aviacionnaya tekhnika* [News of universities. Aviation equipment], 2015, no. 1, pp. 56–60 (in Russian).

7. Petunin V.I., Sibagatullin R.R., Frid A.I. [Robust self-adjusting temperature of the gas meter GTD]. *Vestnik UGATU* [Bulletin of the Ufa State Aviation Technical University], 2015, vol. 19, no. 1(67), pp. 147–155 (in Russian).

8. Petunin V.I., Sibagatullin R.R., Frid A.I. Development of requirements for accuracy of inertia compensation in gas turbine engine control systems with a channel selector. *Russian Aeronautics*, New York, 2015, no. 1(58), pp. 71–77. **DOI:** 10.3103/S1068799815010110

9. Petunin V.I., Sibagatullin R.R., Frid A.I. [Adaptive gas turbine engine temperature measuring instrument with model error correction]. *Vestnik UGATU* [Bulletin of the Ufa State Aviation Technical University], 2017, vol. 21, no. 4(75), pp. 1–8 (in Russian).

10. Pao G.P., Sivakumar L. [Order and Parameter Identification in Continuous Linear Systems via Walsh Functions]. *Trudy institute inzhenerov po elektrotekhnike i radioelektronike (TIIJeR)* [Proceedings of the Institute of Electrical and Electronics Engineers], 1982, vol. 70, no. 7, pp. 89–91 (in Russian).

11. Sherbakov M.A., Iosifov V.P. [Restoration of the input signal based on the results of identification of dynamic characteristics of measuring instruments]. *Izvestija vysshih uchebnyh zavedenij. Povolzhskij region. Tehnicheskie nauki* [Proceedings of the higher educational institutions. Volga region. Technical science], 2007, no. 3, pp. 3–8 (in Russian).

12. Jamroz P. Relationship between dynamic coefficients of two temperature sensors under non stationary flow conditions. *IEEE Sens. J.*, 2011, vol. 11, no. 1–2, pp. 335–340. **DOI:** 10.1109/JSEN.2010.2073463

13. Dubovitskii V.F., Sebina L.P, Godunov M.V., Maksimova E.M. Use of a data measurement system for studying the characteristics of temperature sensors. *Fibre Chemistry*, 2011, vol. 42, no. 6, pp. 399–403.
DOI: 10.1007/s10692-011-9297-0

14. Iosifov V.P. [Determination of the full dynamic characteristics of measuring instruments with the use of recurrent procedures]. *Izvestiya vysshikh uchebnykh zavdenij. Povolzhskij region. Tekhnicheskije nauki* [Proceedings of the higher educational institutions. Volga region. Technical science], 2011, no. 1(17), pp. 126–131 (in Russian).

15. Bekenova Y.A., Komshilova V.A., Komshilova K.O. [Dynamic characteristics of measurements systems based on industrial automation systems]. *Izvestiya Sankt-Peterburgskogo gosudarstvennogo elektrotekhnicheskogo universiteta "LETI"*, 2013, no. 1. pp. 81–86 (in Russian).

16. Froehlich T., Augustin S., Ament C. Temperature-Dependent Dynamic Behavior of Process Temperature Sensors. *International Journal of Thermophysics*, 2015, vol. 36, no. 8, pp. 2115–2123.
DOI: 10.1007/s10765-015-1869-4

17. Marshalov E.D., Nikonorov A.N., Murav'ev I.K. [Determination of thermal reaction time of thermal resistance converters]. *Vestnik Ivanovskogo gosudarstvennogo energeticheskogo universiteta*, 2017, no. 3, pp. 54–59 (in Russian).

18. Vavirovskaja S.L., Zaharov D.L., Korneev M.V. [Automation determination of dynamic and high-speed characteristics of temperature sensors in the installation of air УВ-010 CIAM]. *Avtomatizacia v promyshlennosti* [Automation industry], 2016, vol. 4, pp. 28–29 (in Russian).

19. Sabitov A.F., Safina I.A. [Identification of nominal dynamic characteristics aircraft gas temperature sensors]. *Pribory i metody izmerenii* [Devices and Methods of Measurements], 2017, vol. 8, no. 1, pp. 7–14 (in Russian).
DOI: 10.21122/2220-9506-2017-8-1-7-14

20. Sabitov A.F., Safina I.A. [Method for determination of the characteristic curve of the thermal inertia of aircrcraft gas temperature sensors]. *Pribory i metody izmerenii* [Devices and Methods of Measurements], 2017, vol. 8, no. 4, pp. 357–364 (in Russian).
DOI: 10.21122/2220-9506-2017-8-4-357-364

21. Tyurina M., Sabitov A., Safina I. Identification of Dynamic Characteristics of Temperature Sensors. *Journal of Engineering Thermophysics*, 2020, vol. 29, no. 4, pp. 618–631.
DOI: 10.1134/S1810232820040104

22. Sabitov A.F., Safina I.A. [Implementation of the Spectral Method for Determining of Measuring Instruments' Dynamic Characteristics]. *Pribory i metody izmerenii* [Devices and Methods of Measurements], 2020, vol. 11, no. 2, pp. 155–162 (in Russian).
DOI: 10.21122/2220-9506-2020-11-2-155-162

23. Sabitov A., Safina I. Determining Dynamic Characteristics of Measuring Instruments with a Spectral Method Insensitive to Harmonic Interference. *Journal of Engineering Thermophysics*, 2021, vol. 30, no. 3, pp. 508–514. **DOI:** 10.1134/S1810232821030139

Diffuse Reflectance Spectrophotometers Based on C12880MA and C11708MA Mini-Spectrometers Hamamatsu

V.A. Firago, N.V. Levkovich, K.I. Shuliko

*Belarusian State University,
Nezavisimosty Ave., 4, Minsk 220030, Belarus*

*Received 21.02.2022
Accepted for publication 26.04.2022*

Abstract

Diffuse reflection spectroscopy with spatial resolution is a promising direction of non-destructive control of the properties of a number of scattering fine-dispersed materials, including food products. It can find wide practical application only in the presence of compact, easy-to-use and inexpensive spectrophotometric equipment. The aim of the article is to investigate the possibility of creating portable spectrophotometers based on Hamamatsu mini-spectrometers, which work together with modern computing facilities.

The schematics for connecting the C12880MA and C11708MA mini-spectrometers to portable computing devices are reviewed. Shows the feasibility of using a small-sized microprocessor board ARM STM32F103C8T6 (Blue pill) on the chip STM32F103C8T6. Its use in the connection scheme has simplified data exchange with the control computer via USB interface and the formation of all the signals that are needed to control the mini-spectrometer.

Two experimental samples of spectrophotometers based on C12880MA and C11708MA mini-spectrometers and STM32 microprocessors were created and their characteristics were studied. The calibration procedure and features of the software for these spectrophotometers are presented. The described features ensure the efficiency of software modification for the spectrophotometric problem to be solved. The presence of distortions of the registered spectra in the short-wave part of the spectral range of C12880MA was revealed. They arise due to focusing by the concave diffraction grating of a part of the radiation scattered by it into zero order.

Approbation of developed portable spectrophotometers based on Hamamatsu mini-spectrometers indicates the possibility of their use in portable spectrophotometric equipment and devices for spectral control of optical properties of scattering materials. The described calibration technique allows you to determine the range of the spectrum, in which the distortions of the recorded spectra are minimal. The proposed solutions significantly reduce the cost of diffuse reflectance spectroscopy devices with spatial resolution and expand the possibilities of their use in various branches of science and industry.

Keywords: diffuse reflection, mini-spectrometers, spectral sensitivity, spectrophotometers, calibration of spectrometers.

DOI: 10.21122/2220-9506-2022-13-2-93-104

Адрес для переписки:
*Фираго В.А.
Белорусский государственный университет,
пр-т Независимости, 4, г. Минск 220030, Беларусь
e-mail: firago@bsu.by*

Address for correspondence:
*Firago V.A.
Belarusian State University,
Nezavisimosty ave., 4, Minsk 220030, Belarus
e-mail: firago@bsu.by*

Для цитирования:
V.A. Firago, N.V. Levkovich, K.I. Shuliko.
Diffuse Reflectance Spectrophotometers Based on C12880MA and C11708MA Mini-Spectrometers Hamamatsu.
Приборы и методы измерений.
2022. – Т. 13, № 2. – С. 93–104.
DOI: 10.21122/2220-9506-2022-13-2-93-104

For citation:
V.A. Firago, N.V. Levkovich, K.I. Shuliko.
Diffuse Reflectance Spectrophotometers Based on C12880MA and C11708MA Mini-Spectrometers Hamamatsu.
Devices and Methods of Measurements.
2022, vol. 13, no. 2, pp. 93–104.
DOI: 10.21122/2220-9506-2022-13-2-93-104

Спектрофотометры диффузного отражения на основе мини-спектрометров C12880MA и C11708MA Hamamatsu

В.А. Фираго, Н.В. Левкович, К.И. Шулико

*Белорусский государственный университет,
пр-т Независимости, 4, г. Минск 220030, Беларусь*

*Поступила 21.02.2022
Принята к печати 26.04.2022*

Спектроскопия диффузного отражения с пространственным разрешением – перспективное направление неразрушающего контроля свойств ряда рассеивающих мелкодисперсных материалов, в том числе и продуктов питания. Она может найти широкое практическое применение только при наличии компактной, простой в применении и недорогой спектрофотометрической техники. Цель статьи – исследование возможности создания портативных спектрофотометров на основе мини-спектрометров Hamamatsu, которые работают в комплексе с современными вычислительными средствами.

Рассмотрены схемы подключения мини-спектрометров C12880MA и C11708MA к портативным вычислительным устройствам. Показана целесообразность использования малогабаритной микропроцессорной платы ARM STM32F103C8T6 (Blue pill) на чипе STM32F103C8T6. Её использование в схеме подключения позволило упростить обмен данными с управляющим компьютером по USB интерфейсу и формирование всех сигналов, которые необходимы для управления работой мини-спектрометра.

Созданы два экспериментальных образца спектрофотометров на основе мини-спектрометров C12880MA и C11708MA и микропроцессоров STM32 и исследованы их характеристики. Приведены методика градуировки и особенности программного обеспечения этих спектрофотометров. Описанные особенности обеспечивают оперативность модификации программного обеспечения под решаемую спектрофотометрическую задачу. Выявлено наличие искажений регистрируемых спектров в коротковолновом участке спектрального диапазона C12880MA. Они возникают за счёт фокусировки вогнутой дифракционной решеткой части рассеиваемого ей излучения в нулевой порядок.

Апробация созданных портативных спектрофотометров на основе мини-спектрометров Hamamatsu указывает на возможность их применения в портативной спектрофотометрической технике и устройствах спектрального контроля оптических свойств рассеивающих материалов. Описанная методика градуировки позволяет определять диапазон спектра, в котором искажения регистрируемых спектров минимальны. Предлагаемые решения позволяют существенно снизить стоимость устройств спектроскопии диффузного отражения с пространственным разрешением и расширить возможности их использования в различных отраслях науки и производства.

Ключевые слова: диффузное отражение, мини-спектрометры, спектральная чувствительность, спектрофотометры, градуировка спектрометров.

DOI: 10.21122/2220-9506-2022-13-2-93-104

Адрес для переписки:
*Фираго В.А.
Белорусский государственный университет,
пр-т Независимости, 4, г. Минск 220030, Беларусь
e-mail: firago@bsu.by*

Address for correspondence:
*Firago V.A.
Belarusian State University,
Nezavisimosty ave., 4, Minsk 220030, Belarus
e-mail: firago@bsu.by*

Для цитирования:
V.A. Firago, N.V. Levkovich, K.I. Shuliko.
Diffuse Reflectance Spectrophotometers Based on C12880MA and C11708MA Mini-Spectrometers Hamamatsu.
Приборы и методы измерений.
2022. – Т. 13, № 2. – С. 93–104.
DOI: 10.21122/2220-9506-2022-13-2-93-104

For citation:
V.A. Firago, N.V. Levkovich, K.I. Shuliko.
Diffuse Reflectance Spectrophotometers Based on C12880MA and C11708MA Mini-Spectrometers Hamamatsu.
Devices and Methods of Measurements.
2022, vol. 13, no. 2, pp. 93–104.
DOI: 10.21122/2220-9506-2022-13-2-93-104

Introduction

Optical spectroscopy is widely used in the analysis and control of the composition of various materials and media. Modern microelectronics makes it possible to create portable colorimeters and spectrophotometers, for example, KNFIR-170A (China), which are designed to determine the diffuse reflectance spectra of various materials (granules, powders, fabrics, composite materials, etc.). Modern microelectronics makes it possible to create portable colorimeters and spectrophotometers, for example, KNFIR-170A (China), which are designed to determine the diffuse reflectance spectra of various materials (granules, powders, fabrics, composite materials, etc.) in the visible and infrared regions of the spectrum [1]. Several companies manufacture computerized spectrophotometric systems for measuring diffuse reflectance spectra of inhomogeneous materials. They are equipped with a built-in integrating sphere, for example, the B&W Tek i-Spec Plus series [2]. An example of their use is the operational non-destructive control of the content of nicotine, sugar and chlorides in tobacco based on original algorithms for multiplicative scattering correction.

The use of an integrating sphere is inconvenient at solving many problems of operational optical control of the composition of finely dispersed materials. It is also important to take into account the influence of the unknown coefficient of scattering of the incident radiation by their surface. Therefore, some researchers are developing a new direction of optical control of composite materials and biological tissues, which is called diffuse reflection spectroscopy of light radiation with spatial resolution [3–7]. It is based on the use of narrow beams of probing and backscattered radiation, which are perpendicular to the reflecting surface of the controlled medium. Several reflection spectra are recorded at different distances between the beams. As the amount of data obtained increases at comparison with traditional reflectance spectroscopy, the possibility of creating new methods for processing the recorded spectra appears [5–9]. The reliability of determining the structure of the medium and the volume concentration of the controlled chromophores should also improve significantly.

Existing portable spectrophotometric equipment usually uses mini-spectrometers based on a symmetric Czerny–Turner optical scheme using a concave diffraction grating and a array of photodetectors. The optical path length of the diffracted radiation in these minispectrometers must be at least 70 mm to provide good spectral resolution (on average about 1 nm). This limits the miniaturization of the equipment under discussion. In cases where the device for surface illumination and registration of diffusely reflected radiation must be miniaturized, fiber-optic technique is often used. It is used to inject light radiation into the material sample under study and transmit the reflected radiation to the entrance slit of the spectrometer [4, 5]. The disadvantage of this scheme is the instability of the value of the recorded fluxes, which is caused by uncontrolled bends of the optical fibers during measurements. To eliminate this disadvantage and reduce the cost of equipment, it is necessary to abandon the use of optical fibers and use mini-spectrometers, production of which was mastered by Hamamatsu Corporation. These spectrometers have small dimensions of $20.1\times12.5\times10.1$ mm^3 (C12880MA) [10] and $27.6\times16.8\times13$ mm^3 (C11708MA) [11] and operate in the visible and near-infrared spectrum ranges. They can be used in the creation of compact spectrophotometric devices with limited spectral resolution, which is designed to control the optical characteristics of condensed media with smooth changes in the spectral absorption coefficient of radiation $\mu_a(\lambda)$.

The discussed methods of optical reflectance spectroscopy can find wide practical application in industry, agriculture, biology and medicine only if compact, easy-to-use and inexpensive spectrophotometric equipment is available. Therefore, the aim of the work is to study the possibility of creating portable spectrophotometers based on Hamamatsu C12880MA and C11708MA mini-spectrometers. Also the problems of their complexation with modern computer equipment to provide their expansion of possibilities and convenience of use are considered.

Connection diagrams for mini-spectrometers

The C12880MA and C11708MA spectrometers are miniature devices containing an entrance slit, a concave focusing reflective diffraction grating with a flat field of the formed image of slit [10, 11]. In the plane of the generated image is a CMOS line matrix of photodiodes. The supply voltage of these spectrometers is +5 V. Therefore, TTL control signals must be applied to the outputs of the electronic circuitry of these spectrometers. At the analog output of the spectrometer a series of video pulses are formed, the amplitude of which is proportional to the exposure time of the frame and the photocurrents that are produced by the light-sensitive elements of the line matrix of photodiodes. The best way to connect these spectrometers to a computer is to use a microprocessor-based device with built-in analog-to-digital converters (ADCs).

Market analysis of microprocessor boards shows that the smallest size at a low price has a microprocessor board ARM STM32F103C8T6 STM32 (Blue pill) on a chip STM32F103C8T6, which can be powered from a USB computer port. This board has good performance, all the necessary connectors and interfaces for connecting to a computer and other devices, including the programmer, as well as two built-in 12-bit ADC and 3 timers. The connection diagrams of the C12880MA and C11708MA, developed by the authors of the article, are shown in Figure 1. They are based on Hamamatsu's recommended standard schemes for connecting the necessary external components to them [10, 11].

The microprocessor generates the required CLK and ST logic signals, which are necessary to control the operation of the electronic units of the minispectrometers according to the Hamamatsu recommended timing diagram. Level matching of digital TTL signals used in the microprocessor (from 0 to +3.3 V) and mini spectrometers (from 0 to +5 V) provides the level converter U1 on the SN74ACT04DR. The video signal generated by the spectrometer is fed to the ADC input of the microprocessor through two broadband analog repeaters in series, based on a dual MCP6022-I/SN op-amp. The Blue pill board contains a built-in stabilized power supply with a voltage +3.3 V, which provides the necessary conditions for the stable operation of the built-in ADC with a conversion range from 0 to +3.3 V. The video signal of the mini-spectrometer C12880MA can be changed in the range from 0.3 to 4.3 V. Therefore, in its circuit at the output of the first analog repeater on the operational amplifier a resistive signal divider R3, R4 is used, which ensures the coordination of the variation range of the video signal with the conversion range of the ADC microprocessor.

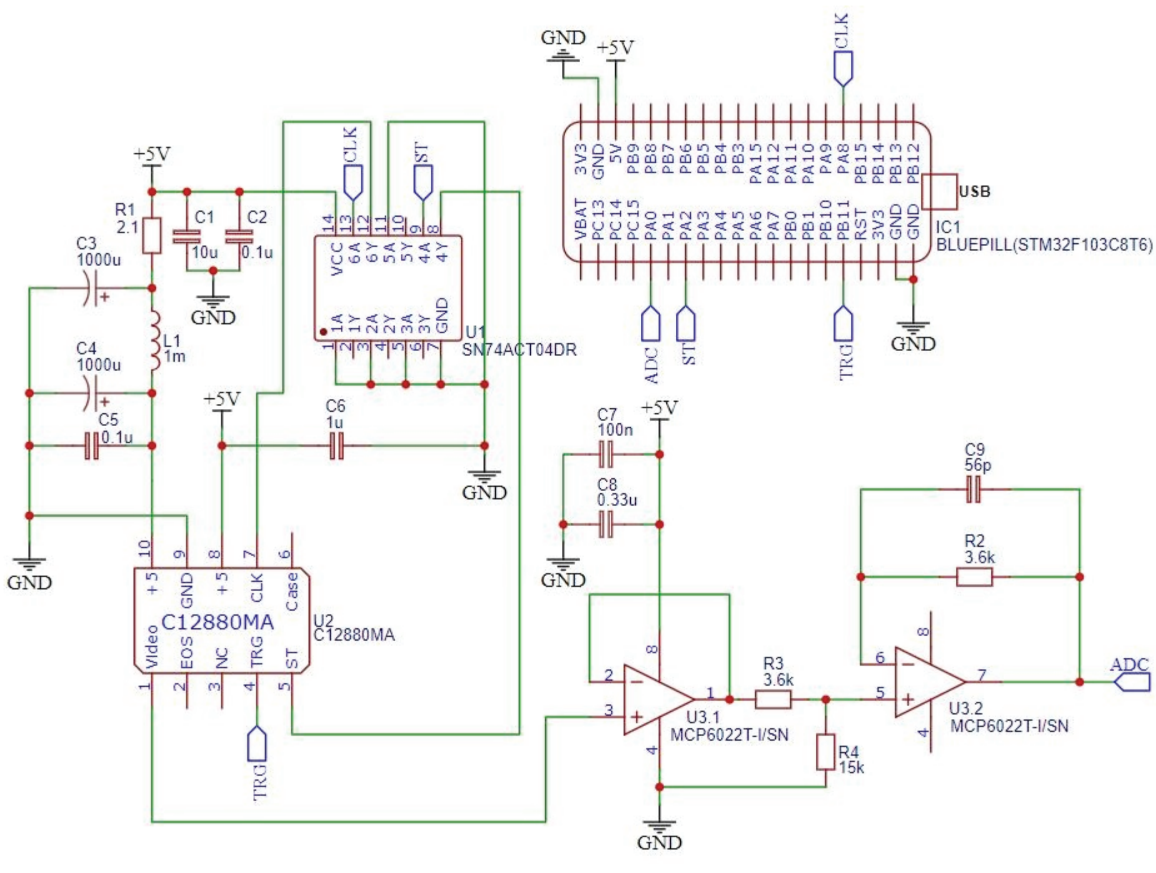

a

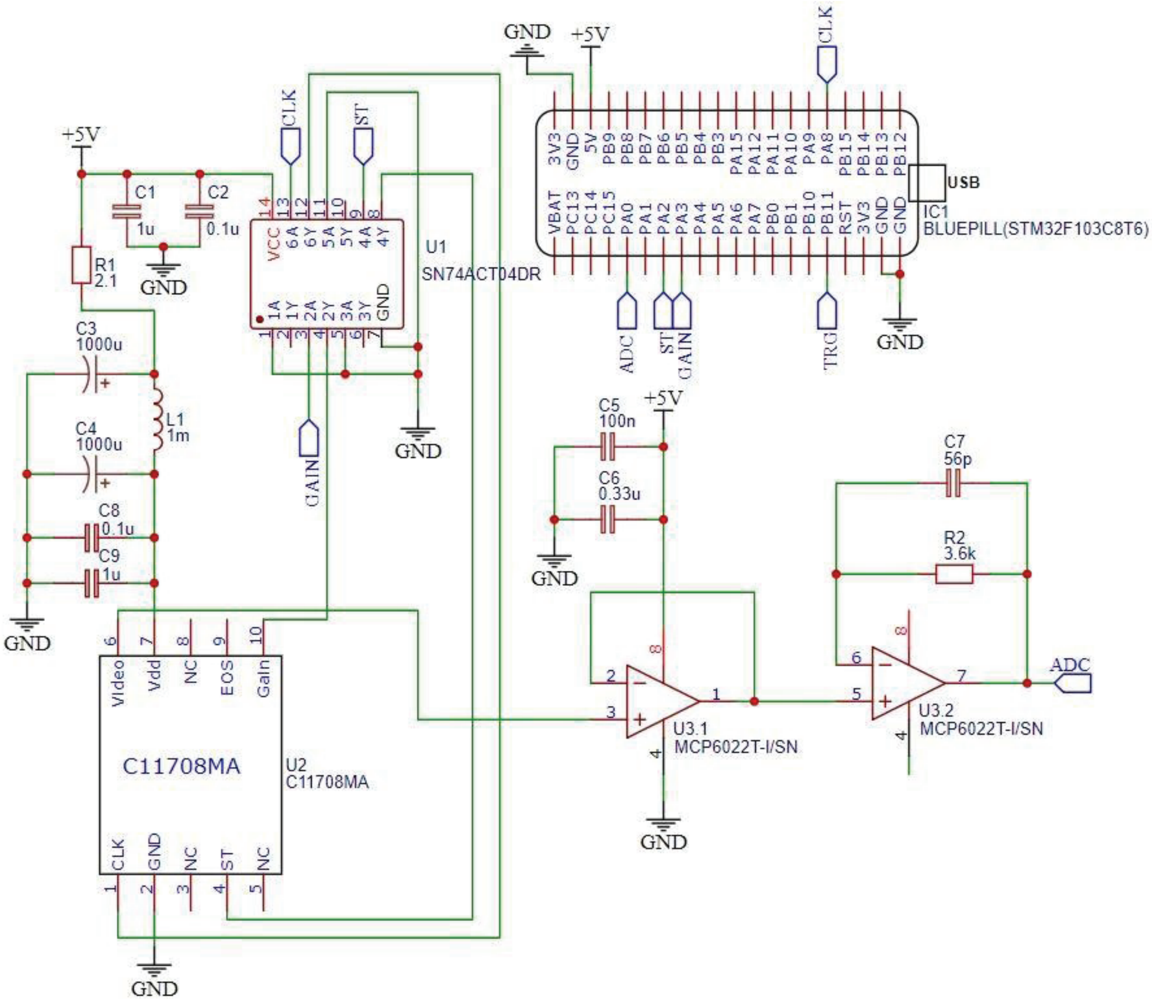

b

Figure 1 – Connection diagram of mini-spectrometrs Hamamatsu C12880MA (*a*) and C11708MA (*b*) to the microprocessor board ARM STM32F103C8T6 STM32

The mini-spectrometer is powered from the +5 V bus of the computer's USB port. The peak values of parasitic pickups on this bus can exceed several tens of millivolts, which can lead to the formation of noticeable interference at the Video output of these mini-spectrometers. Therefore, the LC П-shaped filter is used to filter out the pickups that are inherent to this bus. Therefore, a low-pass LC filter is used to filter out the pickups that are inherent to this bus. The use of low-pass filtering makes it possible to reduce the level of these interferences to the level of the spectrometers' own noise.

The connection scheme of the C11708MA mini-spectrometer differs from that in Figure 1*a* by using a digital Gain signal, which allows increasing the sensitivity of the C11708MA by a factor of 3.5 when a high level is applied to pin 10. At the same time, the capacitor rating of the C11708MA integration node is reduced from 4.8 to 1.4 pF [11]. Also the connection diagram of the C11708MA does not contain a resistive divider at the U3.1 output, because the range of the video signal of this mini-spectrometer is narrower, only from 0.15 to 3.3 V.

Software features

The widespread introduction of diffuse reflectance spectrophotometers is impossible without ensuring the ease of obtaining, storing, and processing the obtained spectra. Therefore, a mandatory requirement for the spectrophotometers under consideration is the ability to easily connect to modern portable computer equipment. For this purpose, the software created by the authors contains two levels. On the lower level, the STM32 firmware generates TTL signal diagrams that define the modes of operation of the mini spectrometer in use. It also provides frame reading, averaging and transmission via the USB bus to the upper level. The upper-level program is specially created on the basis of the powerful Matlab system of computer mathematics. Such a solution provides a quick modification of the applied software when solving spectrophotometric tasks in different branches of science and technology.

The firmware provides continuous control of the mini-spectrometer by commands of the control computer, which are received via the USB bus. A special cascade mode of STM32 timers is used, which ensures the formation of stable time diagrams of the generated TTL signals. In this mode, some timers hardware control start, clocking and dynamic changes in the parameters of other timers, ADCs and STM32 output port states. Therefore, before starting the process of obtaining a frame you only need to set the necessary parameters of the four timers, the ADC and DMA direct memory access block. The program is no longer involved in clocking, setting the exposure time and reading the frame. The proposed solution provides stable operation of the mini-spectrometers in a wide range of frame exposure values from tens of microseconds to tens of seconds.

The top-level software provides the selection of the required measurement modes:

1) a single start with the possibility of accumulating a specified number of frames n for their further averaging;

2) continuous with the possibility of averaging the obtained spectra with the help of a sliding time window with the length of n frames.

The program contains an option for automatically selecting the exposure time or setting its required value. Formation of a scale of counts by wavelength λ_i (this scale is non-linear) and output of the received spectra on the screen is provided. Necessary dialog tools for saving the obtained measurement results to the computer memory in the form of a file are available. The saved file also contains the necessary measurement parameters. The program contains the option of smoothing the obtained spectra on the short-wave and long-wave wings of the spectrophotometer spectral range using the Savitsky–Holley filter. Such a solution significantly improves the visual perception of spectra with insufficient signal-to-noise ratio at the edges of the range. The program contains an option to switch to a linear wavelength scale with a smaller sampling interval, based on the interpolation of the resulting spectrum by cubic splines. The small size of the C12880MA and C11708MA spectrometers can lead to a shift in their wavelength readout scale λ_i, which is due to their aging process. Hamamatsu gives the corresponding polynomial coefficients in the data sheet of each spectrometer. Therefore, the program contains an option for determining the value of the arising shift $\Delta\lambda$ of the scale λ_i by the emission of the He-Ne laser.

Calibration procedure for spectrophotometers

Spectrometer manufacturers calibrate the wavelength scale. In this case the reference gasdischarge sources of radiation and interpolation of values in the intervals between the registered lines of the spectrum are used. The data sheets of the C12880MA and C11708MA minispectrometers contain the p_k coefficients of the 5-th degree polynomial. They are used in the calculation of the wavelengths λ_i which correspond to the indices of the i-th elements of the linear photodiode arrays $\lambda_i = \sum_{k=0}^{5} p_k i^k$. The spectrometers are not usually calibrated by the intensity of the registered radiation $I(\lambda)$.This calibration can be performed by the manufacturer at the request of the user as an option with an additional charge for this service.

Different optical measurement schemes can be used for photometric measurements of the reflection parameters of condensed media. The spectrometer must be supplemented with a lens when it is necessary to determine the spectral density of brightness of radiation $L(\lambda)$ of sufficiently distant objects. In this case, the entrance slit of the spectrometer is placed in the focal plane of the objective, as shown in Figure 2. It is important to make sure that the plane angle, which corresponds to the spatial angle of focus $\Omega = 2\pi[1-\cos(\alpha)]$, fits exactly within the numerical aperture of the NA spectrometer. The numerical aperture NA is defined as the sine of half of the flat angle at the apex of the collecting cone NA = sin(Θ/2). It is NA = 0.22 for the considered spectrometers [10, 11]. The diameter of the exit pupil of the lens used, as shown in Figure 2, must be chosen from the condition that the angle corresponds to 2arcsin(NA) ≈ 26º.

In cases when it is necessary to determine the spectral density of brightness of radiation of a small area of the controlled surface, the measurement scheme with a single magnification is often used. In these cases, the surface of the medium and the spectrometer are placed at distances $2f$ from the front and rear principal planes of the lens used, respectively, as shown by the dashed lines in Figure 2. Note that it is also necessary to observe the conditions of agreement of the spatial angle Ω_{2f} with the aperture NA of the spectrometer when using this measurement scheme.

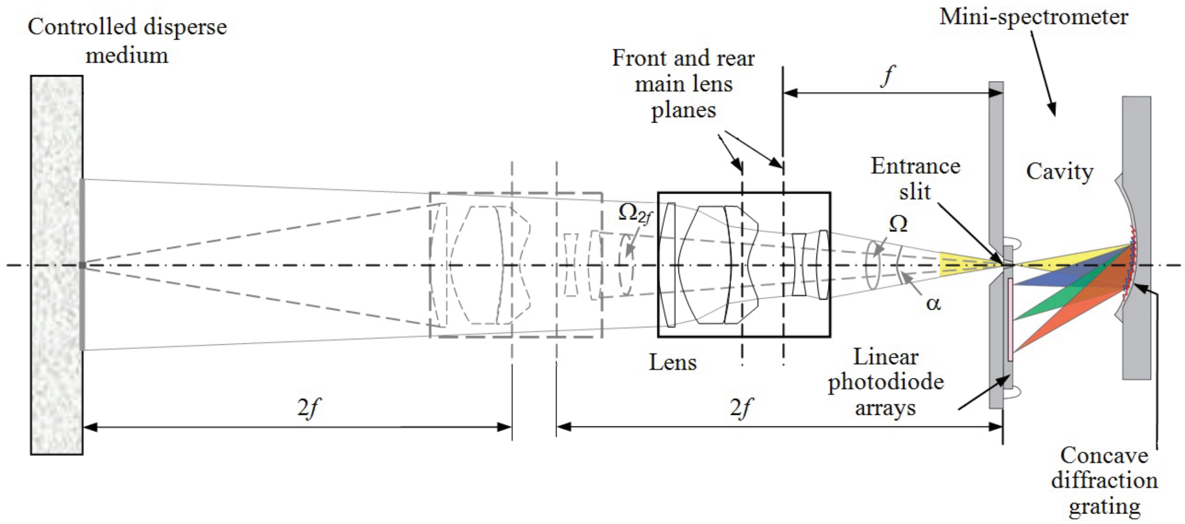

Figure 2 – Optical Scheme of photometry when focusing the lens to infinity (the lens is shown by solid lines) and at a single image magnification (dashed lines)

In cases where the calibration of spectrophotometers is performed by the user himself [12, 13], it is necessary to use standard light sources. The highest accuracy in reproducing the spectral density of surface luminosity $M(\lambda)$ at a given temperature T is provided by the models of black bodies (BB). Other reference emitters with simplified designs, such as a tungsten reference lamp strip, can be used in the absence of a BB. Spectral coefficient of thermal radiation of tungsten $\varepsilon_W(\lambda, T)$ accurately measured. This allows us to calculate its surface spectral luminosity $M_W(\lambda, T)$ quite accurately. The $M_W(\lambda, T)$ dependence is calibrated by the current I through the tungsten strip of the lamp by comparing its luminosity with the spectral luminosity density of the BB, denoted as $M_{\mathrm{BB}}(\lambda)$.The spectral illuminance density of the slit $E(\lambda)$ can be accurately reproduced by projecting the image of the tungsten lamp strip onto the entrance slit of the spectrometer. It is necessary to project an image of the section of the lamp ribbon that has the maximum temperature. This makes it possible to determine the spectral dependence of $E(\lambda, T)$ by setting the necessary values of the spectral luminosity density $M_W(\lambda, T)$ of the tungsten strip.

When calculating it is necessary to take into account that the radiation of the tungsten strip in the direction normal to its surface is close to the radiation of the Lambertian emitters, i. e. the brightness of the strip's radiation $L_{rs} = M_{rs}/\pi$. Then the relationship between the spectral luminosity density $E(\lambda)$ of the reference incandescent lamp strip image and the spectral luminosity density $M_{rs}(\lambda)$ of the strip itself is defined by the expression [14, p. 75]:

$$E(\lambda) = \frac{M_{rs}(\lambda)}{\pi} \frac{(1 - f/z)^2}{f^2} \frac{\pi D_l^2}{4} =$$

$$= \tau_l \frac{D_l^2}{4f^2}\left(1 - \frac{f}{z}\right)^2 M_{rs}(\lambda) = \tau_l K M_{rs}(\lambda),$$

where $K = \left(D_l^2/4f^2\right)(1 - f/z)^2$ is the dimensionless coupling coefficient between the illuminance of the strip image and the luminosity of the tungsten strip; τ_l, D_l and f is transmission, diameter and focal length of the lens used; z is distance from the surface of the reference source to the front main plane of the spectrophotometer objective lens.

The optical scheme with single magnification is the most convenient when calibrating the spectrophotometer by the reference tungsten incandescent lamp, because the size of the area of maximum heating of the lamp strip is small. When using this scheme, the expression for determining the average rate $\overline{V}(\lambda_i)$ (it is proportional to the photocurrents formed in the photosensitive elements of the linear of photodiodes array) of the rise of digital counts $\overline{D}_i(\lambda_i)$, which are formed by the i-th photosensitive elements of the linear array of the spectrometer, has the form:

$$\bar{V}(\lambda_i,T)=\frac{\bar{D}_i(\lambda_i,T,\tau)}{\tau}=\frac{k_iKk_{QD}\left[i_{ph}(\lambda_i)+i_d\right]\tau}{\tau}=k_iKk_{QD}\left[\frac{es_{el}}{hc}\beta(\lambda_i)\eta(\lambda_i)\tau_{wL}\varepsilon_W(\lambda_i,T)M_{\mathrm{BB}}(\lambda_i,T)\lambda_i\Delta\lambda_i+i_d\right]=$$
$$=k_iKk_{QD}\left[\frac{es_{el}}{hc}\beta(\lambda_i)\eta(\lambda_i)\tau_{wL}\varepsilon_W(\lambda_i,T)\frac{c_1}{\lambda_i^4}\left(e^{\frac{c_2}{\lambda_iT}}-1\right)^{-1}\Delta\lambda_i+i_d\right], \quad (1)$$

where λ_i is the wavelength of the registered radiation corresponding to the i-th element of the linear photodiodes array of spectrophotometer; k_i is a coefficient describing the heterogeneity in the sensitivity of the elements of the linear of photodetectors array, which is on average equal to one with a relative standard deviation of about a few percent; T is the temperature of the area of maximum heating of the tungsten strip of the lamp on the Kelvin scale; τ is frame exposure time; k_{QD} is the conversion coefficient of charges Q_i accumulated in the photosensitive elements of the linear of photodetectors array into digital readouts D_i; e, h and c are the electron charge, Planck's constant and the speed of light, respectively; c_1 and c_2 are the first and second radiation constants, respectively; s_{el} is the area of the photosensitive element of the linear of photodetectors array; $\beta(\lambda_i)$ is spectral dependence of the blaze angle of the diffraction grating used in the spectrophotometer; $\eta(\lambda_i)$ is spectral dependence of the quantum efficiency of the elements of linear photodetectors array; $\Delta\lambda_i$ is the width of the elementary segment of the spectrum, falling on one element of the linear of photodetectors array; $K=\tau_l(D_l/4f)^2$ is the relationship coefficient between the illumination of the ruler elements and the luminosity of the tungsten ribbon at $z=2f$; τ_{wL} is the transmittance coefficient of the sapphire window of the lamp; $i_{ph}(\lambda_i)$ is the photogenerated current produced by the i-th photodiode of the linear of photodetectors array; i_d is the average dark current of elements of the linear photodiode array.

The influence of the dark current can be neglected when using the operation of determining the average i_d current, which is then subtracted.

During calibration determine the absolute spectral sensitivity of the spectrophotometer by the brightness of radiation $S_L(\lambda_i)$. This makes it possible to recalculate the spectral dependence $V_i(\lambda_i)$ registered by the spectrophotometer into the spectral density brightness of radiation:

Calculations of the dependence using (1) $L(\lambda_i)=\dfrac{V(\lambda_i)}{S_L(\lambda_i)}$.

will be approximate, due to the inevitable scatter of the spectral characteristics of the spectrometer elements. Therefore, the determination of $S_L(\lambda_i)$ should be performed by calibrating spectrophotometers using a reference emitter [13]. When using a reference tungsten lamp and $z=2f$, the expression applies:

$$S_L(\lambda_i)=\frac{\bar{V}_W^*(\lambda_i,T)}{L_W(\lambda_i,T)}=\frac{\pi\bar{D}_W^*(\lambda_i,T,\tau_{cal})/\tau_{cal}}{\tau_{wL}\varepsilon_W(\lambda_i,T)\left(c_1/\lambda_i^5\right)\left(e^{c_2/\lambda_iT}-1\right)^{-1}}, \quad (2)$$

where $\bar{D}_W^*(\lambda_i,T,\tau_{cal})$ and $\bar{V}_W^*(\lambda_i,T)$ are digital signals recorded during calibration with the frame exposure time τ_{cal} and the rate of their rise, respectively. When applying expression (2), it is convenient to use the dimensionality of the absolute spectral sensitivity $S_L(\lambda_i)$, equal to (cm^2·sr·μm)/(W·ms), so we usually determine $L(\lambda_i)$ with dimensionality in W/(cm^2·sr·μm).

The lens in some applications of diffuse reflectance spectroscopy with spatial resolution can be not used, because the spectrometer collects the reflected radiation from the medium within its numerical aperture. During calibration, when calculating $S_L(\lambda_i)$ in these cases, it is necessary to divide the spectral luminosity of the tungsten in expression (2) by the lens transmittance τ_l.

In many cases of photometry it is necessary to use a field of view of the spectrometer with a weak divergence. Such a measurement scheme, as can be seen in Figure 2, is formed by placing the spectrometer slit in the focal plane of the lens. In this case the linear field of view of the spectrometer is increased and the calibration should be carried out according to the spectral density of brightness radiation of the BB model $L_{\mathrm{BB}}(\lambda_i,T)$. Moreover, it is necessary to make sure that the spectrophotometer's field of view fits into the output aperture of the BB model. In this case, the expression for calculating $S_L(\lambda_i)$ is simplified:

$$S_L(\lambda_i)=\frac{\bar{V}_W^*(\lambda_i,T)}{L_{\mathrm{BB}}(\lambda_i,T)}=\frac{\pi\bar{D}_W^*(\lambda_i,T,\tau_{cal})/\tau_{cal}}{\left(c_1/\lambda_i^5\right)\left(e^{c_2/\lambda_iT}-1\right)^{-1}}.$$

Devices and Methods of Measurements
2022, vol. 13, no. 2, pp. 93–104
V.A. Firago et al.

It should be remembered that the temperature of the emitting core of the BB must be more than 1500 ºC for the calculated $S_L(\lambda_i)$ values in the short-wave region of the spectrum to have a good signal-to-noise ratio. In this case we have to use a neutral attenuating filter with a known spectral transmittance $\tau_{NF}(\lambda_i)$, the attenuation of which must be taken into account when calculating $S_L(\lambda_i)$.

Main parameters, characteristics and examples of applications

The developed spectrophotometers with microprocessor board are 72 mm long and 40 mm wide when assembled without a lens. Therefore, they can be packaged in a cylindrical body with a C-Mount external lens mount. The compact lens "Basler Lens C23-3520-2M F2.0 f35 mm 2/3" with focal length f = 35 mm and f/D = 2.0 ratio was used for performance measurements of the developed spectrophotometers. This lens has a diameter of 35 mm and a length of 43.7 mm. In this case, the angle α at the apex of the assembled radiation cone of the tungsten tape of the reference lamp is not less than 2arcsin(NA), as shown in Figure 2.

Before calibrating the spectrophotometers based on the C12880MA and C11708MA, the offset of their wavelength readout scales λ_i was checked. As a reference monochromatic radiation source the HeNe laser LHN-303 with a wavelength of generation λ = 632.819 nm and the relative stability of the generation frequency not worse than 10^{-8} was used. The resulting readout scale offsets were small and were Δλ = -3.4 nm for C12880MA and Δλ = -2.4 nm for C11708MA. They were entered into the spectrophotometer software to shift the scales λ_i to the right by the corresponding value Δλ. The spectral range of operation of C12880MA was 307.8–878.2 nm, and that of C11708MA was 583.6 to 1086.5 nm. The spectral resolving power of spectrophotometers was determined by the standard technique at the half-height of the hardware function, i. e., the spectrum of diffusely scattered radiation of the LHN-303 laser. For C12880MA it was about 10 nm, for C11708MA it was about 15 nm.

The scheme of the setup used to calibrate the created spectrophotometers corresponded to the scheme shown in Figure 2. The distance between the rear main plane of the lens and the slit of the spectrophotometer, was $2f$, i. e. 70 mm. A neutral attenuation filter with a transmittance factor τ_{NF} = 0.0033 was used to attenuate the illumination of the spectrophotometer slit, which is formed by projecting the image of a glowing tungsten strip of the LI10-300 lamp onto it. The absolute spectral sensitivities of the spectrophotometers that were obtained using (2) are shown in Figure 3.

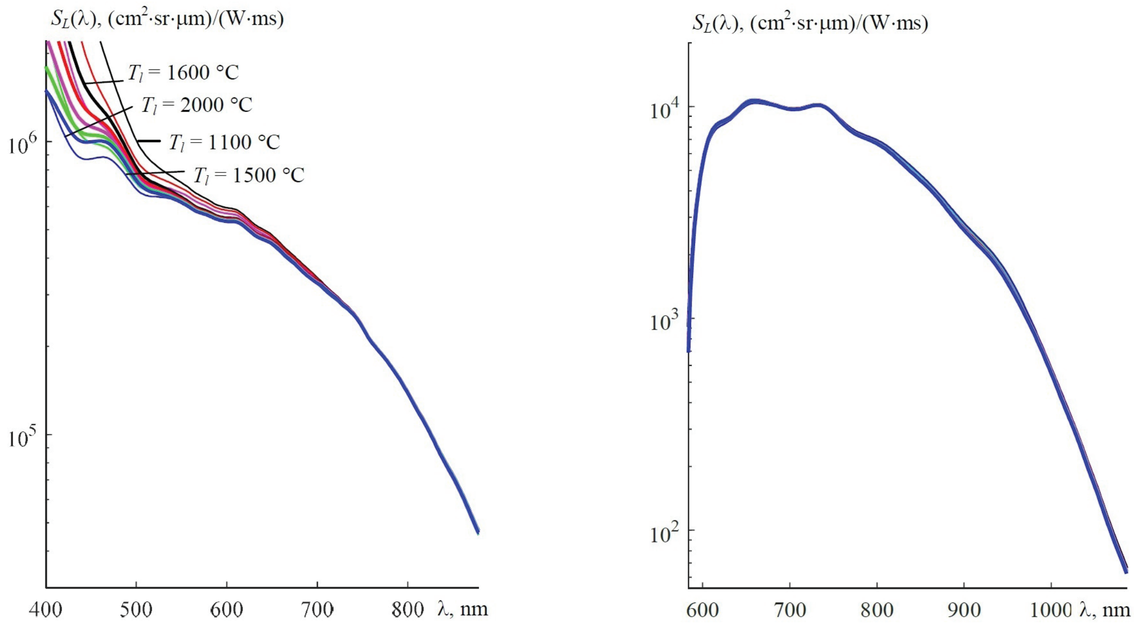

a *b*

Figure 3 – Absolute spectral sensitivities of spectrophotometers based on C12880MA (*a*) and C11708MA (*b*), which are calculated from the emission of a reference SI10-300 tungsten lamp at ten different temperatures were shown in Figure 4

An unpleasant feature of the C12880MA mini-spectrometer was revealed during the calibration work. This is a noticeable addition of radiation, which is scattered by the concave diffraction grating in the zero order of diffraction, to the spectrum recorded in the short-wave part of the spectrum. Many spectrophotometers based on concave diffraction gratings and photodetector arrays have this disadvantage. The C12880MA mini-spectrometer is small, so this effect is much stronger. The dependences shown in Figure 4*a* convincingly illustrate the effect of scattered radiation on the recorded spectra. Therefore, it should be taken into account that the spectra recorded by the C12880MA can be markedly distorted in the short-wave part of the range due to the contribution of powerful spectral components from the longer wavelength part of the spectrum. The spectrophotometer based on C11708MA has practically no marked distortions in the short-wave part of its spectral range. This effect, as follows from Figure 4*b*, appears only near the short-wave boun-dary, i. e. around 584 nm.

The experimentally measured $L_m(\lambda)$ dependences, shown in Figure 4 as solid lines, were determined using the spectral sensitivities of spectrophotometers $S_L(\lambda_i,T_l)$, which were obtained from the radiation of tungsten strip with brightness temperature T_l = 2000 ºC. The dependences of the spectral brightness density $L_m(\lambda)$, which were measured with a spectrophotometer based on C11708MA, turn out to be close to the calculated dependences. Small deviations of $L_m(\lambda)$ values in the long-wave part of the spectral range are caused by an error in determining the spectral transmit-tance of the attenuating neutral filter $\tau_{NF}(\lambda_i)$ in the infrared range. The influence of the effect noted above on the spectrum, which is formed at λ < 480 nm, we found it even in a high-quality fiber-optic spectrometer AvaSpec 2048WL (Holland) [13]. This disadvantage of spectrometers based on concave diffraction gratings and photodetector arrays must necessarily be taken into account when analyzing diffuse reflectance spectra in the short-wave region of the visible spectrum.

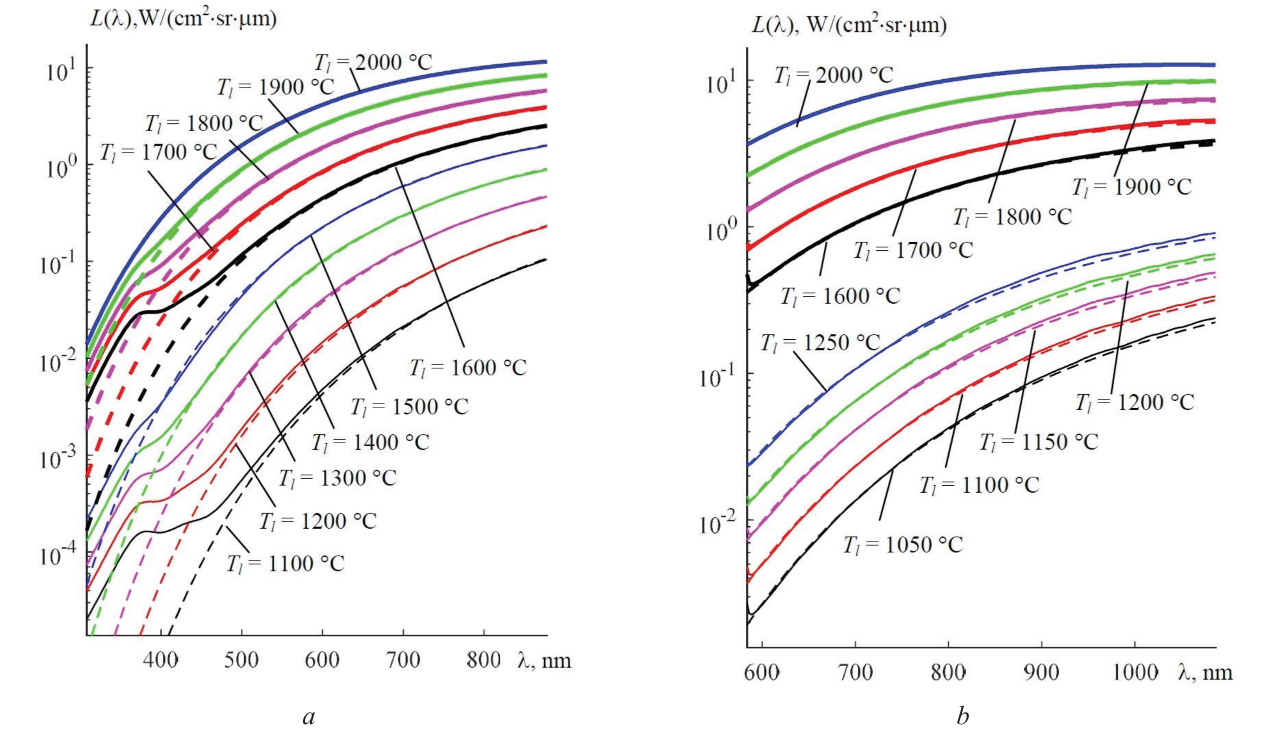

Figure 4 – The calculated spectral brightness $L(\lambda)$ of the tungsten ribbon strip radiation at different brightness temperatures T_l (dashed lines) and spectral dependences measured with the C12880MA (*a*) and C11708MA (*b*) spectrophotometers (solid lines)

Figure 5*a* shows the spectral brightness density of the diffuse reflection of a white sheet illuminated by the Sun. The Earth's atmosphere has a noticeable influence on the spectrum of the illuminating radiation, for example, the absorption bands of O_2 with a maximum at λ = 760 nm and water vapor around 933–960 nm are clearly visible.

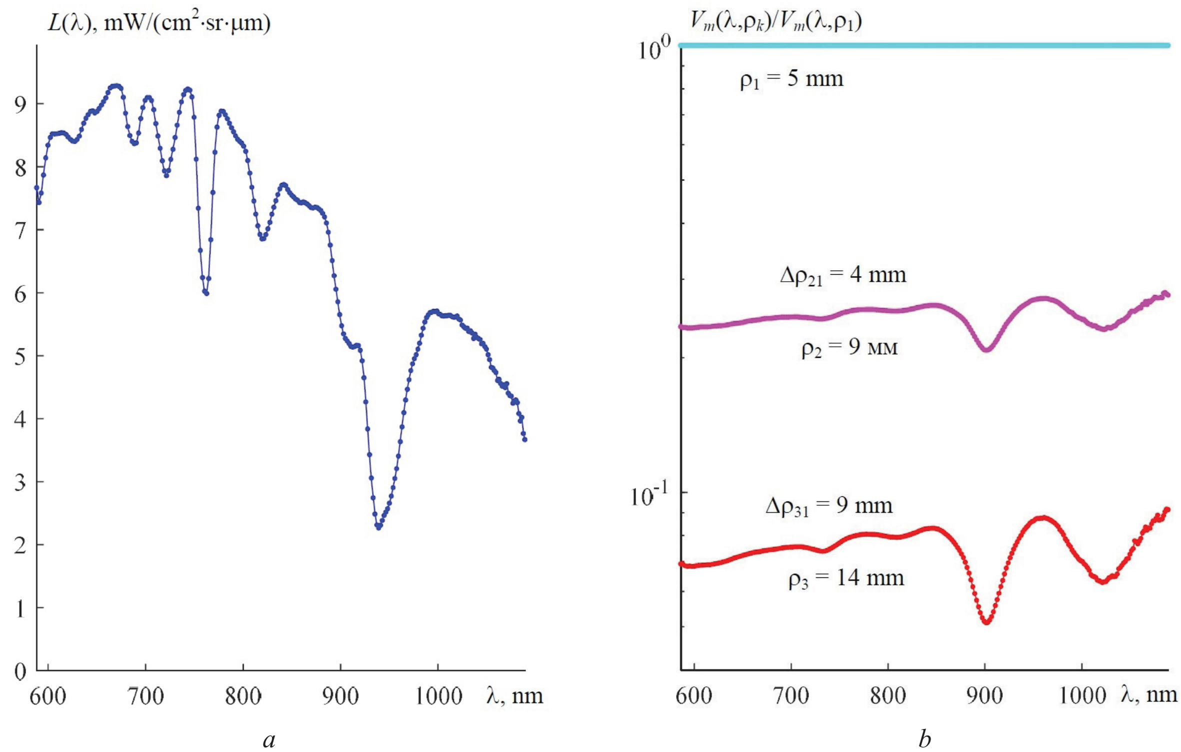

Figure 5 – Spectral brightness $L(\lambda)$ of a sheet of white paper that is illuminated by the sun (*a*), and normalized spectral dependences for plastic Gehr-Pom-C by different distances ρ_k between the input point of the halogen lamp radiation through the optical fiber and the registration point (*b*), which were obtained by a spectrophotometer based on C11708MA

The normed diffuse reflectance spectra of the Gehr-Pom-C matte white plastic, which were obtained using a C11708MA-based spectrophotometer, are shown in Figure 5*b*. The normalization was carried out by dividing the spectra $V_m(\lambda_i,\rho_k)$ by the spectrum $V_m(\lambda_i,\rho_1)$, which was obtained at a minimum distance of $\rho_1 = 5$ mm between the point of radiation input into the plastic and the point of registration. The halogen lamp emission spectrum and spectrometer characteristics do not affect the ratio $V_m(\lambda_i,\rho_k)/V_m(\lambda_i,\rho_1)$ with this normalization. The obtained normalized spectral dependences coincide with similar dependences that were obtained using a spectrophotometer based on the AvaSpec 2048WL spectrometer. It can be clearly seen that the white matte Gehr-Pom-C plastic has radiation absorption bands, which appear stronger with increasing distance ρ between the radiation input point and the registration point.

Conclusion

Progress made in the production of miniature spectrometers and microprocessors opens up the possibility of using the C12880MA and C11708MA in inexpensive spectral techniques, which are designed to control the diffuse reflectance spectra of various materials and media in the visible and near-infrared spectrum ranges. Studies of the characteristics of portable spectrophotometers based on Hamamatsu mini-spectrometers and STM32 microprocessors indicate the prospects for their use in controlling difuse scattering spectra of condensed finely dispersed mediums.

The described graduation method allows you to identify the range of the spectrum, in which its distortion due to the scattering of radiation into the zero order of diffraction of the concave diffraction grating, can not be taken into account.

The conducted studies point to the promising development of inexpensive computerized portable diffuse reflectance spectroscopy techniques with spatial resolution, which can be widely used in various sectors of science and industry.

References

1. Puig-Bertotto J., Coelloa J., Maspoch S. Evaluation of a handheld near-infrared spectrophotometer for quantitative determination of two APIs in a solid

pharmaceutical preparation. *Analytical Methods*, 2019, vol. 11, iss. 3, pp. 327–335.
DOI: 10.1039/C8AY01970C

2. Tang E. Rapid Analysis of Textiles with Portable Near Infrared Spectroscopy. *NIR news*, 2015, vol. 26, iss. 8, pp. 11–12.
DOI: 10.1255/nirn.1566

3. Nicolaï B.M., Beullens K., Bobelyn E., Peirs A., Saeys W., Theron K.I., Lammertyn J. Nondestructive measurement of fruit and vegetable quality by means of NIR spectroscopy: A review. *J. Postharvest Biology Technology*, 2007, vol. 46, iss. 2, pp. 99–118.
DOI: 10.1016/j.postharvbio.2007.06.024

4. Do Trong N.N., Erkinbaev C., Tsuta M., De Baerdemaeker J., Nicolaï B., Saeys W. Spatially resolved diffuse reflectance in the visible and near-infrared wavelength range for non-destructive quality assessment of “Braeburn” apples. *Postharvest Biology and Technology*, 2014, vol. 91, pp. 39–48.
DOI: 10.1016/j.postharvbio.2013.12.004

5. Doornbos R.M., Lang R., Aalders M.C., Cross F.W., Sterenborg H.J.C.M. The determination of in vivo human tissue optical properties and absolute chromophore concentrations using spatially resolved steady-state diffuse reflectance spectroscopy. *Phys. Med. Biol*., 1999, vol. 44, no. 4, pp. 967–981.
DOI: 10.1088/0031-9155/44/4/012

6. Thueler P., Charvet I., Bevilacqua F., Ghislain M. In vivo endoscopic tissue diagnostics based on spectroscopic absorption, scattering, and phase function properties. *J. Biomedical Optics*, 2003, vol. 8, no. 3, pp. 495–503.
DOI: 10.1117/1.1578494

7. Abookasis D., Zafrir E., Nesher E., Pinhasov A., Sternklar S. Diffuse near-infrared reflectance spectroscopy during heatstroke in a mouse model: pilot study. *J. Biomedical Optics*, 2012, vol. 17, no. 10, pp. 105009-1–105009-11. **DOI:** 10.1117/1.JBO.17.10.105009

8. Abookasis D., Shochat A., Marlon S. Monitoring hemodynamic and morphologic responses to closed head injury in a mouse model using orthogonal diffuse near-infrared light reflectance spectroscopy. *J. Biomedical Optics*, 2013, vol. 18, no. 4, pp. 04503-1–04503-11.
DOI: 10.1117/1.JBO.18.4.045003

9. Bevilacqua F., Piguet D., Marquet P., Gross J.D., Tromberg B.J., Depeursinge C. In vivo local determination of tissue optical properties: applications to human brain. *Applied optics*, 1999, vol. 38, no. 22, pp. 4939–4950. **DOI:** 10.1364/ao.38.004939

10. Micro-spectrometr C12880MA. Hamamatsu Photonics K. K. Solid State Division. Cat. No. KAC-C1226E02. Oct. 2015 DN, pp. 1–12.

11. Mini-spectrometers C10988MA-01, C11708MA. Hamamatsu Photonics K. K. Solid State Division. Cat. No. KACC1169E11. Oct. 2014 DN, pp. 1–10.

12. Firago V.A., Sakovich I.A., Sabchuk A.N. [Fiber-optic spectrophotometer to register the spectra of thermal radiation of heated bodies]. *Materialy 4 MNPK “Prikladnyye problemy optiki, informatiki, radiofiziki i fiziki kondensirovannogo sostoyaniya”. 11–12 maya 2017 g., Minsk* [Materials of 4 ISPK “Applied problems of optics, informatics, radiophysics and condensed matter physics”. May 11–12, 2017, Minsk], pp. 148–150 (in Russian).

13. Firago V., Hotra O., Sakovich I. Radiometric calibration of fiber optic spectrophotometers. *Proceedings of SPIE – The International Society for Optical Engineering*, 2019, vol. 11045, pp. 1104516-1–1104516-7. **DOI:** 10.1117/12.2522540

14. Firago V.A. *Tsifrovaya termografiya* [Digital thermography]. Minsk, BSU Publ., 2019, 319 p.

Devices and Methods of Measurements
2022, vol. 13, no. 2, pp. 105–111
V.A. Alekseev et al.

System Eliminating Emergency Discharges in Industrial Facilities Waste Waters Using Relative Signal Description

V.A. Alekseev[1], S.I. Yuran[2], V.P. Usoltsev[1], D.N. Shulmin[1]

*[1]Kalashnikov Izhevsk State Technical University,
Studencheskaya str., 7, Izhevsk 426069, Russia*

*[2]Izhevsk State Agricultural Academy,
Studencheskaya str., 11, Izhevsk 426069, Russia*

Received 18.03.2022
Accepted for publication 30.05.2022

Abstract

Peak emergency discharges of harmful substances to the industrial companies waste waters that normally form coagulates over time present a serious environmental problem. These coagulates can enter natural water bodies during the wastewater discharge. Thus, detecting these coagulates in real-time is a relevant problem.

To solve this problem, the authors suggest building an automated system that shall record and identify the emergency harmful substances discharges to the industrial companies waste waters caused by accidents. This system features a laser probing module which scans waste water at several wavelengths simultaneously and in real time.

Emergency discharge identification is performed based on the substance transmission spectra analysis using the original description of the recorded substance spectra digital signals. The relative description on the components of the lattice function of the spectrum of emergency discharges is used, constructed using the order ratio between the components of the lattice function.

The emergency discharge identification can be implemented by comparing the relative description of the emergency discharge spectrum with the reference spectra for the harmful substances that can be present at the given industrial facility, and the standards of the spectra of these substances are presented in the form of a relative description using the ratio “more”–“less”.

The authors provide a flow chart for the emergency discharge elimination system, describe its operation and the functions fulfilled by its elements. The system features an emergency coagulate identification device, a processing device for the spectrum recorded that can also store the reference spectra of harmful substances, and a valve-control device for the waste water system. Due to installation of laser radiation sources along the perimeter of the pipe along which the liquid moves, simultaneous laser action on the emergency clot of harmful substances passing through the pipe is ensured. The analysis of the clot passing through the sewer pipe allows opening the valves for each of the predicted emergency clots when receiving a command from the control device and diverting the clot that has appeared to the appropriate sump.

Keywords: emergency discharge, laser probing, lattice function, spectrum.

DOI: 10.21122/2220-9506-2022-13-2-105-111

Адрес для переписки:
Юран С.И.
Ижевская государственная сельскохозяйственная академия,
ул. Студенческая, 11, г. Ижевск 426069, Россия
e-mail: yuran-49@yandex.ru

Address for correspondence:
Yuran S.I.
Izhevsk State Agricultural Academy,
Studencheskaya str., 11, 426069, Izhevsk, Russia
e-mail: yuran-49@yandex.ru

Для цитирования:
V.A. Alekseev, S.I. Yuran, V.P. Usoltsev, D.N. Shulmin.
System Eliminating Emergency Discharges in Industrial Facilities Waste Waters Using Relative Signal Description.
Приборы и методы измерений.
2022. – Т. 13, № 2. – С. 105–111.
DOI: 10.21122/2220-9506-2022-13-2-105-111

For citation:
V.A. Alekseev, S.I. Yuran, V.P. Usoltsev, D.N. Shulmin.
System Eliminating Emergency Discharges in Industrial Facilities Waste Waters Using Relative Signal Description.
Devices and Methods of Measurements.
2022, vol. 13, no. 2, pp. 105–111.
DOI: 10.21122/2220-9506-2022-13-2-105-111

Система устранения аварийных сбросов в сточные воды предприятий с использованием относительного описания спектров веществ

В.А. Алексеев[1], С.И. Юран[2], В.П. Усольцев[1], Д.Н. Шульмин[1]

[1]*Ижевский государственный технический университет имени М.Т. Калашникова, ул. Студенческая, 7, г. Ижевск 426069, Россия*

[2]*Ижевская государственная сельскохозяйственная академия, ул. Студенческая, 11, г. Ижевск 426069, Россия*

Поступила 18.03.2022
Принята к печати 30.05.2022

Серьёзной экологической проблемой являются залповые аварийные сбросы вредных веществ в сточные воды предприятий, которые, как правило, представляют сгустки определённой длительности. Образованные сгустки могут попасть в естественные водоёмы при сбросе сточных вод. Поэтому актуальна задача обнаружения указанных сгустков в реальном масштабе времени.

Для решения данной задачи предлагается вариант построения автоматизированной системы фиксации и идентификации аварийных сбросов вредных веществ в сточные воды промышленного предприятия при запроектных авариях. Отличие системы заключается в использовании лазерного зондирования сточных вод одновременно на нескольких длинах волн излучения в реальном масштабе времени.

Идентификация аварийных сбросов производится на основании анализа спектров пропускания веществ с использованием оригинального описания цифровых сигналов регистрируемых спектров веществ. Используется относительное описание на составляющих решетчатой функции спектра аварийных сбросов, построенное с использованием отношения порядка между составляющими решетчатой функции. Идентификация аварийного сброса осуществляется путём сравнения относительного описания спектра аварийного сброса с эталонами спектров возможных вредных веществ для данного предприятия, причём эталоны спектров этих веществ представлены в виде относительного описания с использованием отношения «больше»–«меньше».

Приведена структурная схема системы устранения аварийных сбросов, описана её работа и назначение отдельных элементов системы. Система содержит устройство идентификации аварийных сгустков, устройство обработки регистрируемых спектров и хранения эталонов спектров вредных веществ и устройство управления задвижками в системе сточных вод. За счёт установки источников лазерного излучения по периметру трубы, по которой движется жидкость, обеспечивается одновременное лазерное воздействие на проходящий по трубе аварийный сгусток вредных веществ. Анализ проходящего по сточной трубе сгустка позволяет проводить открытие задвижек для каждого из прогнозируемых аварийных сгустков при получении команды от устройства управления и отвести появившийся сгусток в соответствующий отстойник.

Ключевые слова: аварийный сброс, лазерное зондирование, решетчатая функция, спектр.

DOI: 10.21122/2220-9506-2022-13-2-105-111

Адрес для переписки:
Юран С.И.
Ижевская государственная сельскохозяйственная академия,
ул. Студенческая, 11, г. Ижевск 426069, Россия
e-mail: yuran-49@yandex.ru

Address for correspondence:
Yuran S.I.
Izhevsk State Agricultural Academy,
Studencheskaya str., 11, 426069, Izhevsk, Russia
e-mail: yuran-49@yandex.ru

Для цитирования:
V.A. Alekseev, S.I. Yuran, V.P. Usoltsev, D.N. Shulmin.
System Eliminating Emergency Discharges in Industrial Facilities Waste Waters Using Relative Signal Description.
Приборы и методы измерений.
2022. – Т. 13, № 2. – С. 105–111.
DOI: 10.21122/2220-9506-2022-13-2-105-111

For citation:
V.A. Alekseev, S.I. Yuran, V.P. Usoltsev, D.N. Shulmin.
System Eliminating Emergency Discharges in Industrial Facilities Waste Waters Using Relative Signal Description.
Devices and Methods of Measurements.
2022, vol. 13, no. 2, pp. 105–111.
DOI: 10.21122/2220-9506-2022-13-2-105-111

Introduction

Many modern companies use water from natural water bodies in their production processes and dump the treated waste water in those same water bodies. If any emergencies classified as non-project [1, 2] occur at such companies, harmful substances, including hydrocarbons (oils, alcohols, etc.) may enter the water bodies [3]. The number of such accidents is increasing due to the large amounts of substances stored at the companies' specialized warehouses and unused in the main production processes.

Accidents are mostly attributed to leaks from storage containers, pipelines, loaded vehicles on the move, etc. These accidents are limited in time (peak discharge), meaning that emergencies have to be monitored in real time. Such accidents may also take place at facilities located at sea and on rivers (offshore platforms, moving objects, etc.).

Peak harmful substance discharge instances appear as coagulates of specific length and various densities. The coagulates may disrupt the operation of company treatment systems and enter natural water bodies during waste water discharge. Thus, it is crucial to detect these coagulates in real time and redirect them to harmful substance cesspools [4, 5].

Devices and systems for determining many parameters of aqueous media are known. Optical methods have great diagnostic capabilities for determining harmful substances in an aqueous environment.

In [6], the results of optical measurements of attenuation of light intensity at four different wavelengths (red, green, blue and near infrared) are presented to analyze the turbidity of test liquids in the food industry. For the experiments, the Mettler Toledo Inpro8300RAMS unit was used, which is capable of measuring the intensity of transmitted and backscattered light using radiation from eight LEDs. The experiments were carried out only on static liquids when registering the results for a few seconds. The research is aimed at further use of the method for moni-toring the characteristics of factory wastewater flows in real time.

Article [7] discusses the in situ online optical monitoring system for the concentration of suspended solids in wastewater using digital image analysis. The results of online optical monitoring can be used in predicting the quality of biologically treated wastewater.

In the article [8] the project of an optical system for multiparameter assessment of drinking water quality is considered. The system uses modern lasers operating in the mid-IR range and highly sensitive photodetectors.

A UV-LED spectroscopy system designed to control organic carbon in water is described in [9]. In the optical system, a UV LED with a wavelength of 280 nm was used as a highly efficient light source. The results obtained can significantly expand the scope of studies of the total organic carbon content both in the laboratory and in the field, including the possibility of continuous in situ monitoring.

The article [10] presents an automation system for the elimination of emergency discharge, which contains a liquid analyzer, that continuously monitors the optical density of the aqueous medium. As long as the concentration of controlled substances is within acceptable limits, water enters the filter for further purification. In the case of a salvo discharge of a controlled substance, when its concentration exceeds the specified limit, the liquid analyzer sends a signal to the control computer, which directs the contaminated water into the sump through the discharge valve, and the contamination, instead of passing through the filter and significantly disrupting its operation, goes into the sump for further disposal.

The considered technical solutions do not allow to promptly identify and eliminate an emergency clot, consisting of previously known contaminants. In the event of an emergency discharge in the form of a clot, consisting of several pollutants, the problem arises of identifying the clot to direct it to the filter allocated for it. At the same time, the concentration of the components of the clot may change over time, and the composition of the clot, that is, the ratio between its components, remains unchanged. The use of optical sensors with several wavelengths of radiation in the proposed system makes it possible to more accurately determine the composition of the clot by the ratio of the spectral components of the output signals and promptly select the appropriate purification filter.

Research Essentials

Coagulate identification may take place under the following conditions:

– the coagulate consists of one substance;

– the coagulate contains harmful substances of several types;

– the coagulate consists of several separate coagulates occurring at different times.

Each of the coagulates features specific spectral transmission or absorption parameters in a specific wavelength range from λ_{min} to λ_{max} [11–15].

The majority of spectrum analyzers work with the consecutive analysis of spectra from λ_{min} to λ_{max}, which requires some time and eliminates the possibility of real-time spectrum analysis.

The parallel spectrum scanning requires a lot of detectors for various wavelengths, which may prove impracticable depending on the spectral parameter error.

If the list of emergency substances is limited, we can analyze the spectra of these substances and identify the typical features for specific wavelengths that will become the key spectrum analysis points during the parallel spectrum analysis.

We can review several solution methods for this problem.

1. The lattice function (LF) of the spectrum components can be represented as follows:

$$\{\lambda_{11}\to S_{11}, \lambda_{12}\to S_{12}, \lambda_{13}\to S_{13}, \ldots, \lambda_{1n}\to S_{1n}\};$$
$$\{\lambda_{21}\to S_{21}, \lambda_{22}\to S_{22}, \lambda_{23}\to S_{23}, \ldots, \lambda_{2n}\to S_{2n}\};$$
$$\{\lambda_{31}\to S_{31}, \lambda_{32}\to S_{32}, \lambda_{33}\to S_{33}, \ldots, \lambda_{3n}\to S_{3n}\};$$
$$\ldots\ldots\ldots\ldots\ldots\ldots\ldots\ldots\ldots\ldots\ldots\ldots$$
$$\{\lambda_{k1}\to S_{k1}, \lambda_{k2}\to S_{k2}, \lambda_{k3}\to S_{k3}, \ldots, \lambda_{kn}\to S_{kn}\},$$

where S_{ij} are the LF components located in the typical points on the spectrum curve (dips, swells, etc.); i is the number of spectra (substances) from 1 to k; j is the number of spectrum components from 1 to n.

For each of the substances, specific points are selected on the spectra that characterize the spectrum shape (maximum and minimum extremes). When there are only a few substances (up to 5), a specific spectrum containing up to 3–5 wavelengths are selected for each of them.

2. The lattice function produced has a set increment $\Delta\lambda$ across the spectrum wavelength:

$$\{\lambda_{11}\to S_{11}, \lambda_{11+\Delta\lambda}\to S_{12}, \lambda_{11+2\Delta\lambda}\to S_{13}, \ldots, \lambda_{11+(n-1)\Delta\lambda}\to S_{1n}\},$$

where n is the number of components.

References are constructed for the entire substance (spectrum) list. A specific spectrum length increment is selected (up to 10 in practice), after which spectral parameters of each of the substances at the selected wavelengths are determined.

3. The lattice function using all of the selected wavelengths in the typical points from the list of all spectra:

$$\{\lambda_1\to S_{11}, \lambda_2\to S_{12}, \lambda_3\to S_{13}, \ldots, \lambda_n\to S_{1n}\};$$
$$\{\lambda_1\to S_{21}, \lambda_2\to S_{22}, \lambda_3\to S_{23}, \ldots, \lambda_n\to S_{2n}\};$$
$$\{\lambda_1\to S_{31}, \lambda_2\to S_{32}, \lambda_3\to S_{33}, \ldots, \lambda_n\to S_{3n}\};$$
$$\ldots\ldots\ldots\ldots\ldots\ldots\ldots\ldots\ldots\ldots\ldots\ldots$$
$$\{\lambda_1\to S_{k1}, \lambda_2\to S_{k2}, \lambda_3\to S_{k3}, \ldots, \lambda_n\to S_{kn}\},$$

where k is the number of substances (spectra); n is the total number of the wavelength for the typical points of all the spectra.

Typical points are selected in the spectra for each of the substances (3–5 points), after which an aggregate substance spectrum is constructed containing $n\cdot(3–5)$ points where n is the number of identified substances.

The obtained substance spectra are normally expressed in relative units, however the clean substance spectrum and the substance spectrum obtained through the measurements taken in the waste water may differ due to the different substance concentration and the presence of interfering inclusions from the waste water, as well as the spectrum analyzer error. For relatively clean coagulates, such coagulates may reach 5–10 % of the measured substance concentration.

To identify the substance, it is necessary to produce references, i. e. substance “profiles”. Creating references can be represented as a set of stages:

1. From the known list of substances, we analyze the substance spectra, identify their specific features (spectrum curve extremes), and record wavelengths for the identified points. It is sufficient to identify from 3 to 5 points for each of the substances.

2. We compare the spectrum components at the identified points with other substance spectra. We also determine the wavelengths for the spectrum corresponding to the set error and compare those with other spectra (up to 3 correlations for a list of 10 substances). As a result, there is a set of wavelengths that determines the reference spectra.

3. The lattice function are constructed for each of the substances in the obtained set of wavelengths. The reference substance spectrum profile is represented as a relative description based on a set of LF amplitudes (components) using the more/less relation [16–18]. The relative description of the reference must be different for each of the substances.

To determine the changes in the spectrum due to the inclusion of waste water fractions, we can conduct laboratory experiments to adjust the developed references and improve the detection probability of the substances included in the list of non-project emergency discharges.

Thus, the reference profile is a set of selected components of spectrum S for specific wavelengths.

A reference profile for one of the substances:

$$\{\lambda_1 \rightarrow S_{11},\ \lambda_1 \rightarrow S_{21},\ \lambda_3 \rightarrow S_{31},\ \ldots,\ \lambda_n \rightarrow S_{n1}\};$$
$$\{\lambda_1 \rightarrow S_{12},\ \lambda_2 \rightarrow S_{22},\ \lambda_3 \rightarrow S_{32},\ \ldots,\ \lambda_n \rightarrow S_{n2}\};$$
$$\{\lambda_1 \rightarrow S_{13},\ \lambda_2 \rightarrow S_{23},\ \lambda_3 \rightarrow S_{33},\ \ldots,\ \lambda_n \rightarrow S_{n3}\};$$
$$\cdots\cdots\cdots\cdots\cdots\cdots\cdots\cdots\cdots\cdots\cdots$$
$$\{\lambda_1 \rightarrow S_{1n},\ \lambda_2 \rightarrow S_{2n},\ \lambda_3 \rightarrow S_{3n},\ \ldots,\ \lambda_n \rightarrow S_{nk}\},$$

where n is the number of components in the profile LF corresponding to the number of probing transducers; k is the number of substances in the list of emergency discharges.

Figure 1 shows an example of a profile represented as a LF. The LF curve features a tubular neighborhood of permissible oscillations for components ΔS, where S_0 is the average permissible spectrum oscillations value.

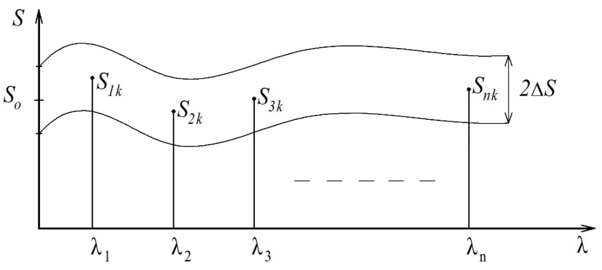

Figure 1 – A profile of a substance spectrum component reference represented as a lattice function

When wastewater fractions enter the coagulate, the spectra may be distorted, which can result in the overrunning of the permissible oscillation tube. In this case, spectrum references should be set as invariable depending on the stretching or contracting of spectrum component amplitudes.

Such properties are typical of a relative description based on the LF components using the ordering relation.

Assume $\{S_1, S_2, S_3, \ldots, S_n\}$ are the components of the LF spectrum. The relative description can be based on the correlations between the adjacent components

$$\{S_1R_{12}S_2,\ S_2R_{23}S_3,\ S_3R_{34}S_4,\ \ldots,\ S_{(n-1)}R_{(n-1)n}S_n\}$$

or the correlations occurring after the next component:

$$\{S_1R_{13}S_3,\ S_2R_{24}S_4,\ S_3R_{35}S_5,\ \ldots,\ S_{(n-2)}R_{(n-2)n}S_n\},$$

where R is the ordering relation between the components.

For the majority of the problems, it is sufficient to determine the relations between the adjacent components.

We confirmed the invariability of such descriptions to the linear stretching and contraction of spectrum component amplitudes. The qualitative parameters in spectrum descriptions are also invariable, including the alternation of extremes, dips, and swells. The more correlations between the LF components are used in the reference, the more complete is the resulting LF description. Its accuracy may reach the size of the lattice within which the LF is determined.

Generally, this description can be represented as an ordering relations matrix based on the LF components:

$$[R] = \left| \begin{array}{cccc} S_1R_{12}S_2 & S_1R_{13}S_3 & S_1R_{14}S_4 \cdots\cdots & S_1R_{1n}S_n \\ & S_2R_{23}S_3 & S_2R_{24}S_4 \cdots\cdots & S_2R_{2n}S_n \\ & \cdots\cdots\cdots & \cdots\cdots\cdots & \cdots\cdots\cdots \\ & & & S_{(n-1)}R_{(n-1)n}S_n \end{array} \right|.$$

The emergency discharge elimination system features an emergency coagulate identification device, a valve control device for the waste water system, and a device that processes the obtained spectrum measurements and stores reference spectra of harmful substances.

The system diagram is shown in Figure 2.

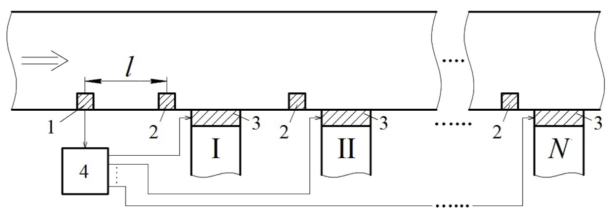

Figure 2 – The flow chart for the emergency discharge elimination system: 1 – the emergency coagulate identification device; 2 – the emergency coagulate front identification elements; 3 – the valves directing the emergency coagulate to the cesspools; 4 – measurement processing, valve control, and reference storage device; I, II, III, …, N – coagulate cesspools

Review the flow chart operation. The emergency coagulate is identified by device 1 featuring n probing transducers with wavelengths $\lambda_1 \ldots \lambda_n$ and photoelectric receivers making a circle on the inner side of the pipe, which helps identify the coagulate in real time at all of the selected wavelengths simultaneously.

The passing of the coagulate through the pipe is detected by elements 2, which allows for the opening of the valves for each of the forecast emergency coagulates (substances) upon receiving a command from the control device 4. At the same time, we can calculate the speed at which the coagulates covers distance l in the pipe. After the coagulate is dumped in the cesspool, the valve gets closed.

To protect the photodetectors from the flares caused by adjacent transducers, two design options can be used:

1 – installing optical filters on the photodetectors;

2 – the probing transducers have modulated-frequency optical emission, and demodulators are installed after the photodetectors.

Conclusion

We analyzed various options for the measurement of the spectral parameters of emergency discharges during the parallel spectrum analysis and the simultaneous measurement of the spectrum components at the selected laser emission wavelengths.

The analysis showed that the identification of the specific features of each of the spectra from the substance list is the most efficient solution for the problem of information in the aggregate reference substance spectrum. To facilitate the reference description invariability for the substance spectrum component contraction and stretching, we used the relative description represented by the more/less relation based on the set of the substance spectrum lattice function components.

The reviewed emergency discharge elimination system for non-project accidents at various production facilities differs from the well-known alternatives because it features emergency discharge detection and identification in real time. Another distinction is the use of relative descriptions for substance spectra obtained through the setting of an ordering relation for the substance spectrum lattice function components.

The suggested solution is crucial for industrial facilities located near natural water bodies and dumping waste water in them.

References

1. Bukrinsky A.M. [Management of non-design accidents in the current regulatory documents of Russia]. *Yadernaya i radiatsionnaya bezopasnost* [Nuclear and radiation safety], 2010, no. 1, pp. 16–25 (in Russian).

2. Bukrinsky A.M., Lankin M.Yu. *Osobennosti protekaniya zaproektnyh avarij i nekotorye aspekty upravleniya imi* [Features of the out-of-design accidents and some aspects of their management]. Moscow, FBI "Scientific and Technical Center for Nuclear and Radiation Safety", 2015, 9 p. Access mode: http://www.gidropress.podolsk.ru/files/proceedings/mntk2015/documents/mntk2015-108.pdf (in Russian).

3. Patin S.L. *Neft' i ekologiya kontinental'nogo shel'fa* [Oil and ecology of the continental shelf]. Vol.1: *Morskoj neftegazovyj kompleks: sostoyanie, perspektivy, faktory vozdejstviya* [Marine oil and gas complex: state, prospects, impact factors]. Moscow, All-Russian Scientific Research Institute of Fisheries and Oceanography, 2017, 326 p.

4. Aleshin I.V., Goncharov V.K. Optical methods in ecological monitoring of the ocean. *Notes of the Mining Institute*, 2008, vol. 176, pp. 88–91. Access mode: https://pmi.spmi.ru/index.php/pmi/article/view/7290 (in Russian).

5. Voronov Yu.V., Yakovlev S.V. *Vodootvedenie i ochistka stochnyh vod* [Drainage and wastewater treatment]. Moscow, Publishing House of the DIA (Association of Construction Universities) Publ., 2006, 704 p.

6. Skouteris G., Webb D. Patrick, Shin Kei Lok Felix, Rahimifard Sh. Assessment of the capability of an optical sensor for in-line real-time wastewater quality analysis in food manufacturing. *Water Resources and Industry*, 2018, vol. 20, December, pp. 75–81.
DOI: 10.1016/j.wri.2018.10.002

7. Tomperi J., Koivuranta E., Leiviskä K. Predicting the effluent quality of an industrial wastewater treatment plant by way of optical monitoring. *Journal of Water Process Engineering*, 2017, vol. 16, April, pp. 283–289.
DOI: 10.1016 / J. JWPE.2017.02.004

8. Doulamis N., Voulodimos A., Doulamis A., Bimpas M., Angeli A., Bakalos N., Giusti A., Philimis P., Varriale A., Ausili A., D'Auria S., Lampropoulos G., Baer M., Schmauss B., Freitag S., Lendl B., Młynarczyk K., Sosna-Głębska A., Trajnerowicz A., Pawluczyk J. WaterSpy: A High Sensitivity, Portable Photonic Device for Pervasive Water Quality Analysis. *Sensors*, 2019, vol. 19, iss. 1, p. 33. **DOI:** 10.3390/s19010033

9. Kim Chihoon, Ji Taeksoo, Eom Joo Beom. Determination of organic compounds in water using ultraviolet LED. *Measurement Science and Technology*, 2018, vol. 29, p. 045802, 6 p. **DOI:** 10.1088/1361-6501/aaa364

10. Alekseev V.A., Usoltsev V.P., YUran S.I., Shulmin D.N. [Complex for monitoring of sewage optical density changes]. *Devices and Methods of Measurements*, 2018, vol. 9, no. 1, pp. 7–16 (in Russian).
DOI: 10.21122/2220-9506-2018-9-1-7-16

11. Smirnov S.V. [Fiber-optic technologies for offshore oil and gas fields]. *Business Journal NEFTEGAZ.RU*, 2017, no. 8(68), pp. 72–78 (in Russian).

12. Li M.E., Martynov O.V., Shibanov E.B. [Improvement of methods for measuring the spectral angular index of light scattering by seawater]. *Sovremennye problemy optiki estestvennyh vod: trudy mezhdunarodnoj konferencii* [Modern problems of optics of natural waters: Proceedings of the International Conference]. St. Petersburg, 2015, vol. 8, pp. 262–267 (in Russian).

13. Klimkov Yu.M., Mayorov V.S., Khoroshev M.V. *Vzaimodejstvie lazernogo izlucheniya s veshchestvom: uchebnoe posobie* [Interaction of laser radiation with matter: textbook]. Moscow, Moscow State University of Geodesy and Cartography (MIIGAiK), 2014, 108 p.

14. Bhargava R. Infrared Spectroscopic Imaging: The Next Generation. Applied Spectroscopy, 2012, vol. 66, no. 10, pp. 1091–1120. **DOI:** 10.1366/12-06801

15. Obukhov A.E. Optical spectroscopy and the structure of polyfunctional hydrocarbon compounds and oil products. *Optics and Spectroscopy*, 2018, vol. 124, no. 5, pp. 696–702.
DOI: 10.1134/S0030400X18050168

16. SHrejder YU.A. *Logika znakovyh sistem: elementy semiotiki* [Logic of sign systems: elements of semiotics]. Moscow, Librocom Publ., 2012, 64 p.

17. Alekseev V.A., Dizendorf K.I., YUran S.I. Classifier of pulse curves using ratio matrices. *Intelligent systems in manufacturing*, 2010, no. 1(15), pp. 231–235 (in Russian).

18. Alekseev V.A., Yuran S.I., Usoltsev V.P., Shulmin D.N. System of Laser Monitoring of Water Pollution with Application of Relative Description of Signal Shape. *Devices and Methods of Measurements*, 2020, vol. 11, no. 2, pp. 114–121.
DOI: 10.21122/2220-9506-2020-11-2-114-121

Devices and Methods of Measurements
2022, vol. 13, no. 2, pp. 112–116
O.D. Kanafyev et al.

Influence of Cylindrical Shield Dimensions on Shielding Effectiveness

O.D. Kanafyev, A.V. Trukhanov, T.I. Zubar, S.S. Grabchikov, M.I. Panasiuk, A.N. Kotelnikova, V.A. Fedkin, V.M. Fedosyuk

Scientific and Practical Materials Research Centre
of the National Academy of Sciences of Belarus,
P. Brovki str., 19, Minsk 220072, Belarus

Received 07.04.2022
Accepted for publication 18.05.2022

Abstract

Study of dimensional parameters' influence on shielding properties of cylindrical shields will allow to optimise the fusion process, as well as to reduce production costs by reducing the material used. The purpose of this work was to compare results of theoretical calculation of shielding effectiveness of an infinite cylindrical shield with the data obtained in real conditions.

A cylindrical Ni-Fe shield was synthesised by electrochemical deposition with length of 32 cm, diameter of 4.5 cm and shielding thickness of ≈ 100 μm. The cylinder length was then reduced from 32 cm to 6 cm in 4 cm increments and for each cylinder length shielding effectiveness was measured using three-coordinate Helmholtz field-forming system.

The measurement results show that the calculation of shielding effectiveness of infinite cylindrical shield is valid for cylinder lengths $l \geq 18–20$ cm. Shielding effectiveness is markedly reduced at values of $l < 15$ cm.

Analysis of data obtained allowed to conclude that it is necessary to determine the correction factor when calculating a cylindrical screen shielding efficiency.

Keywords: shielding, magnetostatic fields, cylindrical shields.

DOI: 10.21122/2220-9506-2022-13-2-112-116

Адрес для переписки:
Канафьев О.Д.
НПЦ НАН Беларуси по материаловедению,
ул. П. Бровки, 19, г. Минск 220072, Беларусь
e-mail: olegkan96@mail.ru

Address for correspondence:
Kanafyev O.D.
Scientific and Practical Materials Research Centre of the National Academy of Sciences of Belarus,
P. Brovki str., 19, Minsk 220072, Belarus
e-mail: olegkan96@mail.ru

Для цитирования:
O.D. Kanafyev, A.V. Trukhanov, T.I. Zubar, S.S. Grabchikov, M.I. Panasiuk, A.N. Kotelnikova, V.A. Fedkin, V.M. Fedosyuk.
Influence of Cylindrical Shield Dimensions on Shielding Effectiveness.
Приборы и методы измерений.
2022. – Т. 13, № 2. – С. 112–116.
DOI: 10.21122/2220-9506-2022-13-2-112-116

For citation:
O.D. Kanafyev, A.V. Trukhanov, T.I. Zubar, S.S. Grabchikov, M.I. Panasiuk, A.N. Kotelnikova, V.A. Fedkin, V.M. Fedosyuk.
Influence of Cylindrical Shield Dimensions on Shielding Effectiveness.
Devices and Methods of Measurements.
2022, vol. 13, no. 2, pp. 112–116.
DOI: 10.21122/2220-9506-2022-13-2-112-116

Влияние габаритных параметров цилиндрического экрана на эффективность экранирования

О.Д. Канафьев, А.В. Труханов, Т.И. Зубарь, С.С. Грабчиков, М.И. Панасюк, А.Н. Котельникова, В.А. Федькин, В.М. Федосюк

Научно-практический центр Национальной академии наук Беларуси по материаловедению, ул. П. Бровки, 19, г. Минск 220072, Беларусь

Поступила 07.04.2022
Принята к печати 18.05.2022

Изучение влияния габаритных параметров на экранирующие свойства цилиндрических экранов позволит оптимизировать процесс синтеза, а также снизить затраты на производство, за счёт уменьшения используемого материала. Целью данной работы было сравнение результатов теоретического расчёта эффективности экранирования бесконечного цилиндрического экрана и данных, полученных в реальных условиях.

Методом электрохимического осаждения был синтезирован цилиндрический экран Ni-Fe, длина которого составила 32 см, диаметр 4,5 см, толщина экранирующего покрытия составила ≈ 100 мкм. Затем длина цилиндра уменьшалась от 30 до 6 см с шагом в 4 см, для каждой длины цилиндра была измерена эффективность экранирования с помощью полеобразующей системы трёхкоординатных катушек Гельмгольца.

Результаты измерений показали, что расчёт эффективности экранирования бесконечного цилиндрического экрана справедлив при длине цилиндра $l \geq 18$–20 см. При значениях $l < 15$ см эффективность экранирования заметно снижается.

Анализ полученных данных позволил сделать вывод о необходимости определения поправочного коэффициента при расчётах эффективности экранирования цилиндрического экрана.

Ключевые слова: экранирование, магнитостатические поля, цилиндрические экраны.

DOI: 10.21122/2220-9506-2022-13-2-112-116

Адрес для переписки:
Канафьев О.Д.
НПЦ НАН Беларуси по материаловедению,
ул. П. Бровки, 19, г. Минск 220072, Беларусь
e-mail: olegkan96@mail.ru

Address for correspondence:
Kanafyev O.D.
Scientific and Practical Materials Research Centre of the National Academy of Sciences of Belarus,
P. Brovki str., 19, Minsk 220072, Belarus
e-mail: olegkan96@mail.ru

Для цитирования:
O.D. Kanafyev, A.V. Trukhanov, T.I. Zubar, S.S. Grabchikov, M.I. Panasiuk, A.N. Kotelnikova, V.A. Fedkin, V.M. Fedosyuk.
Influence of Cylindrical Shield Dimensions on Shielding Effectiveness.
Приборы и методы измерений.
2022. – Т. 13, № 2. – С. 112–116.
DOI: 10.21122/2220-9506-2022-13-2-112-116

For citation:
O.D. Kanafyev, A.V. Trukhanov, T.I. Zubar, S.S. Grabchikov, M.I. Panasiuk, A.N. Kotelnikova, V.A. Fedkin, V.M. Fedosyuk.
Influence of Cylindrical Shield Dimensions on Shielding Effectiveness.
Devices and Methods of Measurements.
2022, vol. 13, no. 2, pp. 112–116.
DOI: 10.21122/2220-9506-2022-13-2-112-116

Introduction

Global electrification along with the undeniable benefits poses many threats, of which electromagnetic radiation is the most significant. One of the particularly difficult cases of protection from the impact of external electromagnetic fields is shielding of static magnetic fields.

This type of magnetic fields can have a negative impact on the human body, disable devices and their elements and is also widely used in the military industry [1, 2]. To minimize the effects of magnetostatic fields magnetically soft materials (steel, permalloy, amorphous metal alloys are usually used). Study of magnetostatic shielding is based on the principle of magnetic field shunting by a ferromagnetic material [3, 4]. The basis of this principle is the closure of the field lines through the material with low resistance to magnetic flux which means that the shielding efficiency is directly proportional to the value of magnetic permeability (μ) of the shielding material and inversely proportional to the area of its cross section. However we have previously shown [5, 6] that a number of experimental results on the magnetostatic shielding does not agree with the provisions of the shunt principle.

Thus the purpose of this work was to investigate the shielding effectiveness of the cylindrical shield and to find out the effect of the cylinder length changing on shielding effectiveness. This will reduce the error in theoretical calculations which in turn will have a positive impact on the quality of development of highly effective protection of devices and equipment for a wide range of applications.

Measurement technique

An aluminum cylinder with a single layer Ni shielding coating $Ni_{80}Fe_{20}$ with a copper underlayer was made as the test sample with the following parameters: 32 cm long, diameter is 4.5 cm. The average thickness of the coating was 132 μm.

The aluminum surface preparation process was carried out in several stages such as trichloroethylene treatment degreasing with Vienna lime, chemical etching, chemical galvanizing and copper undercoating was then applied to increase of adhesion.

The shielding coating was synthesised by electrochemical deposition using nickel anodes at 35–40 °C. The current density was 25 mA/cm^2. The composition of the electrolyte solution is shown in Table.

Table

The composition of the electrolyte solution

№	Reactive	Content, *g*/*l*
1	$NiSO_4 \cdot 6H_2O$	210
2	$NiCl_2 \cdot 6H_2O$	20
3	$FeSO_4 \cdot 7H_2O$	15
4	$KNaC_4H_4O_6 \cdot 4H_2O$	30
5	$MgSO_4$	60
6	H_3BO_3	30
7	Saccharine	2
8	Ascorbic acid	2

The thickness of the resulting shielding coating was ≈ 100 μm.

From the resulting cylinder with the shielding coating, 4 cm were cut off (Figure 1), then at each length, the shielding effectiveness was measured.

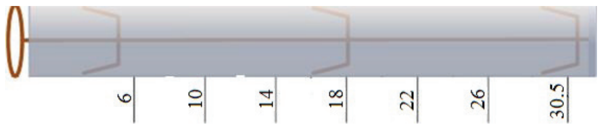

Figure 1 – Schematic representation of the test sample

The efficiency of the shielding was measured by means of a three-coordinate Helmholtz field-forming system.

Results and discussion

The most complex case of shielding against external sources of electromagnetic radiation is that of static magnetic fields [5]. Usually when considering magnetostatic shielding the principle of the magnetic field shunting with a ferromagnetic material is used. The basic essence of this principle is to short circuit the field lines through a material with low resistance to magnetic flux. According to this approach the effectiveness of the shielding is constant and directly proportional to the magnetic permeability of the shield material and inversely proportional to its cross-sectional area [7, 8]. For an infinite cylindrical shield, the calculation of the shielding effectiveness is carried out according to the formula:

$$Oe_{cyl.} = 0.57\mu d/r,$$

where μ is the magnetic constant, d is shield thickness [mm]; r is outer radius [mm].

As we know [9], in theoretical calculations of shielding efficiency usually use ideal geometric shapes of samples (infinite plane and infinite cylinder, sphere). In real conditions the situation is much more complicated – bodies, blocks to be shielded have finite dimensions, irregular shape and may contain holes and apertures. Therefore, for practical purposes, it is important to know how the screen size affects such characteristics as the maximum screening efficiency $Oe_{мах}$ and the magnetic field strength corresponding to the maximum screening efficiency $HOe_{мах}$.

To check the validity of the above formula, the shielding effectiveness was measured at cylinder lengths l = 6–30 cm, in 4 cm increments. Figure 2 shows the obtained results of shielding efficiency depending on the length of the cylinder. It can be seen that reducing the cylinder length to 14 cm does not result in a significant change in shielding effectiveness. When the cylinder length is further reduced from 14 cm to 6 cm, there is a sharp decrease in shielding effectiveness.

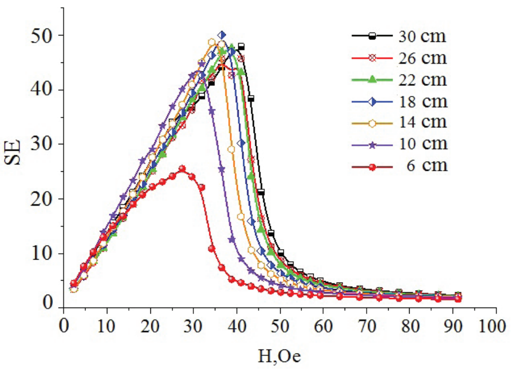

Figure 2 – Shielding efficiency depending on the length of the cylinder

Figure 3 shows the dependencies of $Oe_{мах}$ and $HOe_{мах}$ on the length of the cylindrical shield.

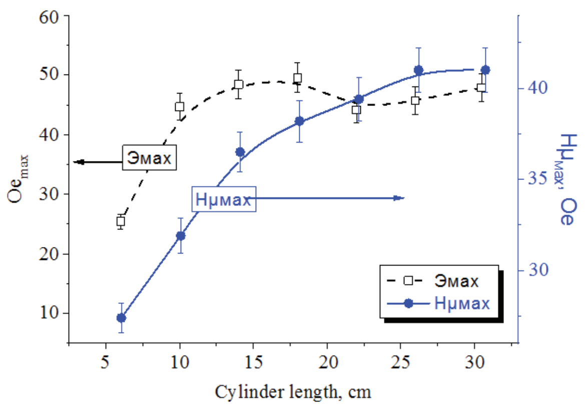

Figure 3 – Changing the position of the maximum shielding efficiency depending on the length of the cylinder

It can be seen, the parameters $Oe_{мах}$ and $HOe_{мах}$ become very stable at values of $l \geq$ 18–20 cm. At values of $l <$ 15 cm, the shielding efficiency decreases markedly. For example, the $Oe_{мах}$ values of a 6 cm long sample are 2 times lower than those of a 26–30 cm long sample. At the same time, the $HOe_{мах}$ shifts to a lower field region from 44 to 26 Oe.

Conclusion

Studies have been carried out on the shielding effectiveness of an aluminum cylinder with Ni-Fe shielding.

It is found that the theoretical calculations of shielding efficiency differ from the data obtained under real conditions. Parameters as the maximum screening efficiency $Oe_{мах}$ and the magnetic field strength corresponding to the maximum screening efficiency $HOe_{мах}$ are stable at values $l \geq$ 18–20 cm, so maximum shielding efficiency of the obtained sample holds within 45–50 times. Reducing the length of the cylinder to a value of $l <$ 15 cm leads to a significant decrease in the maximum shielding efficiency from 42 to 25 times. At the same time the $HOe_{мах}$ shifts to a lower field region.

This result is due to the effect of the magnetic field flowing into the open sample of finite size. Thus in order to reduce the influence of the dimensional effect of cylindrical and close-shaped shields the l/r ratio must be $\geq$ 8–9.

Further it is planned to extend the research range to obtain a correction factor to calculate the shielding effectiveness of real cylindrical shields.

The findings are to be used in the manufacture of shields to protect sensitive components of various kinds of devices.

References

1. Zhang C., Han Y., Zhang P., Song G., Zhou C. Research on modern radar emitter modelling technique under complex electromagnetic environment. *The Journal of Engineering*, 2019, vol. 2019, iss. 20, pp. 7134–7138. **DOI:** 10.1049/joe.2019.0579

2. Kechiev L.N., Akbashev B.B., Stepanov P.V. Shielding of technical means and shielding systems. Because, "ITD Group" Publ., 470 p.

3. Zhang Q., Liang Q., Zhang Z., Kang Z., Liao Q., Ding Y., Ma M., Gao F., Zhao X., Zhang Y. Electromagnetic Shielding Hybrid Nanogenerator for Health Monitoring and Protection. *Advanced Functional*

Materials, 2018, vol. 28, iss. 1, p. 1703801.
DOI: 10.1002/adfm.201703801

4. Panagopoulos D.J., Chrousos G.P. Shielding methods and products against man-made Electromagnetic Fields: Protection versus risk. *Science of the total environment*, 2019, vol. 667, pp. 255–262.
DOI: 10.1016/j.scitotenv.2019.02.344

5. Grabchikov S.S., Trukhanov A.V., Trukhanov S.V., Kazakevich I.S., Solobay A.A., Erofeenko V.T., Vasilenkov N.A., Volkovad O.S., Shakin A. Effectiveness of the magnetostatic shielding by the cylindrical shells. *Journal of Magnetism and Magnetic Materials*, 2016, vol. 398, pp. 49–53.
DOI: 10.1016/j.jmmm.2015.08.122

6. Grabchikov S.S., Gromyko G.F., Erofeenko V.T., Zayats G.M. The Shielding Effectiveness of Static Magnetic Fields by Cylindrical Screen Taking Into Account Nonlinear Effects. *Physical Bases of Instrumentation*, 2015, vol. 4, no. 4, pp. 30–39.

7. Appolonsky S.M., Gorsky A.N. Calculations of electromagnetic fields. M.: Route Publ., 2006, 992 p.

8. Reutov Y.Y. Physical interpretation of magnetostatic shielding. *Russ. J. Nondestruct. Test*., 2000, vol. 36, pp. 117–126.

9. Shapiro D.N. Electromagnetic shielding. Dolgoprudny: Publishing House “Intellect” Publ., 2010, 120 p.

An Approach to Monitoring of Magnetic Parameters of Cores of a Chain of Spheres. Diagnostics of Different Chain's Length and Core's Radius

A.A. Sandulyak, D.A. Sandulyak, Y.O. Gorpinenko, A.V. Sandulyak, V.A. Ershova

*MIREA – Russian Technological University,
Stromynka str., 20, Moscow 107996, Russia*

*Received 26.02.2022
Accepted for publication 01.06.2022*

Abstract

The basic structural elements of the magnetized granular medium (effectively used, in particular, in apparatus of thin magnetic separation) are granule chains (according to channel-by-channel model), in connection with which there is a need to detail the features of their magnetization. The purpose of the work is to develop and implement an approach to measuring magnetic (micro)flows along the cores of different radius r in the chain of granules using a specially developed (by printed circuit board technology) sensor, with high radius R (15 and 20 mm) spheres available for such measurements.

From the data of measuring magnetic (micro)flows data of average induction in each of the quasi-continuous cores of the spheres chain are obtained, as well as data of magnetic permeability and susceptibility of these cores, their magnetization for different values of the intensity of the magnetizing field. It is shown that dependences of mentioned magnetic parameters from number n spheres in a chain are generalized on r/R for different R.

These relationships, increasing as n increases due to a decrease in the demagnetizing factor N of any of the cores and the chain as a whole, demonstrate the achievement of individually limiting values of magnetic parameters and corresponding auto-model regions where $N \to 0$. At the same time, the transition to each of these regions, manifesting almost independently of r/R and intensity, falls on the value of n = 10–12 = [n]. Thus, in fact, such a criterion value [n] distinguishes chains by sufficiently "long" – when $n \geq [n]$ and "short" – when $2 \leq n < [n]$. Data of demagnetizing factor for different cores of "short" chains of spheres are obtained and phenomenologically described.

Keywords: chain of granules, sensor contour on a printed circuit board, magnetic permeability, susceptibility, demagnetizing factor.

DOI: 10.21122/2220-9506-2022-13-2-117-127

Адрес для переписки:
*Сандуляк Д.А.
МИРЭА – Российский технологический университет,
ул. Стромынка, 20, г. Москва 107996, Россия
d.sandulyak@mail.ru*

Address for correspondence:
*Sandulyak D.A.
MIREA – Russian Technological University,
Stromynka str., 20, Moscow 107996, Russia
d.sandulyak@mail.ru*

Для цитирования:
A.A. Sandulyak, D.A. Sandulyak, Y.O. Gorpinenko, A.V. Sandulyak, V.A. Ershova.
An Approach to Monitoring of Magnetic Parameters of Cores of a Chain of Spheres. Diagnostics of Different Chain's Length and Core's Radius.
Приборы и методы измерений.
2022. – Т. 13, № 2. – С. 117–127.
DOI: 10.21122/2220-9506-2022-13-2-117-127

For citation:
A.A. Sandulyak, D.A. Sandulyak, Y.O. Gorpinenko, A.V. Sandulyak, V.A. Ershova.
An Approach to Monitoring of Magnetic Parameters of Cores of a Chain of Spheres. Diagnostics of Different Chain's Length and Core's Radius.
Devices and Methods of Measurements.
2022, vol. 13, no. 2, pp. 117–127.
DOI: 10.21122/2220-9506-2022-13-2-117-127

Подход к контролю магнитных параметров сердцевин цепочки шаров. Диагностика разных по длине цепочки и радиусу сердцевин

А.А. Сандуляк, Д.А. Сандуляк, Ю.О. Горпиненко, А.В. Сандуляк, В.А. Ершова

*МИРЭА – Российский технологический университет,
ул. Стромынка, 20, г. Москва 107996, Россия*

*Поступила 26.02.2022
Принята к печати 01.06.2022*

Базовыми структурными элементами намагничиваемой гранулированной среды (эффективно используемой, в частности, в устройствах для тонкой магнитной сепарации) являются цепочки гранул (согласно поканальной модели), в связи с чем возникает необходимость в детализации особенностей их намагничивания. Цель работы – разработка и реализация подхода к измерениям магнитных (микро) потоков по сердцевинам разного радиуса r в цепочке гранул при помощи специально разработанного (по технологии печатных плат) датчика, используя доступные для таких измерений шары повышенного радиуса R (15 и 20 мм).

По данным измерений магнитных (микро)потоков получены данные средней индукции в каждой из квазисплошных сердцевин цепочки шаров, а также данные магнитной проницаемости и восприимчивости этих сердцевин, их намагниченности для разных значений напряжённости намагничивающего поля. Показано, что зависимости указанных магнитных параметров от числа шаров n в цепочке обобщаются по r/R для разных R.

Эти зависимости, возрастая по мере увеличения n вследствие уменьшения размагничивающего фактора N любой из сердцевин и цепочки в целом, демонстрируют достижение индивидуально предельных значений магнитных параметров и соответствующих автомодельных областей, где $N \to 0$. При этом переход к каждой из этих областей, проявляющийся практически независимо от r/R и напряжённости, приходится на значение n = 10–12 = $[n]$. Тем самым такое, по сути критериальное, значение $[n]$ разграничивает цепочки на достаточно «длинные» – когда $n \geq [n]$ и «короткие» – когда $2 \leq n < [n]$. Получены и феноменологически описаны данные размагничивающего фактора для разных сердцевин «коротких» цепочек шаров.

Ключевые слова: цепочка гранул, датчик-контур на печатной плате, магнитная проницаемость, восприимчивость, размагничивающий фактор.

DOI: 10.21122/2220-9506-2022-13-2-117-127

Адрес для переписки:
*Сандуляк Д.А.
МИРЭА – Российский технологический университет,
ул. Стромынка, 20, г. Москва 107996, Россия
d.sandulyak@mail.ru*

Address for correspondence:
*Sandulyak D.A.
MIREA – Russian Technological University,
Stromynka str., 20, Moscow 107996, Russia
d.sandulyak@mail.ru*

Для цитирования:
A.A. Sandulyak, D.A. Sandulyak, Y.O. Gorpinenko, A.V. Sandulyak, V.A. Ershova.
An Approach to Monitoring of Magnetic Parameters of Cores of a Chain of Spheres. Diagnostics of Different Chain's Length and Core's Radius.
Приборы и методы измерений.
2022. – Т. 13, № 2. – С. 117–127.
DOI: 10.21122/2220-9506-2022-13-2-117-127

For citation:
A.A. Sandulyak, D.A. Sandulyak, Y.O. Gorpinenko, A.V. Sandulyak, V.A. Ershova.
An Approach to Monitoring of Magnetic Parameters of Cores of a Chain of Spheres. Diagnostics of Different Chain's Length and Core's Radius.
Devices and Methods of Measurements.
2022, vol. 13, no. 2, pp. 117–127.
DOI: 10.21122/2220-9506-2022-13-2-117-127

Introduction

The concept of the so-called effective medium is traditional in studies of any type of inhomogeneous magnets [1–8]. These magnets are used in various physical and applied problems. Effective medium is medium as a formally quasi-continuous volume of a magnet with its inherent magnetic parameters.

We used the concept of a quasi-continuous magnet for such types of inhomogeneous magnets as granular media (in particular, which are the key working bodies of fine magnetic separation devices). Concept could be efficient only to a chain of granules (and not the environment as a whole). This concept helped to study magnetic parameters. The model of channel-by-channel magnetization of a granular medium [9, 10] provided an information that a chain of granules was the basic structural element of this medium and a carrier of information about its magnetic parameters. At the same time, the chains of granules performed the function of a "bundle" of conductors-channels similar to each other for the generated magnetic flux. The example of comparing the corresponding magnetization curves proved the similarity of the magnetic parameters of the chain of granules and the granular medium as a whole [10].

The following must be said about the nature of the magnetization of such a quasi-continuous magnet as a chain of granules (for example, spheres). There was a pronounced redistribution of the magnetic flux over the cross section in contrast to the variant of magnetization of a solid (continuous) bar magnet. The flux density decreased as you moved away from the axis of the chain. Hence there was also a decrease in this density in one or another of its conditional core with an increase its radius r. This was due to an increase in the magnetic resistance of the "thickening" core of such a specific magnet due to decreasing volumes of metal in the core and increasing volumes of gaps between the surfaces of adjacent granules.

Direct measurements of magnetic fluxes proved that. We measured magnetic fluxes (with a microwebermeter) Φ through concentric loops of thin wire with different radii $r \leq R$, located in a hollow volume between the spheres in the chain, surrounding the contact point of the spheres with a radius R [9]. Thus, we obtained Φ in the corresponding in radius r cores of the chain of spheres. It became possible to obtain Φ values in the cores of even a small relative radius r/R by deeping the sensor loops into the inter-ball space. Use of chains with spheres of increased radius and loops of very thin wire was advisable here. The wire was so much thin as to place them as deep as possible in the thinning (when approaching the contact point of the spheres) volume between the surfaces of the spheres.

Then we had to develop ideas about the nature and features of the magnetization of chains of granules. It became necessary to expand the volume of this kind of labor-intensive research. Therefore, the issue of justified simplification in the manufacture and fixation of magnetic flux sensors (with the rejection of the traditional use for such purposes of a thin wire, which is not so practical here), became relevant. For example, by creating appropriate sensors. Printed-circuit technique could be sufficient to create appropriate sensors for such tasks [11–13].

Circular circuit on a thin printed board with a mounting hole like a magnetic flux sensor in the core of the chain of spheres

To measure the magnetic flux in one or another core of a magnetizable chain of spheres, we adhered to the classical principle. This was the principle of using a conductive sensor with a circular shape. A sensor in the form of a thin printed board with a conductive circular circuit or a block of concentric circuits made on it was preferable [11]. At the same time, each of the circuits had to have a small gap for the wire connection of its free ends with the microwebermeter.

With this approach to the implementation of the above magnetic measurements, which increases the reliability and quality of control, it is easy to ensure the required strict shape of the sensor circuit and/or each of the sensor circuits in the block (as geometrically ideal circles on a flat surface) and the concentricity of the sensor circuits with respect to the point of contact of the spheres and to each other.

It was also easy to ensure the correct positioning (Figure 1) of this working printed board 1 in the plane of symmetry of the volume between the contacting sphere 2 with radius R. The mounting hole ensured the correct positioning. The hole was made in the middle part of the working board concentric to the circuit-sensor or the block of circuits-sensors. The diameter d_0 corresponded to the recommendation: $d_0 = [\delta(4R–\delta)]^{0.5}$ [11], where δ was the board thickness. The edges of the board, formed around the circumference of the hole, fit snugly against the surfaces of the opposing spheres (without preventing their mutual contact). They fixed the working board in the required symmetry plane of the volume between the spheres.

Magnetic induction data in different cores of the chain of spheres, corresponding data on their magnetic permeability, susceptibility and magnetization

The board described above contained measuring circuits-sensors with a relative radius from $r/R = 0.2$ to $r/R = 0.9$, its positioning was in the middle of the studied chains of spheres (Figure 1). The board made it possible to obtain the necessary experimental data on the magnetic fluxes Φ in the cores of the chains of spheres corresponding in r/R. In this experiment, we used chains of different lengths, i. e. with a different (even) number n of spheres in one or another chain, namely from $n = 2$ to $n = 14$.

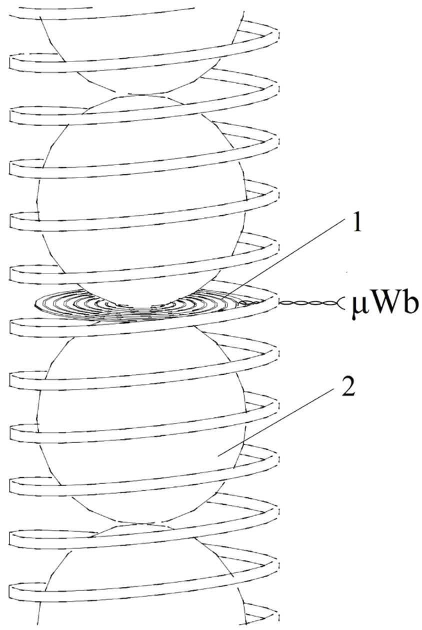

Figure 1 – The location of printed circuit board 1 with a sensor contour (sensor contours) of the magnetic flux values in the volume between the middle spheres 2 of the magnetized (in the solenoid) chain with even number n of contacting spheres

There were two identical series of experiments. In one of them, the chains consisted of spheres with a radius $R = 15$ mm, the other one contained spheres with a radius $R = 20$ mm (for subsequent comparison of the results of experiments on such a dimensionless parameter, which claims to be universal, as r/R). The spheres had an increased radius due to the need to place a sufficient number of measuring sensors as deep as possible in the volume between the surfaces of adjacent spheres. This volume thinned as it approached the contact point of the spheres, i. e. with the smallest possible relative radius r/R of the measuring circuit-sensor. The magnetization of the chains took place in a sufficiently long solenoid by a field strength from $H = 4.8$ kA/m to $H = 54.5$ kA/m.

According to the experimental data of the magnetic flux Φ, one could judge its density:

$$B = \Phi / \left(\pi r^2\right), \tag{1}$$

i. e. about the data of the average induction B in each of the studied quasi-continuous cores of the chain of spheres. These data, obtained on the basis of formula (1), were shown in Figure 2 in the form of combined (for both series of experiments) families of dependencies B on the number of spheres n in chains at different values of r/R and H.

The resulting families of dependences B on n (Figure 2) were very informative for the qualitative and quantitative characteristics of the cores of chains of spheres as quasi-continuous magnets. This helped to visually illustrate the following notable features.

Firstly, the data of induction B in the cores of chains of spheres with a radius $R = 15$ mm corresponded to the data of induction B in the cores of chains similar in relative radius r/R with the same number n of spheres, but with a radius $R = 20$ mm. This can be seen in Figure 2 by the coincidence of the compared data B (points • and ○). This, quite expected (based on the principle of similarity), fact testified to the possibility of applying the obtained induction data (Figure 2) to the corresponding chains of spheres of a different identical radius.

Secondly, the larger the relative radius r/R of the core of the chain of spheres, the lower the values of induction B in the core were (Figure 2) due to a decrease in the proportion of ferromagnetic metal in the core and vice versa.

Thirdly, all dependences of the induction B (in the cores of the chain of spheres with different r/R) on the number n of spheres in the chain increased with increasing n due to a decrease in the demagnetizing factor N of each of the cores and the chain as a whole. Then they demonstrated the onset a characteristic self-similar region (Figure 2) with an individually limiting value B. This indicated the disappearance of the demagnetizing factor. The beginning of this region manifested itself almost independently of the relative radius r/R of the core and the intensity H of the magnetizing field, fell on the value $n = 10$–12 (starting from which $N \to 0$). Thus, such a transitional, but essentially criterial, value $n = 10–12 = [n]$ delimited both chains of spheres and their cores along the length (multiple of n) of the chain itself. They divided into quite "long" – when $n \geq [n] = 10$–12 and "short" – when $n < [n] = 10$–12.

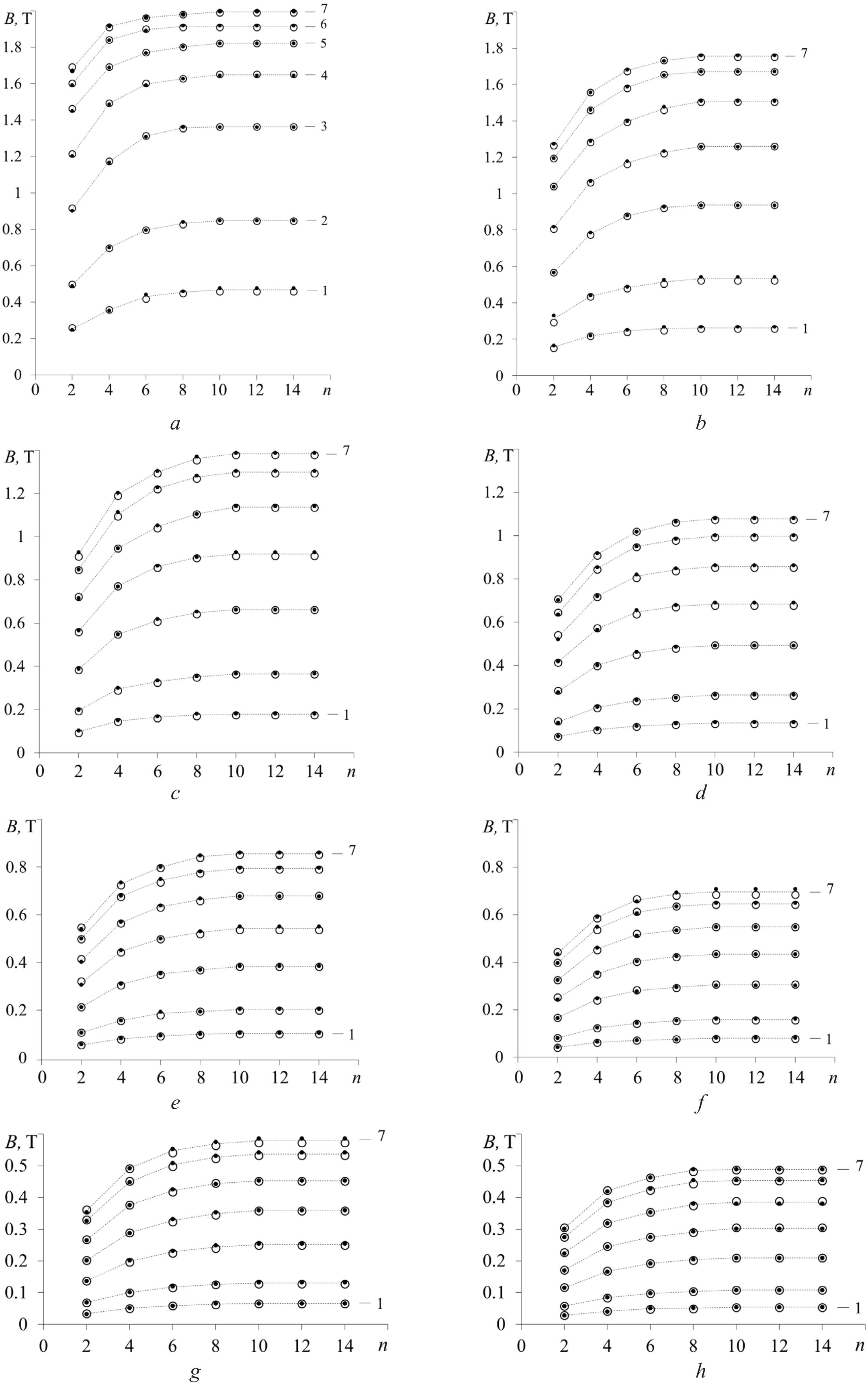

Figure 2 – Magnetic flux density in quasi-continuous cores of a chain of spheres, different in relative radius r/R, depending on the number n of spheres; a – r/R = 0.2; b – r/R = 0.3; c – r/R = 0.4; d – r/R = 0.5; e – r/R = 0.6; f – r/R = 0.7; g – r/R = 0.8; h – r/R = 0.9; 1 – magnetic field strength H = 4.8 kA/m; 2 – 10 kA/m; 3 – 20 kA/m; 4 – 29.7 kA/m; 5 – 39.5 kA/m; 6 – 48.7 kA/m; 7 – 54.5 kA/m; designations • and ○ are spheres with radius R = 15 mm and R = 20 mm, respectively

Devices and Methods of Measurements
2022, vol. 13, no. 2, pp. 117–127
A.A. Sandulyak et al.

Mentioned specifics, including the fact of the manifestation of self-similar regions, which are fundamental here, were also valid with respect to other key magnetic parameters: magnetic permeability μ of the cores of chains of spheres (Figure 3), the magnetic susceptibility χ (Figure 4) and their magnetization M (Figure 5). The following relations were used to determine the values of μ, χ and M:

$$\mu = \frac{B}{\mu_0 H}; \qquad (2)$$

$$\chi = \frac{\mu}{\mu_{N\to 0}}\left(\mu_{N\to 0} - 1\right); \qquad (3)$$

$$M = \chi H, \qquad (4)$$

where $\mu_0 = 4\pi\cdot 10^{-7}$ H/m is magnetic constant; $\mu_{N\to 0}$ and $\chi_{N\to 0}$ are attainable limit individual values (in the corresponding self-similar region – according to Figures 3 and 4: at $n \geq [n] = 10$–12) magnetic permeability and susceptibility. Regarding the relationship (3), that is nonspecific and rarely appears in the literature, it was valid precisely with respect to "short" magnets (including the cores of chains studied here as quasi-continuous magnets). This was so because the parameters of susceptibility and permeability of the "short" and "long" magnets were, as is known, in the ratio $\chi/\chi_{N\to 0} = \mu/\mu_{N\to 0}$. The use of the well-known classical relation $\chi = \mu - 1$ was valid for a magnet devoid of a demagnetizing factor, for example, a classic toroidal or "long" cylindrical, but for a "short" magnet, this was not correct. Ignoring this circumstance, as, for example, in [14], turned out to be an unjustified simplification and led to the appearance of an error in the corresponding results.

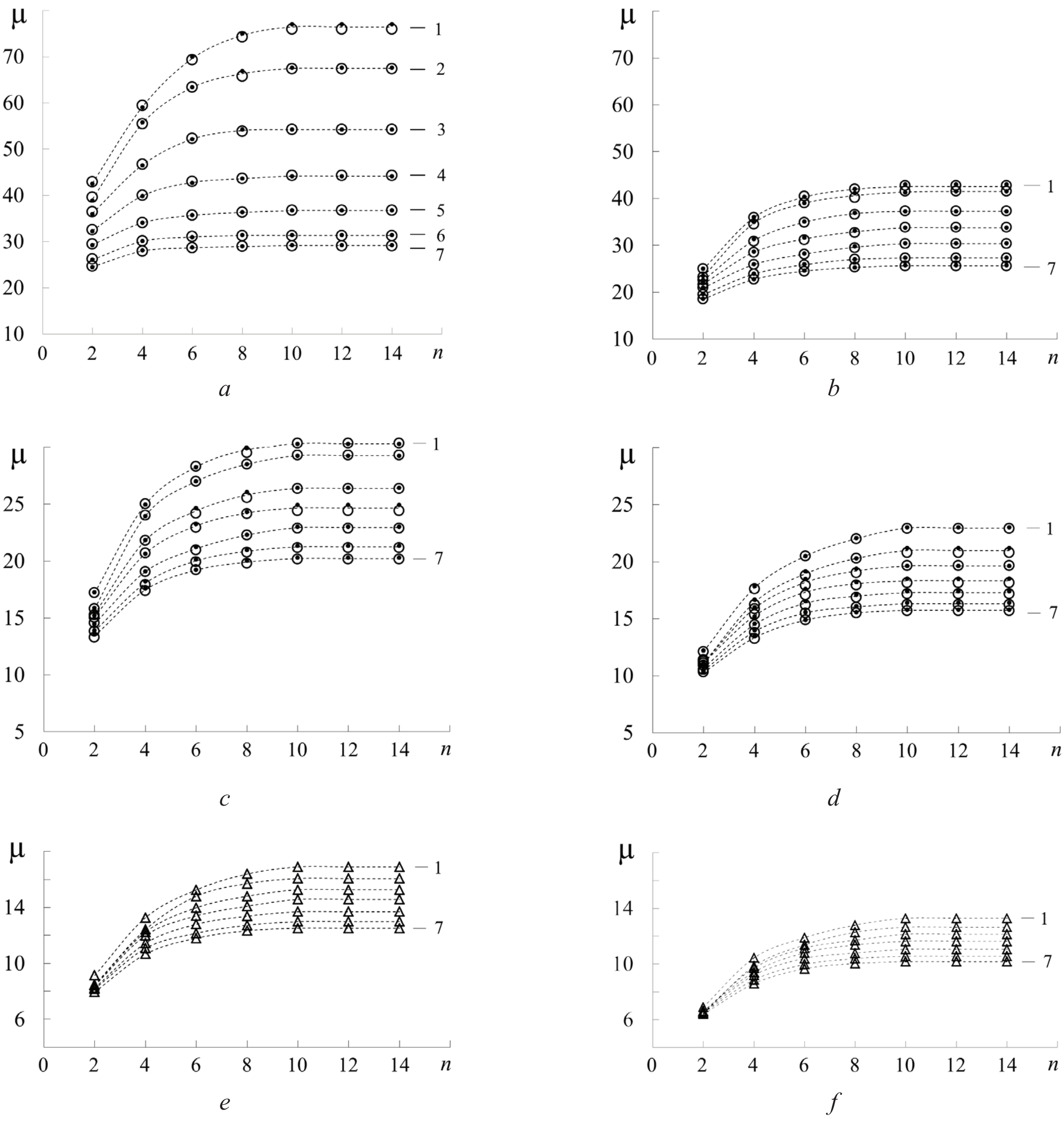

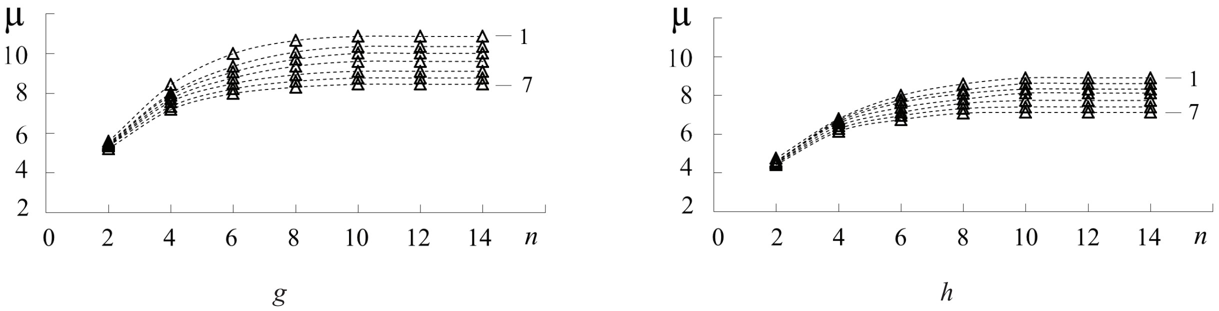

Figure 3 – Magnetic permeability μ of different (by relative radius r/R) quasi-continuous cores of a chain of spheres, depending on the number n of spheres; designations – according to Figure 2 (on e, f, g, h the designations Δ are generalized data for R = 15 mm and R = 20 mm); calculations – according to (2)

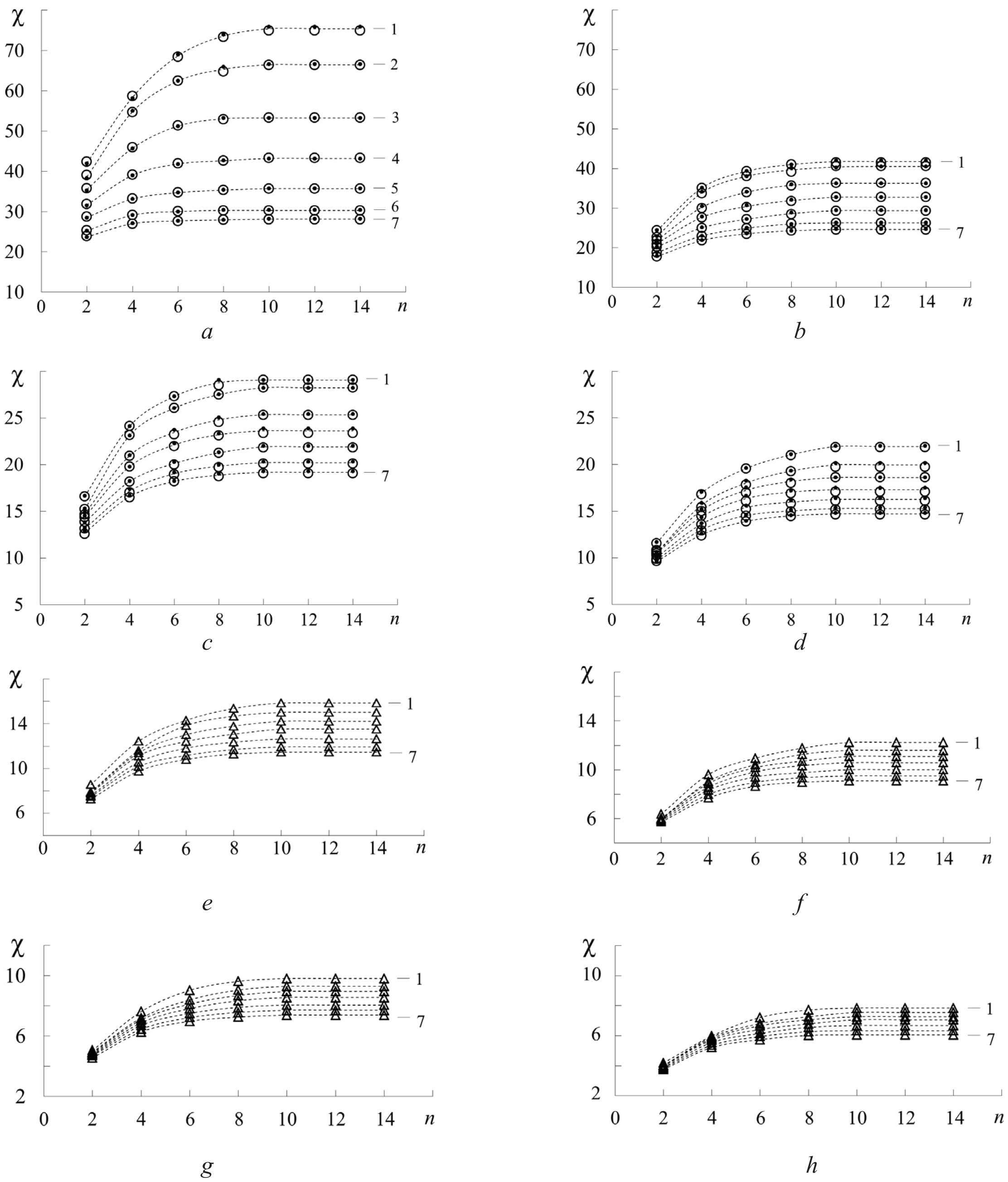

Figure 4 – Magnetic susceptibility χ of different (by relative radius r/R) quasi-continuous cores of a chain of spheres, depending on the number n of spheres; designations – according to Figure 2; calculations – according to (3)

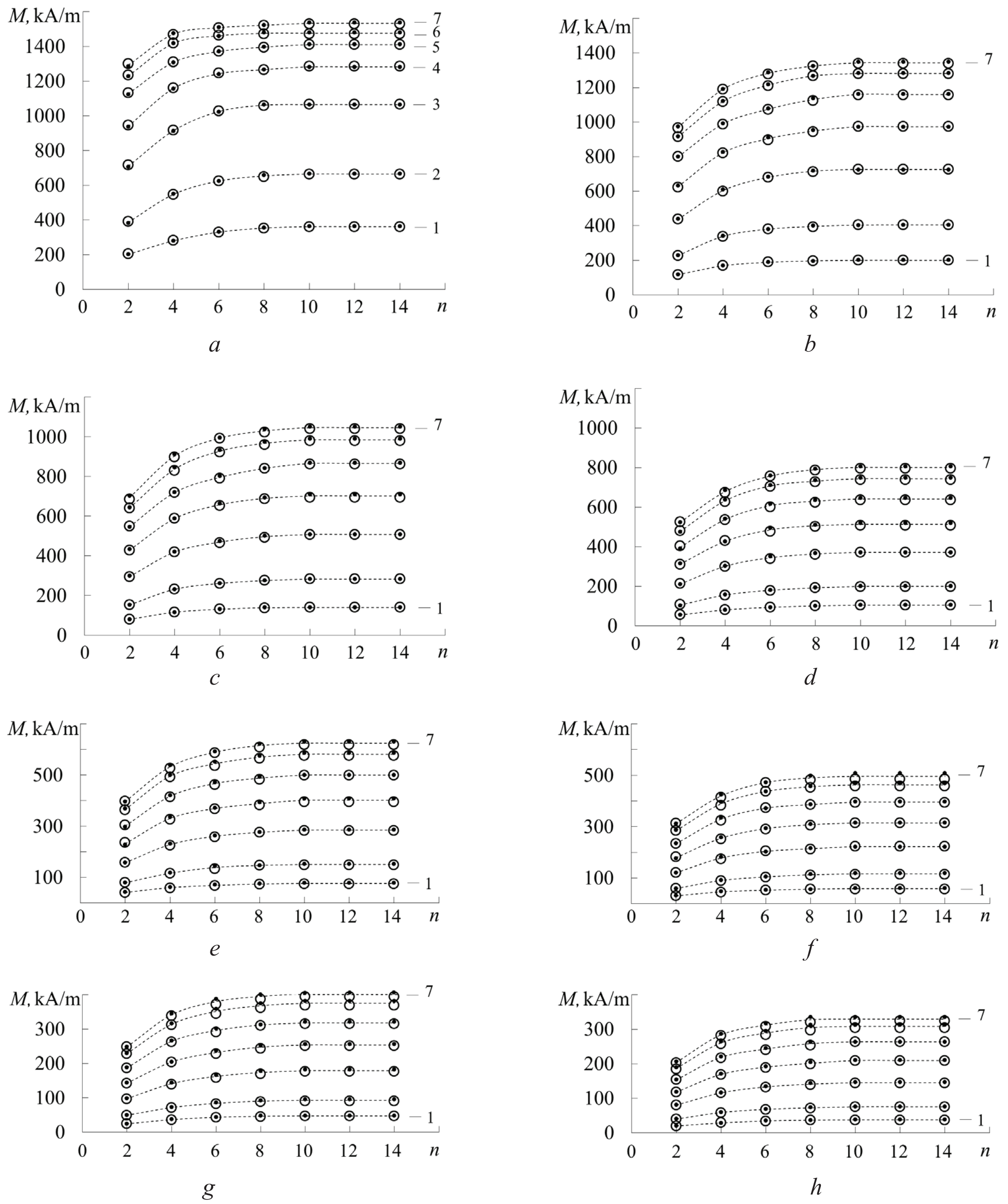

Figure 5 – The magnetization *M* of different (by relative radius r/R) quasi-continuous cores of a chain of spheres, depending on the number *n* of spheres; designations – according to Figure 2; calculations – according to (4)

Data of the demagnetizing factor of different cores of "short" chains of spheres. Functional approximation of these data

Figure 4 showed the values of the magnetic susceptibility χ of the cores of "short" chains of spheres with different relative radius r/R. These chains consisted of $n < [n] = 10–12$ spheres: $n = 2$, $n = 4$, $n = 6$, and $n = 8$. The individual limit values of the magnetic susceptibility $\chi_{N\to 0}$ for the cores of a "long" chain of spheres are also given. These chains consisted of $n \geq [n] = 10–12$ spheres. Therefore, it was possible to obtain data on the demagnetizing factor *N* of the cores of "short" chains, in particular, by the expression:

$$N = \frac{1}{\chi} - \frac{1}{\chi_{N\to 0}}, \tag{5}$$

depending on the number *n* of spheres in the chain, as in Figure 6*a*.

Each of the N values here is averaged for the entire studied range of field intensity $H = 4.8–54.5$ kA/m due to the fact that the influence of H (in this range) on the values of N was very weak. Here, in Figure 6*a*, it is shown that as the chain lengthened from $n = 2$ to $n = 8$, the demagnetizing factor N of its cores decreased. The decline was very significant – more than an order of magnitude.

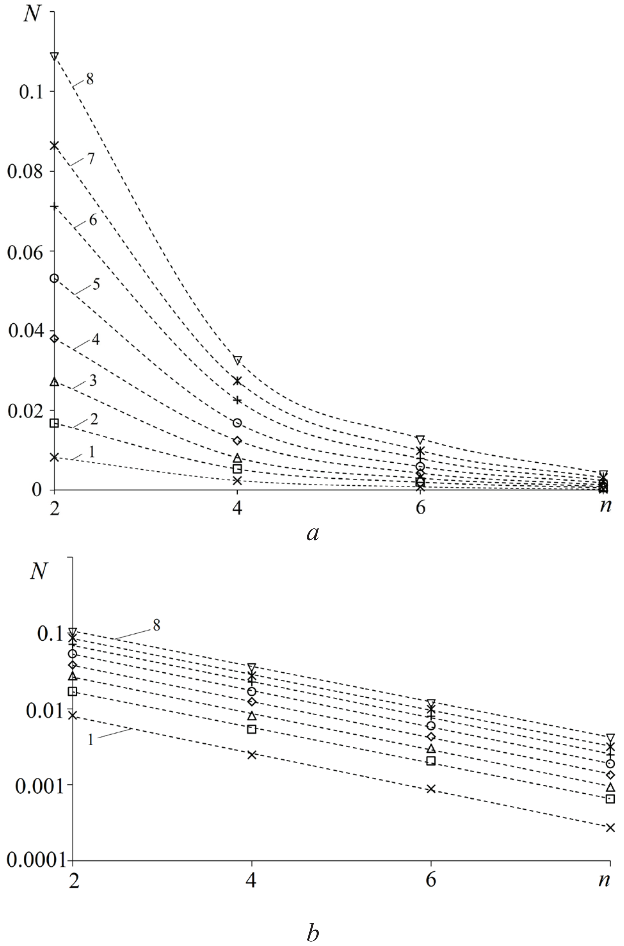

Figure 6 – Data of the demagnetizing factor of different (by relative radius r/R) quasi-continuous cores of a chain of spheres, depending on the number n of spheres: in ordinary (*a*) and semi-logarithmic (*b*) coordinates; 1 – r/R = 0.2; 2 – 0.3; 3 – 0.4; 4 – 0.5; 5 – 0.6; 6 – 0.7; 7 – 0.8; 8 – 0.9

The data N established according to (5) (Figure 6*a*) for the cores of "short" ($n < [n]$) chains of spheres succumbed to generalization by a functional (phenomenological) dependence. These data were presented in semi-logarithmic coordinates, as in Figure 6*b*. The fact of their quasi-linearization precisely in such coordinates testified to the exponential relationship between N and n:

$$N = A\exp(-kn), \tag{6}$$

moreover, with a practically constant phenomenological parameter $k = 0.54$. At the same time, the phenomenological parameter A in (6) is quasi-linearized in logarithmic coordinates (Figure 7).

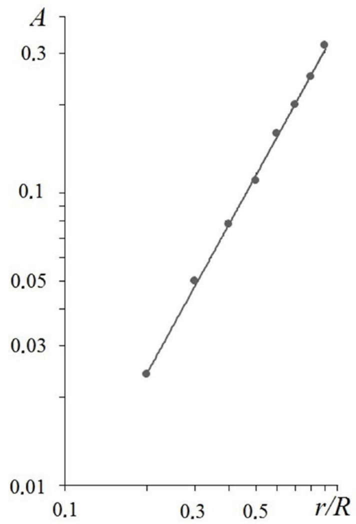

Figure 7 – On the power-law relationship (7) – due to the fact of quasi-linearization of the values of the phenomenological parameter A, which, in accordance with Figure 6*b*, depends on the relative radius r/R of the quasi-solid cores of the chain of spheres, in logarithmic coordinates

The parameter values were individual for one or another core (relative radius r/R). The fact of quasi-linearization of A parameter indicated a power-law relationship $A = a(r/R)^{1.7}$ with the value of the phenomenological parameter $a = 0.37$.

Then, taking into account this connection, expression (6) for the demagnetizing factor N of the cores of "short" ($n < [n]$) chains of spheres took the expanded form:

$$N = a(r/R)^{1.7}\exp(-kn), \tag{7}$$

representing the product of power and exponential functions for the values of the phenomenological parameters $k = 0.54$ and $a = 0.37$ aforementioned. Expression (7) made it possible to determine the demagnetizing factor of any (by the relative radius r/R) "short" core of a chain, i. e. consisting of $2 \le n \le 8$ spheres.

Conclusion

The relevance of direct control of the magnetic parameters of the cores of a chain of granules is noted as one of the basic structural elements of a granular medium (according to the model of its channel-by-channel magnetization). It contained information about the magnetic parameters of a granular medium that was the main working body of fine magnetic separation devices, particularly. For such control, a magnetic (micro) flux sensor Φ was preferable. It consisted of a circular circuit (a block of concentric circuits) on a thin printed circuit board that made it possible to carry out measurements in narrow slotted gaps between contacting granules-spheres. A clear fixation (positioning) of the board between the spheres was provided due to the presence in the board of a mounting hole of a certain diameter, depending on the radius of the spheres and the thickness of the board. In the experiments chains of spheres of different lengths were used, i. e. with a different number n of identical spheres in a chain (moreover, with spheres with a radius of R = 15 mm or R = 20 mm). Based on the results of measuring Φ in one or another core with a radius $r < R$, data on the average induction B in each of the quasi-continuous cores of the chain were obtained as well as data on the magnetic permeability μ and susceptibility χ of these cores, their magnetization M.

The resulting informative families of dependencies made it possible to establish the following. First, the data of the parameters B, μ, χ and M for the cores of chains of spheres with a radius R = 15 mm corresponded to the data of these parameters for the cores of chains similar in relative radius r/R with the same n, but with a radius R = 20 mm. This testified to the possibility of applying the obtained data to similar chains of spheres of a different radius, i. e. about their versatility. Second, the larger was the relative radius r/R of the core of the chain of spheres, the smaller the values of B, μ, χ and M were for it. This was due to a decrease in the proportion of ferromagnetic metal in the core and vice versa. Thirdly, all dependences of B, μ, χ and M (for different cores of the chain of spheres) on n initially increased as n increased due to a decrease in the demagnetizing factor N of each of the cores and the chain as a whole. Subsequently, they demonstrated the achievement of individually limiting values of these magnetic parameters and the corresponding self-similar regions (where $N \rightarrow 0$). In this case, the beginning of each of these regions, which manifested themselves almost independently of r/R and the field intensity H, fell on the value n = 10–12 (starting from which $N \rightarrow 0$). Thus, such an established, in fact, criterial, value n = 10–12 = $[n]$ made it possible to distinguish both chains of spheres and their cores. The groups were as follows: sufficiently "long" – when $n \geq [n]$ and "short" – when $2 \leq n < [n]$. N data were obtained for different cores of "short" chains of spheres and described by a phenomenological expression. This expression was a product of a power (in r/R) and exponential (in n) functions.

Acknowledgments

This research was supported by the Ministry of Science and Higher Education of the Russian Federation, project 0706-2020-0024.

References

1. Périgo E.A., Weidenfeller B., Kollár P., Füzer J. Past, present, and future of soft magnetic composites. *Applied Physics Review*, 2018, vol. 5, no. 3, p. 031301. **DOI:** 10.1063/1.5027045

2. Strečková M., Füzer J., Kobera L., Brus J., Faberova M., Bures R., Kollar P., Lauda M., Medvecky L., Girman V., Hadraba H., Bat'kova M., Bat'ko I. A comprehensive study of soft magnetic materials based on FeSi spheres and polymeric resin modified by silica nanorods. *Materials Chemistry and Physics*, 2014, vol. 147, iss. 3, pp. 649–660. **DOI:** 10.1016/j.matchemphys.2014.06.004

3. Kanhe N.S., Kumar A., Yusuf S.M., Nawale A.B., Gaikwad S.S., Raut Suyog A., Bhoraskar S.V., Sheng Wu Yun, Das A.K., Mathe V.L. Investigation of structural and magnetic properties of thermal plasma-synthesized Fe1−xNiχ alloy nanoparticles. *Journal of Alloys and Compounds*, 2016, vol. 663, pp. 30–40. **DOI:** 10.1016/j.jallcom.2015.11.190

4. Birčáková Z., Kollár P., Weidenfeller B., Füzer J., Fáberová M., Bureš R. Reversible and irreversible DC magnetization processes in the frame of magnetic, thermal and electrical properties of Fe-based composite materials. *Journal of Alloys and Compounds*, 2015, vol. 645, pp. 283–289. **DOI:** 10.1016/j.jallcom.2015.05.121

5. Kollár P., Birčáková Z., Vojtek V., Füzer J., Bureš R., Fáberova M. Dependence of demagnetizing fields in Fe-based composite materials on magnetic particle size and the resin content. *Journal of Magnetism and Magnetic Materials*, 2015, vol. 388, pp. 76–81. **DOI:** 10.1016/j.jmmm.2015.04.008

6. Bai K., Casara J., Nair-Kanneganti A., Wahl A., Carle F., Brown E. Effective magnetic susceptibility of suspensions of ferro-magnetic particles. *Journal of*

Applied Physics, 2018, vol. 124, p. 123901.
DOI: 10.1063/1.5041750

7. Moore R.L. Development of a volume fraction scaling function for demagnetization factors in effective media theories of magnetic composites. *AIP Advances*, 2019, vol. 9, p. 035107.
DOI: 10.1063/1.5078736

8. Moore R.L. Development and test of concentration scaled demagnetization in effective media theories of magnetic composites. *Journal of Applied Physics*, 2019, vol. 125, p. 085101. **DOI:** 10.1063/1.5053791

9. Sandulyak A.A., Sandulyak D.A., Ershova V.A., Sandulyak A.V. Ferrous Material Fill: Magnetization Channels, Layer-by-Layer and Average Permeability, Element-to-Element Field. *Analysis and Modelling of Advanced Structures and Smart Systems*, 2017, vol. 81, pp. 191–210.
DOI: 10.1007/978-981-10-6895-9_9

10. Sandulyak A.V., Sandulyak A.A., Ershova V.A. Magnetization curve of a granulated medium in terms of the channel-by-channel magnetization model (new approach). *Doklady Physics*, 2007, vol. 52, pp. 179–181.
DOI: 10.1134/S1028335807040027

11. Sandulyak A.V., Gorpinenko Yu.O., Polismakova M.N., Sandulyak D.A., Sandulyak A.A. Magnetic flow and induction in the hearts of magnetizable ball chains. *Engineering*, 2020, no. 6(96), pp. 96–110.
DOI: 10.23670/IRJ.2020.96.6.017

12. Kolomeitsev A.A., Zatonov I.A., Pischanskaya M.I., Baranov P.F., IlyaschenkoD.P., Verkhoturova E.V. Designing a Planar Fluxgate Using the PCB Technology. *Devices and Methods of Measurements*, 2021, vol. 12, no. 2, pp. 117–123.
DOI: 10.21122/2220-9506-2021-12-2-117-123

13. Uchaikin S., Likhachev A., Cioata F., Perminov I., Sanghera H., Singh I., Spear P., Chavez P., Han X., Petroff C., Rich C. 3D magnetometer for a dilution refrigerator. *Journal of Physics: Conference Series*, 2012, vol. 400, p. 052037.
DOI: 10.1088/1742-6596/400/5/052037

14. Chen D.X., Pardo E., Zhu Y.-H., Xiang L.-X., Ding J.-Q. Demagnetizing correction in fluxmetric measurements of magnetization curves and hysteresis loops of ferromagnetic cylinders. *Journal of Magnetism and Magnetic Materials*, 2018, vol. 449, pp. 447–454.
DOI: 10.1016/j.jmmm.2017.10.069

Dynamic Features of Spectra of Single and Quasi-Periodic Measuring Signals

U.V. Suchodolov[1], A.V. Isaev[1], A.A. Sheinikau[2]

*[1]Belarusian National Technical University,
Nezavisimosty Ave., 65, Minsk 220013, Belarus*

*[2]Military Academy of the Republic Belarus,
Nezavisimosty Ave., 220, Minsk 220057, Belarus*

Received 28.01.2022
Accepted for publication 30.05.2022

Abstract

Solving the problems of spectral processing of single and quasi-periodic signals in measurement and diagnostic systems is directly related to their isolation against the background of external interference or noise. The purpose of this work was to study single and quasi-periodic signals, i. e. signals limited in time, presented as separate components; development of a mathematical apparatus that connects the individual components of the original, time-limited signal, with the spectral characteristics of the periodic signal, which is obtained from the original by its periodization.

The paper analyzes the spectrum of a quasi-periodic signal, which is presented from spectral density regions separated by spectral components with zero amplitude. The process of signal periodization is considered on the example of unipolar rectangular pulses. The representation of the analyzed complex single signal in the form of a linear combination of given functions, limited in time by the duration of the considered signal, was chosen, and it was determined that it is most logical and efficient to use radio-frequency pulses. The spectral density of the signal under consideration is presented as the sum of the spectral densities of radio-frequency pulses of the same width with a varying carrier frequency. The original signal is presented as the sum of the constituent components (radio-frequency pulses), which form a time-limited frequency spectrum – a quastr. As a result, the correlation of the considered quasi-periodic signal with the parameters of the periodic signal (amplitude, period, and initial phase) is shown.

A format for representing time-limited signals in the form of components related to the spectral characteristics of a periodic signal, obtained from the original signal by periodization, has been developed. The formed mathematical apparatus allows simplifying the algorithmic support of measuring systems by eliminating the correlation signal processing.

Keywords: quasi-periodic measuring signals, spectrum harmonics, spectral density, decomposition basis.

DOI: 10.21122/2220-9506-2022-13-2-128-138

Адрес для переписки:
Суходолов Ю.В.
Белорусский национальный технический университет,
пр-т Независимости, 65, г. Минск 220013, Беларусь
e-mail: suhodolov@bntu.by

Address for correspondence:
Suchodolov U.V.
Belarusian National Technical University,
Nezavisimosty Ave., 65, Minsk 220013, Belarus
e-mail: suhodolov@bntu.by

Для цитирования:
U.V. Suchodolov, A.V. Isaev, A.A. Sheinikau.
Dynamic Features of Spectra of Single and Quasi-Periodic Measuring Signals.
Приборы и методы измерений.
2022. – Т. 13, № 2. – С. 128–138.
DOI: 10.21122/2220-9506-2022-13-2-128-138

For citation:
U.V. Suchodolov, A.V. Isaev, A.A. Sheinikau.
Dynamic Features of Spectra of Single and Quasi-Periodic Measuring Signals.
Devices and Methods of Measurements.
2022, vol. 13, no. 2, pp. 128–138.
DOI: 10.21122/2220-9506-2022-13-2-128-138

Спектральное представление измерительных одиночных и квазипериодических сигналов

Ю.В. Суходолов[1], А.В. Исаев[1], А.А. Шейников[2]

*[1]Белорусский национальный технический университет,
пр-т Независимости, 65, г. Минск 220013, Беларусь*

*[2]Военная академия Республики Беларусь,
пр-т Независимости, 220, г. Минск 220057, Беларусь*

Поступила 28.01.2022
Принята к печати 30.05.2022

Решение задач по спектральной обработке одиночных и квазипериодических сигналов в системах измерения и диагностики непосредственно связанно с их выделением на фоне внешних помех или шумов. Целью работы являлось исследование одиночных и квазипериодических сигналов, т. е. сигналов, ограниченных во времени, представленных в виде отдельных компонент; разработка математического аппарата, связывающего отдельные компоненты исходного, ограниченного во времени сигнала, со спектральными характеристиками периодического, который получен из исходного путём его периодизации.

В работе проведён анализ спектра квазипериодического сигнала, который представлен из участков спектральной плотности, разделённых спектральными составляющими с нулевой амплитудой. Рассмотрен процесс периодизации сигнала на примере однополярных прямоугольных импульсов. Выбрано представление анализируемого сложного одиночного сигнала в виде линейной комбинации заданных функций, ограниченных по времени длительностью рассматриваемого сигнала. Определено, что наиболее логично и эффективно в качестве линейной комбинации заданных функций использовать радиоимпульсы. Представлена спектральная плотность исследуемого сигнала в виде суммы спектральных плотностей радиоимпульсов той же длительности с изменяющейся несущей частотой. Исходный сигнал представлен как сумма составляющих компонент (радиоимпульсов), которые формируют ограниченный во времени частотный спектр – квастр. В результате показана корреляция рассматриваемого квазипериодического сигнала с параметрами периодического сигнала (амплитудой, периодом и начальной фазой).

Разработан формат представления ограниченных во времени сигналов в виде компонент, связанных со спектральными характеристиками периодического сигнала, который получен из исходного путём его периодизации. Сформированный математический аппарат позволяет упростить алгоритмическое обеспечение измерительных систем за счёт исключения корреляционной обработки сигнала.

Ключевые слова: квазипериодический измерительный сигнал, гармонические составляющие спектра, спектральная плотность, базис разложения.

DOI: 10.21122/2220-9506-2022-13-2-128-138

Адрес для переписки:
Суходолов Ю.В.
Белорусский национальный технический университет,
пр-т Независимости, 65, г. Минск 220013, Беларусь
e-mail: suhodolov@bntu.by

Address for correspondence:
Suchodolov U.V.
Belarusian National Technical University,
Nezavisimosty Ave., 65, Minsk 220013, Belarus
e-mail: suhodolov@bntu.by

Для цитирования:
U.V. Suchodolov, A.V. Isaev, A.A. Sheinikau.
Dynamic Features of Spectra of Single and Quasi-Periodic Measuring Signals.
Приборы и методы измерений.
2022. – Т. 13, № 2. – С. 128–138.
DOI: 10.21122/2220-9506-2022-13-2-128-138

For citation:
U.V. Suchodolov, A.V. Isaev, A.A. Sheinikau.
Dynamic Features of Spectra of Single and Quasi-Periodic Measuring Signals.
Devices and Methods of Measurements.
2022, vol. 13, no. 2, pp. 128–138.
DOI: 10.21122/2220-9506-2022-13-2-128-138

Introduction

Measuring signals are the main physical quantities parameters information carriers in measuring systems. In case of this signal being random, the aggregate of individual instantaneous values of its main parameter is considered to be information. Pulse measuring systems most often use the frequency-domain parameters of the signal. However, the spectral method is used to analyze the measuring signals most often in both cases.

According to the Fourier transform theory, the representation of any signal in the frequency domain is valid only when it meets the Dirichlet conditions, i. e. the signal must start at infinity and end at infinity, and, therefore, it must be stable over the entire time interval in which its spectral characteristic will not be a function of time [1]. This condition is not feasible for the analysis of real quasi-periodic processes and signals. Usually in this case window Fourier transforms [2] or wavelet transforms [3, 4] are used. However, the wavelet transform theory also contains a number of simplifications that use orthogonal basis systems, which, in turn, are mathematical abstractions.

Distortion in the operation of individual elements of various measuring and diagnostic systems leads to the formation of additional non-normalized quasi-periodic signal structures [5]. Therefore, when developing algorithms to automatically remove interference from a useful signal, the main condition is to establish an accurate dependence between local signal disturbances and changes in the values of individual components of its spectrum. It was shown in [6] that changes in the values of signal parameters lead to a significant violation of the initial distribution of spectral components, some of the latter undergoing more significant changes than others. Therefore, to increase measurement accuracy one can replace the low-sensitivity registration of the signal temporal parameters changes with the registration of the characteristic spectral components parameters changes, the latter being more sensitive to deviations of the measured parameter and less sensitive to deviations that are due to the instability of the elements in the measuring systems.

Having taken recent development of modern computing base into account, using a hardware-mathematical approach to study of quasi-periodic signals is most efficient, since by controlling individual parameters of the signal under study (amplitude, pulse-repetition interval, pulse duration, and other time parameters), it is possible to indirectly control the parameters of its spectrum. One also can distinguish useful signal from interference using the numbers of the necessary spectral components. In this case to select the numbers of spectral components with minimum measuring signal parameters instability sensitivity one must study the dynamic features of measuring signal spectrum.

The purpose of this work was to develop a mathematical apparatus that allows one to represent single and quasi-periodic time-limited signals as a set of spectral components, the basis of which are impulses, parameters of said impulses being determined by conditional periodization, to provide a unified approach to describing the spectra of these signals over finite time intervals.

Main part

Quasi-periodic signals, which occupy an intermediate position between periodic and non-periodic signals, are among the most common signals used in measurement and diagnostic systems, said signals reflect the process of transforming spectral density into a discrete spectrum. Their main feature is that they are time-limited [7, 8]. Therefore, given the different approach to describing the spectra of periodic and non-periodic signals, this creates difficulties when considering quasi-periodic signals. At the same time, modeling the discrete spectrum formation process from the spectral density provides a general description for both types of spectra. This problem can be solved in two ways. The first one considers the process of a discrete spectrum formation from the spectral density during signal periodization. However, a spectrum-limited signal is a signal that is infinite in time. Consequently, when sampling such a signal, an infinite number of samples will be obtained. Then, to restore the original signal (including obtaining its discrete spectrum), it is necessary to take into account all the readings, which is impossible due to its unlimited duration [7].

The second method involves obtaining a periodic sequence of signals, which is the sum of individual signals delayed relative to each other in time [1]. However, such treatment of a real signal as a periodic one leads to an error due to the finite duration of the measurement process. And in this case, it is necessary to determine the influence of the discrete spectrum formation error that depends on the number of repetitions in the periodization process. Thus, with an increase in the number of pulses more and more zeros appear in the spectral density of the signal during periodization [1]. Taking into account that each zero of the spectral density is at a strictly defined frequency and has a strictly defined and measurable zero amplitude at the same time, it can be assumed that it is the spectral component of the discrete spectrum, which was formed as a result of full periodization, and it is a part of a continuous spectrum at the same time. This representation is the main connecting component. Therefore, the spectrum of the quasi-periodic signal itself can be considered combined, i. e. consisting of spectral density regions separated by spectral components with zero amplitude. For example, consider the process of periodization of a signal represented as unipolar rectangular pulses (Figure 1).

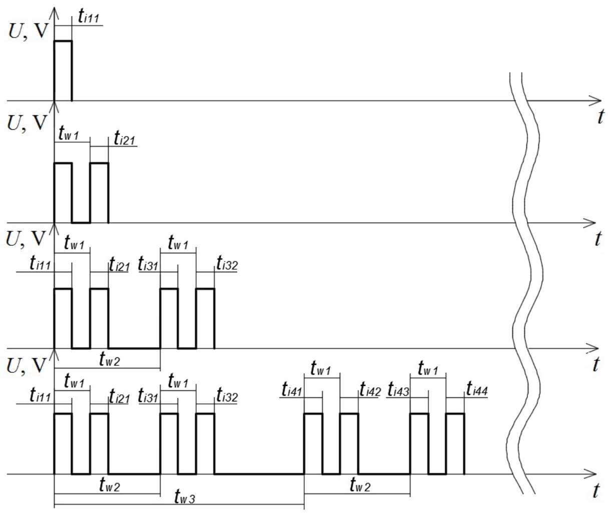

Figure 1 – Periodization of rectangular pulses

Let's set the following conditions:

$t_{i11} = t_{i12} = t_{i21} = t_{i22} = t_{ixx} = t_i$.

Then, according to [9], the complex spectral density of such a sequence is defined as the spectral densities sum of the pulses, that are presented in the sequence. The equation for the first pulse in the sequence can be written as:

$$S_{11}(\omega)=\frac{E}{\pi j}(1-e^{-j\omega t_i}), \quad (1)$$

where E is pulse amplitude; t_i is pulse duration; ω is current frequency of the rectangular pulse sequence.

Accordingly, the equation for the second pulse is:

$$S_{12}(\omega)=\frac{E}{\pi j}(1-e^{-j\omega t_i})e^{-j\omega t_{w1}}, \quad (2)$$

where t_{w1} is delay between two pulses.

The expression for the sequence of these two pulses is:

$$S_{p1}(\omega)=S_{11}(\omega)+S_{12}(\omega)=\frac{E}{\pi j}(1-e^{-j\omega t_i})+\frac{E}{\pi j}(1-e^{-j\omega t_i})e^{-j\omega t_{w1}}=$$
$$=\frac{E}{\pi j}(1-e^{-j\omega t_i})(1+e^{-j\omega t_{w1}}). \quad (3)$$

According to the displacement theorem [9], for the second same pair of pulses with numbers 3 and 4, the equation will look like:

$$S_{p2}(\omega)=S_{21}(\omega)+S_{22(\omega)}=\frac{E}{\pi j}(1-e^{-j\omega t_i})e^{-j\omega t_{w2}}+$$
$$+\frac{E}{\pi j}(1-e^{-j\omega t_i})e^{-j\omega t_{w2}}e^{-jn\omega t_{w1}}= \quad (4)$$
$$=\frac{E}{\pi j}(1-e^{-j\omega t_i})(1+e^{-j\omega t_{w1}})e^{-j\omega t_{w2}},$$

where t_{w2} is delay between double pulses.

Then the complex spectral density of the sum of two identical double pulses has the form:

$$S_{pp1}(\omega)=S_{p1}(\omega)+S_{p2}(\omega)=\frac{E}{\pi j}(1-e^{-j\omega t_i})(1+e^{-j\omega t_{w1}})+$$
$$+\frac{E}{\pi j}(1-e^{-j\omega t_i})(1+e^{-j\omega t_{w1}})e^{-j\omega t_{w2}}= \quad (5)$$
$$=\frac{E}{\pi j}(1-e^{-j\omega t_i})(1+e^{-j\omega t_{z1}})(1+e^{-j\omega t_{z2}}).$$

Transforming this expression, we will have:

$$S_{pp1}(\omega)=$$
$$=\frac{8E}{\pi j}(\sin\frac{\omega t_i}{2})(\cos\frac{\omega t_{z1}}{2})(\cos\frac{\omega t_{z2}}{2})e^{-j\omega\frac{\omega t_i}{2}}e^{-j\omega\frac{\omega t_{z1}}{2}}e^{-j\omega\frac{\omega t_{z2}}{2}}. \quad (6)$$

Repeating the resulting impulse combination after a delay time t_{w3} and taking into account the displacement theorem, we obtain an expression for its complex amplitude:

$$S_{pp2}(\omega)=\frac{E}{\pi j}(1-e^{-j\omega t_i})(1+e^{-j\omega t_{w1}})(1+e^{-j\omega t_{w2}})e^{-j\omega t_{w3}}. \quad (7)$$

Then the general expression for the complex spectral density of the resulting pulse train will be as follows:

$$S_{ppp1}(\omega) = S_{pp1}(\omega) + S_{pp2}(\omega) = \frac{E}{\pi nj}(1 - e^{-j\omega t_i})(1 + e^{-j\omega t_{w1}})(1 + e^{-j\omega t_{w2}}) + \frac{E}{\pi j}(1 - e^{-j\omega t_i})(1 + e^{-j\omega t_{w1}})(1 + e^{-j\omega t_{w2}})e^{-j\omega t_{w3}}. \quad (8)$$

Transforming this expression, we will have:

$$S_{ppp1}(\omega) = \frac{16E}{\pi j}(\sin\frac{\omega t_i}{2})(\cos\frac{\omega t_{w1}}{2})(\cos\frac{\omega t_{w2}}{2})(\cos\frac{\omega t_{w3}}{2})e^{-j\omega\frac{\omega t_i}{2}}e^{-j\omega\frac{\omega t_{w1}}{2}}e^{-j\omega\frac{\omega t_{w2}}{2}}e^{-j\omega\frac{\omega t_{w3}}{2}}. \quad (9)$$

Therefore, the general expression for the spectral densities modulus of the constructed impulse arrays can be written as:

$$|S(\omega)| = \frac{2EK}{\pi}|\sin\frac{\omega t_i}{2}| \times \prod_{L=1}^{K}|\cos\frac{\omega t_{zL}}{2}|, \quad (10)$$

where E is pulse amplitude; t_{zL} is delay between sets of impulse combinations; t_i is pulse duration; ω is current spectral density frequency; K is number of consecutive rectangular pulses combinations.

Accordingly, the spectral density modulus envelope zeros are determined from the expressions:

$$\sin\frac{\omega t_i}{2} = 0 \text{ and } \cos\frac{\omega t_{zL}}{2} = 0. \quad (11)$$

Therefore,

$$\omega_{0t_i} = N \cdot 2\pi / t_i, \quad \omega_{0w} = N \cdot \pi / Kt_w, \quad (12)$$

where $N = 1, 2, 3...$ etc. is zero number.

From expressions (10), it can be concluded that with an increase in the number of zeros the distance between them decreases and the spectral density increases in the region of frequencies that are multiples of the periodization frequency, and, therefore, the components of the expected discrete spectrum are formed. This suggests that with such a periodization, due to an increase in the number of zeros, the process of transformation of the spectral density into a discrete spectrum occurs. However, with such a signal analysis, it is impossible to determine a discrete spectrum formation end time, since with each new periodization step and regardless of the number of steps, the amplitudes of the spectral components change to indicate that in order to obtain high accuracy, it is necessary to obtain an amplitude-frequency spectrum corresponding to the maximum number of repetitions, and this leads to an increase in the analysis time. An increase in the analysis time in turn leads to the additional error appearance, the latter associated with the signal under study repetition parameters instability.

To analyze a single signal, let's represent it as a linear combination of given functions, which are limited in time by the duration of the consi-dered signal. According to the signal Fourier series expansion theory, only signals of infinite duration have physical meaning, which does not reflect real processes [2]. Thus such a method cannot be used to expand a time-limited quasi-periodic signal. Therefore, when choosing the expansion basis, it is most expedient to represent it as a set of harmonic signals, taking into account the limitations imposed by practice. A solution that satisfies the requirements is the use of various time-limited and often encountered in real life signals as a basis. Various types of sequences can serve as such signals, the most optimal of them being various damped oscillations with fast Fourier series convergence. For example, sinusoidal pulses with exponentially decaying amplitude, or a limited spectrum signal of the form $\sin(\omega t)/\omega t$, the general form and spectral density of which are shown in Figure 2.

However, the construction and circuit implementation of complex pulse sequences are associated with the introduction of additional errors associated with the limited stability of such circuits. In addition, on the signal duration limiting the amplitude-frequency spectrum for a signal in the form $\sin(\omega t)/\omega t$, ideally having a finite spectrum, is strongly distorted, up to the loss of the advantage in limiting the spectrum. Therefore, when analyzing quasi-periodic sequences, it is most optimal to use radio pulses, as presented in [10, 11], but it has to be taken into account that generally the initial phase is not equal to zero inside each radio pulse.

Thus, the signal will be decomposed into radio pulses with different multiple carrier frequencies [12], the initial phases and amplitudes being obtained as a result of the Fourier expansion of the generated periodic signal, and the carrier frequency of an individual radio pulse will then correspond to the frequency of a separate spectral component of the periodized signal. Consequently, the analyzed signal spectral density will consist of the sum of its constituent radio pulses spectral densities. Figure 3 shows the decomposition of a sequence of bipolar rectangular pulses into time-limited spectrum components – radio pulses.

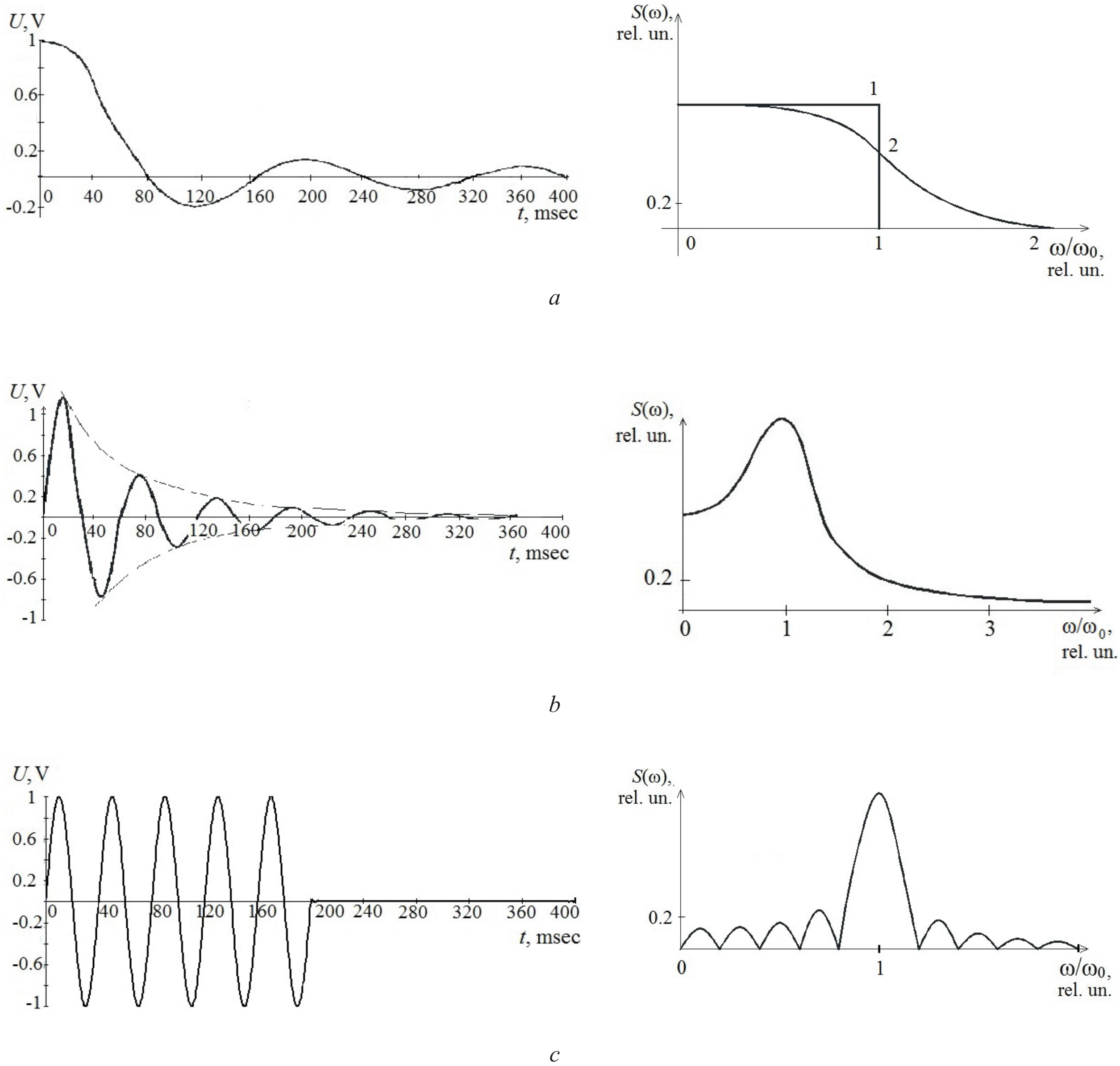

Figure 2 – General view and spectral density of signals limited in time: *a* – sinusoidal signal with exponentially decaying amplitude; *b* – signal of the form $\sin(\omega t)/\omega t$; *c* – radio pulse

Therefore, a time-limited quasi-periodic signal $S(t_1,t_2)$ (i. e., a signal existing in the time interval $[t_1,t_2]$) can be represented as the sum of time-limited spectral densities $\varphi_k(t_1,t_2)$, which are a set of non-periodic signals (radio pulses) described in the frequency domain by the spectral density [13]:

$$S(t_1,t_2)=\sum_{k=0}^{K} C_k \phi_k(t_1,t_2), \qquad (13)$$

where C_k is expansion coefficients that determine the spectrum of a quasi-periodic signal.

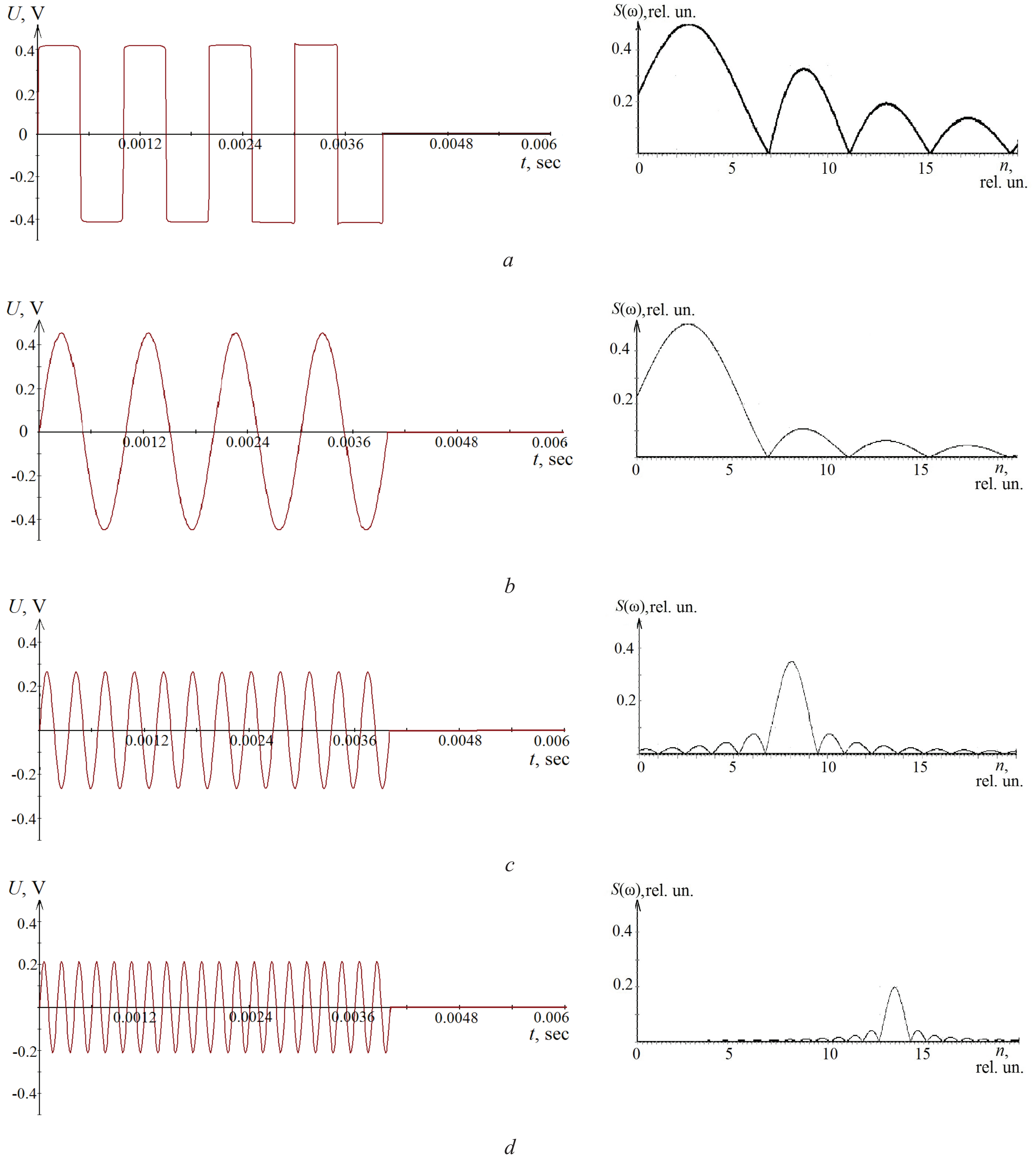

Figure 3 – An example of the spectral density of a quasi-periodic signal and its components: *a* – a limited pulse sequence and its spectral density; *b*, *c*, *d* – constituent radio pulses and their spectral densities

The result of such an expansion is the total spectral density of the studied pulse sequence shown in Figure 4. For convenience, it was proposed to name this kind of expansion a quastr.

At the same time, it should be noted that a separate component of the quastr has a physical meaning, since it is essentially a radio pulse with quite simply measurable parameters. This distinguishes it from the representation of the investigated pulse only in the form of spectral density, the latter having frequency components with infinitely small amplitudes and continuous frequency components. At the same time, the quastr reflects the real process and corresponds to practice [8, 12]. The components of the quastr (radio pulses) being not periodic functions, they are described in the frequency domain by the spectral density, which links the quasi-periodic signal to its representation in the form of a spectral density. In this case, the spectral density of each component of the quastr, as well as the spectral density of the other components, is distributed over the entire frequency range, and the value of the spectral signal density sum of all radio pulses at a certain frequency can be calculated. Thus, the gain in the transition from the spectrum to the quastr is associated with the emerging opportunity to calculate and to measure the components of a non-periodic signal, and hence the opportunity to localize errors due to measuring systems individual elements functional peculiarities. This will make it possible to establish an unambiguous relationship between local signal variations and changes in its quastr components, which will allow the development of algorithms for automatic noise suppression in measuring systems, express diagnostics of malfunctions in electrical machines and other electrical equipment using one or more signals, and so on.

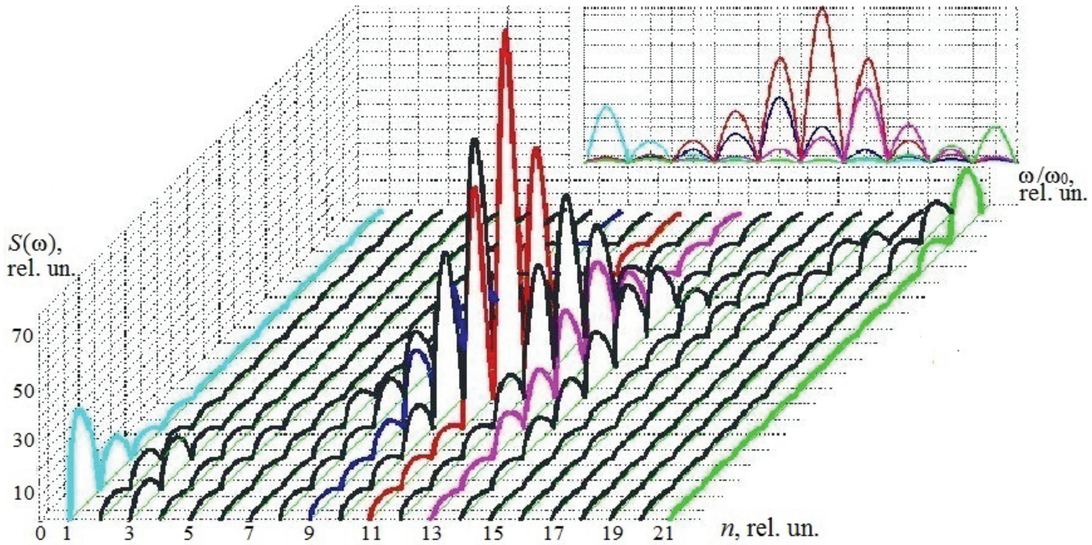

Figure 4 – Volumetric representation of a quasi-periodic signal in the form of a quastr

Let us obtain an expression for the spectral density, presented as the sum of the spectral densities of its constituent radio pulses. The use of coherent radio pulses as frequency components, as it is shown in [8, 12], does not allow one to accurately and fully relate the processes and parameters of the quastr and spectral density components, i. e. the absence of phase shift in radio pulses is a special case, and the general view of a radio pulses sequence with an arbitrary phase delay is shown in Figure 5.

Let's represent the signal under consideration as a sum of four separate pulse components:

1. θ is incomplete pulse period associated with the phase shift θ;

2. 1, 2, ..., m is full periods of the harmonic signal delayed in time by T_c relative to each other together with the delay time t_θ;

3. P_+ is completed half-cycle of the last pulse;

4. P_- is incomplete part of the half-cycle of the last pulse.

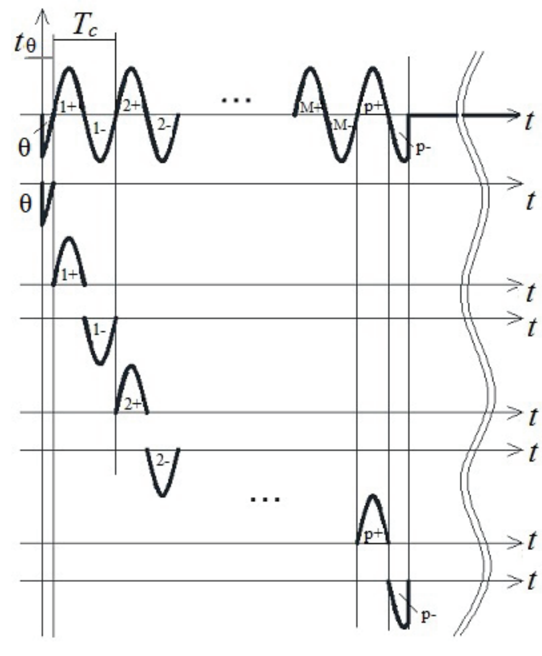

Figure 5 – Representation of a phase-delayed signal of a sequence of radio pulses

Thus, taking into account the phase shift by time t_Θ, the presented harmonic signal spectral density will be determined by the expression:

$$S_c(\omega) = S_{i\theta}(\omega) + \sum\nolimits_{k=1}^{m} S_{i_k}(\omega) + S_{ip+}(\omega) + S_{ip-}(\omega), \qquad (14)$$

where $S_\theta(\omega)$ is spectral density of a part of the sig is number of complete periods of the harmonic signal; $S_{ip+}(\omega)$ is spectral density of the completed part of the last signal period; $S_{ip-}(\omega)$ is the spectral density of the last incomplete pulse.

According to [1], the spectral density of a sinusoidal pulse is determined by the formula:

$$S_i(\omega) = \int_{t_1}^{t_2} (-1)\sin\left(\frac{2\pi}{T_c}t\right) e^{-j\omega t}dt, \qquad (15)$$

where t_1 and t_2 is start and finish times of the impulse under consideration; T_c is full period of the signal under study; ω is current frequency.

Taking into account expression (15), expression (14) will be of the form:

$$S_c(\omega) = \int_0^{t_\theta} E_m \sin\left(\frac{2\pi}{T_c}t\right) e^{-j\omega t}dt + \int_{t_\theta}^{t_\theta+mT_c} E_m \sin\left(\frac{2\pi}{T_c}t\right) e^{-j\omega t}dt + \int_{t_\theta+mT_c}^{t_\theta+mT_c+T_c/2} E_m \sin\left(\frac{2\pi}{T_c}t\right) e^{-j\omega t}dt + \int_{t_\theta+mT_c+T_c/2}^{(m+1)T_c} E_m \sin\left(\frac{2\pi}{T_c}t\right) e^{-j\omega t}dt, \qquad (16)$$

where E_m is amplitude of impulse under consideration.

Or, using the displacement theorem [9]:

$$S_c(\omega) = \int_0^{t_\theta} E_m \sin\left(\frac{2\pi}{T_c}t\right) e^{-j\omega t}dt + \int_0^{mT_c} E_m \sin\left(\frac{2\pi}{T_c}t\right) e^{-j\omega t} e^{-j\omega t_\theta}dt + \int_0^{T_c/2} E_m \sin\left(\frac{2\pi}{T_c}t\right) e^{-j\omega t} e^{-j\omega(t_\theta+mT_c)}dt +$$
$$+ \int_0^{T_c/2-t_\theta} E_m \sin\left(\frac{2\pi}{T_c}t\right) e^{-j\omega t} e^{-j\omega(t_\theta+mT_c+T_c/2)}dt. \qquad (17)$$

Let us form an expression for each part of the expression (17).

1. The solution of equation for $S_\theta(\omega)$ will look like:

$$S_\theta(\omega) = \int_0^{t_\theta} E_m \sin\left(\frac{2\pi}{T_c}t\right) e^{-j\omega t}dt = E_m \left(\frac{(-j\omega)\sin\left(\frac{2\pi}{T_c}t\right) - \left(\frac{2\pi}{T_c}\right)\cos\left(\frac{2\pi}{T_c}t\right)}{(-j\omega)^2 + \left(\frac{2\pi}{T_c}\right)^2} e^{-j\omega t} \right)\Bigg|_0^{t_\theta}. \qquad (18)$$

After a series of transformations and calculations, equation (18) has the following form:

$$S_\theta(\omega) = E_m \frac{\frac{2\pi}{T_c}}{\omega^2 + \left(\frac{2\pi}{T_c}\right)^2} \left(\left(j\omega \frac{T_c}{2\pi}\sin\left(\frac{2\pi}{T_c}t_\theta\right) + \cos\left(\frac{2\pi}{T_c}t_\theta\right)\right) e^{-j\omega t_\theta} + 1 \right). \qquad (19)$$

2. Let us write the spectral density of the full period of the impulse under consideration as the sum of two identical pulses, opposite in sign and shifted relative to each other by a time $t_{w1} = T_c/2$, i. e.:

$S_i(\omega) = S_{i+}(\omega) + S_{i-}(\omega)$.

Then the spectral density of the first positive pulse will have the form:

$$S_{i_1+}(\omega) = \int_0^{T_c/2} (-1)\sin\left(\frac{2\pi}{T_c}t\right) e^{-j\omega t} e^{-j\omega t_\theta}dt. \qquad (20)$$

After integration, expression (20) has the form:

$$S_{i_1+}(\omega) =$$
$$= \left(E_m \frac{(-j\omega)\sin\left(\frac{2\pi}{T_c}t\right) - \left(\frac{2\pi}{T_c}\right)\cos\left(\frac{2\pi}{T_c}t\right)}{(-j\omega)^2 + \left(\frac{2\pi}{T_c}\right)^2} e^{-j\omega t_\theta} e^{-j\omega t} \right)\Bigg|_0^{T_c/2}$$

or

$$S_{i_1+}(\omega) = E_m \frac{\frac{2\pi}{T_c}}{\omega^2 + \left(\frac{2\pi}{T_c}\right)^2} e^{-j\omega t_\theta} \left(1 - e^{-j\omega \frac{T_c}{2}}\right). \qquad (21)$$

Then, according to displacement theorem, the spectral density of the negative half-wave of the first pulse, delayed by time $t_{w1} = T_c/2$, is determined by the expression:

$$S_{i_1-}(\omega) = E_m \frac{\frac{2\pi}{T_c}}{\omega^2 + \left(\frac{2\pi}{T_c}\right)^2} e^{-j\omega t_\theta} e^{-j\omega T_c/2} \left(1 - e^{-j\omega\frac{T_c}{2}}\right). \quad (22)$$

Then the expression for the spectral density of a single period of the radio pulse will have the form:

$$S_i(\omega) = S_{i_1+}(\omega) + S_{i_1-}(\omega) =$$

$$= E_m \frac{\frac{2\pi}{T_c}}{\omega^2 + \left(\frac{2\pi}{T_c}\right)^2} \left(1 - e^{-j\omega\frac{T_c}{2}}\right)\left(1 + e^{-j\omega\frac{T_c}{2}}\right) e^{-j\omega t_\theta}. \quad (23)$$

The total spectral density of the full periods of the considered harmonic signal has the form:

$$S_i(\omega) = \sum_{k=1}^{m} S_{i_k}(\omega) e^{-j\omega k T_c} = E_m \frac{\frac{2\pi}{T_c}}{\omega^2 + \left(\frac{2\pi}{T_c}\right)^2} e^{-j\omega t_\theta} \times$$

$$\times \left(1 - e^{-j\omega\frac{T_c}{2}}\right)\left(1 + e^{-j\omega\frac{T_c}{2}}\right)\left(\frac{\sin\frac{\omega m T_c}{2}}{\sin\frac{\omega T_c}{2}}\right) e^{-j\omega\frac{(m-1)T_c}{2}}. \quad (24)$$

3. Similarly to the previous calculations, let us define the spectral densities of the considered signal remaining components. The expression for the spectral density of the completed half-cycle of the last pulse has the form:

$$S_{P+}(\omega) = E_m \frac{\frac{2\pi}{T_c}}{\omega^2 + \left(\frac{2\pi}{T_c}\right)^2} \left(1 - e^{-j\omega\frac{T_c}{2}}\right) e^{-j\omega t_\theta} e^{-j\omega m T_c}, \quad (25)$$

and for the incomplete one:

$$S_{p-}(\omega) = E_m \frac{\frac{2\pi}{T_c}}{\omega^2 + \left(\frac{2\pi}{T_c}\right)^2} \left(\left(j\omega \frac{T_c}{2\pi} \sin\left(\frac{2\pi}{T_c} t_\theta\right) + \cos\left(\frac{2\pi}{T_c} t_\theta\right)\right) e^{-j\omega\left(\frac{T_c}{2} - t_\theta\right)} + 1 \right) e^{-j\omega(t_\theta + mT_c + T_c/2)}. \quad (26)$$

Then the general expression for the spectral density of the considered signal can be represented as:

$$S(\omega) = E_m \frac{\frac{2\pi}{T_c}}{\omega^2 + \left(\frac{2\pi}{T_c}\right)^2} \left(\left(1 - e^{-j\omega\frac{T_c}{2}}\right) e^{-j\omega t_\theta} \left(\left(1 + e^{-j\omega\frac{T_c}{2}}\right)\left(\frac{\sin\frac{\omega m T_c}{2}}{\sin\frac{\omega T_c}{2}}\right) e^{-j\omega\frac{(m-1)T_c}{2}} + e^{-j\omega m T_c} \right) + \right.$$

$$\left. + \left(\left(j\omega \frac{T_c}{2\pi} \sin\left(\frac{2\pi}{T_c} t_\theta\right) + \cos\left(\frac{2\pi}{T_c} t_\theta\right)\right) e^{-j\omega t_\theta} + 1 \right) + \left(\left(j\omega \frac{T_c}{2\pi} \sin\left(\frac{2\pi}{T_c} t_\theta\right) + \cos\left(\frac{2\pi}{T_c} t_\theta\right)\right) e^{-j\omega\left(\frac{T_c}{2} - t_\theta\right)} + 1 \right) e^{-j\omega(t_\theta + mT_c + T_c/2)} \right). \quad (27)$$

It follows from expression (26) that the signal spectral density is directly related to the periodic signal through its main parameters – amplitude (E_m), period (T_c) and initial phase (t_θ), and, therefore, to study single and quasi-periodic signals, instead of the spectral density, one can use the quastr, which represents the time-limited amplitude-frequency spectrum of the signal. Such a representation will simplify the algorithmic support of measuring systems by eliminating the correlation signal processing, which requires large computational resources [13].

Conclusion

A format has been developed to represent single and quasi-periodic, time-limited signals in the form of components that are associated with the spectral characteristics of a periodic signal obtained by periodization and the development of a mathematical apparatus for performing these procedures.

The presented approach to the analysis of quasi-periodic signals makes it possible to simplify the algorithmic support of measuring systems by eliminating the correlation processing of the signal, which requires large computational resources. The practical implementation of the proposed technique will reduce the measurement time and design parameters of the measuring systems elements.

References

1. Petre Stoica, Randolph Moses, Spectral Analysis of Signals. PRENTICE HALL, *Upper Saddle River*, New Jersey, 2005, 512 p.

2. Batura M.P., Kuznetsov A.P., Kurulev A.P. *Teoriya elektricheskikh tsepey* [Theory of electrical circuits]. Minsk: Higher School Publ., 2015, 608 p.

3. Gribunin V.G. *Vvedeniye v veyvlet-preobrazovaniye* [Introduction to Wavelet Transform]. St. Petersburg: AVTEKS Publ., 2009, 70 p.

4. Qian Tao, Vai Mang I., Xu Yuesheng (ed.). Wavelet analysis and applications. *Springer Science & Business Media*, 2007, 588 p.

5. Panfilov V.A. *Elektricheskiye izmereniya* [Electrical measurements]. Moscow: Akademiya Publ., 2008, 288 p.

6. Malashin A.N., Sukhodolov YU.V., Sheynikov A.A. *Povysheniye pomekhoustoychivosti kontrolya mezhvitkovoy izolyatsii kollektornykh elektricheskikh mashin postoyannogo toka s pomoshch'yu volnovykh zatukhayushchikh kolebaniy* [Improving the noise immunity of the control of inter-turn insulation of DC collector electric machines using wave damped oscillations]. *Sb. nauch. st. Voyen. akad. Resp. Belarus* [Collection of scientific articles of the military academy of the Republic of Belarus], 2010, no. 19, pp. 67–72 (in Russian).

7. Trukhachev A.A. *Radiolokacionnye signaly i ih primenenie* [Radar signals and their applications]. Moscow: Voyennoye izdatel'stvo Publ., 2005, 320 p.

8. GómezG., Mondelo J.M., Simó C. A collocation method for the numerical Fourier analysis of quasi-periodic functions. I: Numerical tests and examples. *Discrete and Continuous Dynamical Systems B.*, 2010, vol. 14, no. 1, pp. 41–74.
DOI: 10.3934/dcdsb.2010.14.41

9. Kharkevich A.A. *Spektry i analiz* [Spectra and analysis]. Izd. 6, URSS Publ., 2018, 240 p.

10. Gutnikov V.S. *Fil'tratsiya izmeritel'nykh signalov* [Filtering measurement signals]. L.: Energoatomizdat Publ., 1990, 192 p.

11. Zelenko V.V., Sheynikov A.A., Sukhodolov YU.V. [Accounting for instrumental errors in the control of windings of electrical machines using quasi-periodic test signals]. *Energetika. Izvestiya vysshikh uchebnykh zavedeniy i energeticheskikh ob"yedineniy SNG* [Energy. News of higher educational institutions and energy associations of the CIS], 2018, vol. 61, no. 3, pp. 235–245 (in Russian).
DOI: 10.21122/1029-7448-2018-61-3-235-245

12. Sheynikov A.A., Sukhodolov YU.V. [The use of the dynamic properties of spectra of sequences of radio pulses to ensure high sensitivity of test control windings of asynchronous motors]. *Energetika. Izvestiya vysshikh uchebnykh zavedeniy i energeticheskikh ob"yedineniy SNG* [Energy. News of higher educational institutions and energy associations of the CIS], 2018, vol. 61, no. 1, pp. 36–46 (in Russian).
DOI: 10.21122/1029-7448-2018-61-1-36-46

13. Shirman YA.D. *Radioelektronnyye sistemy: Osnovy postroyeniya i teoriya Izd. 2-ye, pererab. i dop.* [Radioelectronic systems: Fundamentals of construction and theory. Ed. 2nd, revised. and additional]. Moscow: Radiotekhnika, 2007, 512 p.

Probability of Erroneous Data Registration in a Single Photon Erasure-Type Communication Channel with a Receiver Based on a Photon Counter

A.M. Timofeev

*Belarusian State University of Informatics and Radioelectronics,
Brovki str., 6, Minsk 220013, Belarus*

*Received 20.04.2022
Accepted for publication 25.05.2022*

Abstract

When measuring low-power optical signals, it is necessary to ensure the highest reliability of the received data, which is especially important for single-photon communication channels. This determines the expediency of using photon counters as receiving modules for such channels. They are highly sensitive, but are characterized by data recording errors. Therefore, the purpose of this work was to investigate the influence of the intensity of the registered optical radiation J_0 during the transmission of binary symbols “0” on the probability of registering symbols “1” at the output of the communication channel in the presence of symbols “0” at its input $P(1/0)$.

The statistical distributions of the mixture of the number of dark and signal pulses at the output of the photon counter during the registration of binary symbols “0” $P_{st0}(N)$ were determined. To do this, a technique was used to reduce information loss. As a result, the minimum probability $P(1/0)$ was reached.

The probabilities $P(1/0)$ were calculated for a communication channel containing a photon counter as a receiving module. This calculation was carried out at different values of the supply voltage of the avalanche photodetector U and the intensity of the optical signal used to transmit the binary symbols “0” J_0.

The experimental results showed that with increasing optical signal intensity J_0, the dependences $P(1/0)$ on J_0 initially remain almost unchanged and retain a constant value. However, with a further increase in J_0, there is a linearly increasing character of the dependences $P(1/0)$ on J_0. Moreover, with other equal reception parameters, such a character of the dependences $P(1/0)$ on J_0 begins to manifest itself at higher intensities of the optical signal J_0 with an increase in the supply voltage of the avalanche photodetector.

Keywords: photon counter, single photon communication channel, probability of erroneous registration of binary symbols.

DOI: 10.21122/2220-9506-2022-13-2-139-146

Адрес для переписки:
Тимофеев А.М.
Белорусский государственный университет информатики и радиоэлектроники,
ул. П. Бровки, 6, г. Минск 220013, Беларусь
e-mail: tamvks@mail.ru

Address for correspondence:
Timofeev A.M.
Belarusian State University of Informatics and Radioelectronics,
Brovki str., 6, Minsk, 220013, Belarus
e-mail: tamvks@mail.ru

Для цитирования:
A.M. Timofeev.
Probability of Erroneous Data Registration in a Single Photon Erasure-Type Communication Channel with a Receiver Based on a Photon Counter.
Приборы и методы измерений.
2022. – Т. 13, № 2. – С. 139–146.
DOI: 10.21122/2220-9506-2022-13-2-139-146

For citation:
A.M. Timofeev.
Probability of Erroneous Data Registration in a Single Photon Erasure-Type Communication Channel with a Receiver Based on a Photon Counter.
Devices and Methods of Measurements.
2022, vol. 13, no. 2, pp. 139–146.
DOI: 10.21122/2220-9506-2022-13-2-139-146

Вероятность ошибочной регистрации данных в однофотонном канале связи стирающего типа с приёмником на основе счётчика фотонов

А.М. Тимофеев

Белорусский государственный университет информатики и радиоэлектроники, ул. П. Бровки, 6, г. Минск 220013, Беларусь

Поступила 20.04.2022
Принята к печати 25.05.2022

При измерении маломощных оптических сигналов, передаваемых в каналах однофотонной связи, приёмные модули должны обеспечивать наибольшую достоверность принятых данных.

В этой связи целесообразно использовать счётчики фотонов, которые являются высокочувствительными, однако характеризуются ошибками регистрации данных. Поэтому цель работы – исследовать влияние интенсивности регистрируемого оптического излучения J_0 при передаче двоичных символов «0» на вероятность регистрации на выходе канала связи символов «1» при наличии символов «0» на его входе $P(1/0)$.

На основе методики уменьшения потерь информации определены статистические распределения смеси числа темновых и сигнальных импульсов на выходе счётчика фотонов при регистрации двоичных символов «0» $P_{st0}(N)$, при которых вероятность $P(1/0)$ минимальная.

Определены вероятности $P(1/0)$ для канала связи, содержащего в качестве приёмного модуля счётчик фотонов при различных значениях напряжения питания лавинного фотоприёмника $U_{\text{пит}}$ и интенсивности оптического сигнала, используемого для передачи двоичных символов «0» J_0.

Экспериментальные результаты показали, что с увеличением интенсивности оптического сигнала J_0 зависимости $P(1/0)$ от J_0 вначале практически не изменяются и сохраняют постоянную величину. Однако при дальнейшем увеличении J_0 имеет место линейно возрастающий характер зависимостей $P(1/0)$ от J_0. Причём при прочих равных параметрах приёма такой характер зависимостей $P(1/0)$ от J_0 начинает проявляться при бóльших интенсивностях оптического сигнала J_0 с увеличением напряжения питания лавинного фотоприёмника.

Ключевые слова: счётчик фотонов, канал однофотонной связи, вероятность ошибочной регистрации двоичных символов.

DOI: 10.21122/2220-9506-2022-13-2-139-146

Адрес для переписки:
Тимофеев А.М.
Белорусский государственный университет информатики и радиоэлектроники,
ул. П. Бровки, 6, г. Минск 220013, Беларусь
e-mail: tamvks@mail.ru

Address for correspondence:
Timofeev A.M.
Belarusian State University of Informatics and Radioelectronics,
Brovki str., 6, Minsk, 220013, Belarus
e-mail: tamvks@mail.ru

Для цитирования:
A.M. Timofeev.
Probability of Erroneous Data Registration in a Single Photon Erasure-Type Communication Channel with a Receiver Based on a Photon Counter.
Приборы и методы измерений.
2022. – Т. 13, № 2. – С. 139–146.
DOI: 10.21122/2220-9506-2022-13-2-139-146

For citation:
A.M. Timofeev.
Probability of Erroneous Data Registration in a Single Photon Erasure-Type Communication Channel with a Receiver Based on a Photon Counter.
Devices and Methods of Measurements.
2022, vol. 13, no. 2, pp. 139–146.
DOI: 10.21122/2220-9506-2022-13-2-139-146

Introduction

When building modern infocommunication systems, it is necessary to ensure sufficiently high reliability of the technical means used for this [1–7]. This is especially important for systems that solve certain problems in the field of information security, for example, by organizing single photon communication channels [8–21]. In such communication channels, each binary bit (symbol) is transmitted using extremely weak optical radiation with an average number of photons no more than several tens. As a result, it becomes possible to ensure absolute secrecy and confidentiality of the transmitted information through the use of a quantum mechanical resource when encoding the transmitted data.

When implementing single-photon communication channels, a number of rather complex technical problems arise, in particular, the problem of registering such a weak optical radiation. In this regard, it is advisable to use photon counters in such communication channels, which have a sufficiently high sensitivity [22–25]. It should be noted that, due to the imperfection of their characteristics, photon counters can lead to errors in data registration, the causes of which are, in particular, non-zero dead time, quantum registration efficiency different from unity, etc. [24].

Quantum detection efficiency is the ratio of the number of optical radiation photons registered by the photon counter to the total number of photons received [24].

The dead time of the photon counter is the time during which the photon counter is not sensitive to the optical radiation incident on it [24].

Known methods for estimating the probabilities of erroneous data recording for single photon communication channels [5, 7] are not applicable to single photon communication channels with erasure. Such communication channels do not require additional communication lines for transmitting and receiving clock pulses, which distinguishes them favorably from other communication channels. At the same time, they are characterized by the presence of errors of two types, one of which is the registration of characters with different names. A mathematical model for the specified communication channel was built in [25], and in [26], theoretical studies were carried out to estimate the probability of erroneous data recording. However, in the literature there is no assessment of the influence of the intensity of the detected optical radiation during the transmission of information in a single photon communication channel with erasure, which contains a photon counter as a receiving module, on the probability of registering unlike symbols.

The object of study was an asynchronous binary asymmetric homogeneous fiber-optic communication channel without memory and with erasure, containing as a receiving module a photon counter based on an avalanche photodetector FD-115L, connected according to the scheme of passive avalanche suppression. The choice of such a communication channel as the object of study is due to the fact that the fiber optic channel is characterized by the highest bandwidth compared to other data transmission media, for example, metal wires, open space, etc. The passive damping scheme has a lower measurement error of the detected radiation due to the absence of forced avalanche breakdown quenching, which distinguishes it favorably from other schemes – active quenching and pulsed *p-n*-junction bias (with gating). Avalanche photodetectors FD-115L are used to operate in the near-IR range and, due to the silicon semiconductor material used in their manufacture, they are characterized by lower noise associated with carrier multiplication and better threshold sensitivity compared to germanium and gallium photodetectors. It should also be noted that silicon avalanche photodetectors make it possible to implement the photon counting mode at room temperatures [24].

The subject of the study was to establish the influence of such parameters of an avalanche photodetector as the intensity of the registered optical radiation and the supply voltage on the probability of registering the symbol “1” at the output of the communication channel in the presence of the symbol “0” at the input of the communication channel.

The purpose of this work was to study the influence of the intensity of the detected optical radiation during the transmission of binary symbols “0” on the probability of registering opposite symbols in a single photon communication channel containing a photon counter as a receiving module.

Description of the procedure for conducting experimental studies

Further reasoning will be based on the fact that the communication channel is created on the basis of transceivers [27]. The mathematical model of this communication channel was built in [25].

To estimate the probability of registering the symbol “1” at the output of the communication channel in the presence of the symbol “0” at its input, we use the formula [25]:

$$P(1/0) = 1 - \sum_{N=0}^{N_2} P_{st0}(N), \tag{1}$$

where N_2 is the upper threshold level of registration, $P_{st0}(N)$ is the statistical distribution of the mixture of the number of dark and signal pulses at the output of the photon counter during the registration of binary symbols “0”.

The upper threshold level of registration is the largest number of pulses registered at the output of the photon counter, at which it is concluded that the symbol “0” has been transmitted. When the registered pulses exceed the number N_2, it is concluded that the symbol “1” has been transmitted [25, 27].

Dark and signal pulses are pulses that appear at the output of the photon counter, respectively, in the absence of an optical signal and as a result of the action of photons of the detected radiation [24].

Using the setup [27], *I* obtained the statistical distributions of the mixture of the number of dark and signal pulses at the output of the photon counter when registering binary symbols “0” $P_{st0}(N)$. To achieve the least loss of information in the studied communication channel, the technique [27] was used, on the basis of which the lower and upper threshold levels of registration were chosen, as well as the statistical distributions of the mixture of the number of dark and signal pulses at the output of the photon counter when registering binary symbols “0” $P_{st0}(N)$.

The lower threshold level of registration is the smallest number of pulses registered at the output of the photon counter, at which it is concluded that the symbol “0” has been transmitted. When registering pulses in an amount less than N_1, a decision is made that the symbol is absent [25, 27].

The parameter [27] was used as a criterion for the implementation of the applied technique:

$$K_P = \frac{1 - \sum_{N=N_1}^{N_2} P_{st0}(N) + \sum_{N=0}^{N_2} P_{st1}(N)}{1 + \sum_{N=N_1}^{N_2} P_{st0}(N) - \sum_{N=0}^{N_2} P_{st1}(N)}. \tag{2}$$

where N_1 is the lower threshold level of registration, $P_{st1}(N)$ is the statistical distribution of the mixture of the number of dark and signal pulses at the output of the photon counter during the registration of binary symbols “1”.

It is also important to note that during the research, both the symbols “0” and the symbols “1” were applied to the input of the experimental setup due to the following features of the studied communication channel. The intensity of optical radiation used to transmit a given binary symbol affects not only the probability of erroneous registration of the symbol of the same name, but also the probability of erroneous registration of another binary symbol [25]. Thus, the intensity J_0 affects not only the probability of erro-neous registration of the symbol “0”, but also the probability of erroneous registration of the symbol “1”, and the intensity J_1 affects not only the probability of erroneous registration of the symbol “1”, but also the probability of erroneous registration of the symbol “0”. Given this, as well as the fact that for the considered communication channel, the information transfer rate is maximum with the equiprobable occurrence of binary symbols “0” and “1” at the input of the communication channel [25, 28], the number of binary symbols “0” supplied to the input of the experimental setup, it is advisable to choose equal to the number of binary characters “1”. Thus, the condition was fulfilled:

$$P_s(0) = P_s(1) = 0.5, \tag{3}$$

where $P_s(0)$ and $P_s(1)$ are the probabilities of occurrence of symbols “0” and “1”, respectively, at the input of the communication channel.

The calculation of the probability $P(1/0)$ was performed for a communication channel containing a photon counter as a receiving module for various values of the supply voltage of the avalanche photodetector U and the intensity of the optical signal used to transmit binary symbols “0” J_0.

Experimental results and their discussion

Figure 1 shows the dependence of the probability of registering the symbol “1” at the output of the communication channel in the presence of the symbol “0” at the input of the communication channel on the intensity of the registered optical radiation used to transmit these symbols.

Devices and Methods of Measurements
2022, vol. 13, no. 2, pp. 139–146
A.M. Timofeev

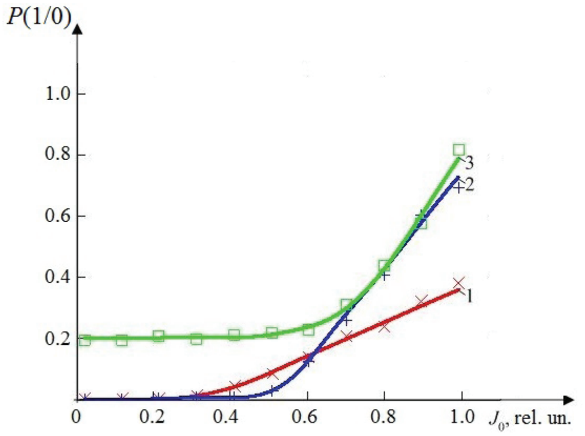

Figure – Dependence of the probability of registering the symbol "1" at the output of the communication channel in the presence of the symbol "0" at the input of the communication channel on the intensity of the optical signal used to transmit these symbols; supply voltage of the FD-115L avalanche photodetector: 1 – 52.48 V; 2 – 52.54 V; 3 – 52.65 V

Note that to implement the photon counting mode, the supply voltages of the avalanche photodetector were chosen near the voltage of its avalanche breakdown, which was determined by the method [29] and amounted to 52.71 V. The intensities of optical radiation J_0 used to transmit binary symbols "0" are normalized to the maximum value from the studied range. All studies were carried out at a temperature of 293 K.

From the results presented in Figure, it can be seen that each of the dependences $P(1/0)$ on J_0 has similar trends for all studied supply voltages of the avalanche photodetector. As the intensity of the optical signal J_0 increases, the dependences $P(1/0)$ on J_0 initially remain virtually unchanged and remain constant. In this section, the probabilities $P(1/0)$ are approximately equal to the lowest values obtained for the corresponding supply voltages of the avalanche photodetector. With a further increase in J_0, a linearly increasing character of the dependences of $P(1/0)$ on J_0 is observed.

The indicated character of the change in the dependences $P(1/0)$ on J_0 with increasing J_0 agrees quite well with the results of mathematical modeling of the considered communication channel, performed in [25] when studying the dependences $P(1/0)$ on n_{s0}, where n_{s0} is the average counting rate signal pulses at the output of the photon counter when transmitting the symbols "0".

Note that the count rate of signal pulses during the transmission of "0" symbols is defined as the number of pulses generated at the output of the receiving module per unit time when exposed to radiation photons corresponding to the registered binary symbols "0" [21, 24]. To estimate the count rate of signal pulses during the transmission of symbols "0", its average value n_{s0} is used [21, 24].

The presence of segments of dependences $P(1/0)$ on J_0 with constant values is explained as follows. At low optical signal intensities J_0, the average count rate of signal pulses at the output of the photon counter during the transmission of symbols "0" n_{s0} is small. Therefore, the probability of registration at the output of the counter of photons of pulses in an amount exceeding the upper threshold level of registration N_2 is also small. As a result, the probabilities of registering the symbol "1" at the output of the communication channel in the presence of the symbol "0" at the input of the communication channel $P(1/0)$ are equal to the smallest values obtained for the corresponding supply voltages of the avalanche photodetector. With an increase in the intensity of the optical signal J_0, the probability of registering pulse photons at the output of the counter in the range from the lower threshold level of registration N_1 to the upper threshold level of registration N_2 increases. At the same time, the probability of registration at the output of the counter of photons of pulses in an amount exceeding the upper threshold level of registration N_2 remains rather low. Thus, the probabilities of registering the symbol "1" at the output of the communication channel in the presence of the symbol "0" at the input of the communication channel $P(1/0)$ are also equal to the smallest values obtained for the corresponding supply voltages of the avalanche photodetector. Therefore, in these J_0 ranges, the probabilities $P(1/0)$ remain the least constant (see Figure).

A further increase in the intensity J_0 with other equal reception parameters leads to an increase in the probability of registration at the output of the counter of photons of pulses in an amount exceeding the upper threshold level of registration N_2. Therefore, the probabilities $P(1/0)$ increase (see Figure). Moreover, with other equal reception parameters, the linearly increasing nature of the dependences $P(1/0)$ on J_0, which was determined by the 5 % excess of the probability $P(1/0)$ from the smallest value of the corresponding dependences, begins to manifest itself at higher intensities of the optical signal J_0 with increasing supply voltage of the avalanche photodetector:

at $J_0 \geq 1.88 \times 10^{-2}$ rel. units for $U = 52.48$ V;

at $J_0 \geq 2.25 \times 10^{-2}$ rel. units for $U = 52.54$ V;

at $J_0 \geq 49.33 \times 10^{-2}$ rel. units for $U = 52.65$ V.

This is explained as follows. With an increase in the supply voltage of the avalanche photodetector, the smallest value of the criterion K_P, which was used in the research, is provided at higher values of the lower threshold level of registration N_1. Therefore, with other receiving parameters being equal, the shift in the statistical distributions of the mixture of the number of dark and signal pulses during the transmission of symbols "0" $P_{st0}(N)$, which results in an increase in the probability $P(1/0)$ [25–27], occurs at higher intensities of the optical signal J_0 with an increase in the supply voltage of the avalanche photodetector.

It is also seen from the presented results that at sufficiently large values of U, the probability $P(1/0)$, corresponding to the section of the dependence of $P(1/0)$ on J_0 with constant values, turns out to be higher than at lower supply voltages of the avalanche photodetector (see Figure). For example, the probabilities $P(1/0)$ corresponding to $J_0 = 21.23 \times 10^{-2}$ rel. units, are respectively:

0.20×10^{-2} at $U = 52.48$ V and 20.89×10^{-2} at $U = 52.65$ V.

This is due to the fact that at low values of the supply voltage of the avalanche photodetector, the dark pulse count rate is low [24], so the probability $P(1/0)$ does not reach large values and is close to zero.

It is important to note that the dark pulse count rate is defined as the number of pulses generated at the output of the receiving module per unit time when there is no detected optical radiation. The greater the number of dark pulses will be formed per unit time, the greater the probability that the symbol "0" and the symbol "1" will be received, respectively, in the absence of the binary symbol "0" and its presence at the input of the communication channel [25–27].

As the supply voltage of the avalanche photodetector increases, the dark pulse count rate nt increases [24]. This leads to the fact that even at the lowest of the studied optical signal intensities J_0, the probability $P(1/0)$ is very high (see Figure).

Conclusion

As applied to an asynchronous binary asymmetric homogeneous fiber optic communication channel without memory and with erasure, containing as a receiving module a photon counter based on an avalanche photodetector FD-115L with switching on according to the passive avalanche suppression scheme. The probability of registering the symbol "1" at the output of the communication channel in the presence of the symbol "0" at its input $P(1/0)$ is made.

Based on the information loss reduction technique, the statistical distributions of the mixture of the number of dark and signal pulses at the output of the photon counter during the registration of binary symbols "0" $P_{st0}(N)$ are determined, at which the probability $P(1/0)$ is minimal.

The dependences of the probability $P(1/0)$ on the intensity of the optical signal J_0 used to transmit binary symbols "0" are established. It is found that, as the intensity of the optical signal J_0 increases, the dependences $P(1/0)$ on J_0 initially remain almost unchanged and retain a constant value. However, with a further increase in J_0, there is a linearly increasing character of the dependences $P(1/0)$ on J_0. Moreover, with other equal reception parameters, such a character of the dependences $P(1/0)$ on J_0 begins to manifest itself at higher intensities of the optical signal J_0 with an increase in the supply voltage of the avalanche photodetector.

The performed experimental results showed that in order to reduce the probability of registering the symbol "1" at the output of the communication channel in the presence of the symbol "0" at its input $P(1/0)$, it is important to select not only the intensity of the used optical radiation J_0, but also the supply voltage of the avalanche photodetector U. This makes it possible to achieve minimal information loss in the studied communication channel.

The results obtained in this work can be used to create quantum cryptographic asynchronous communication systems containing photon counters with extended dead time as receiving modules and characterized by high reliability of received data.

The author of this work considers research aimed at substantiating the choice of an avalanche photodetector used in the construction of a photon counter to be very topical. Such photodetectors can differ both in the structure of the semiconductor regions and in the area of the photosensitive surface. In this regard, in the course of further comprehensive studies, it is planned to determine how these parameters affect the probability of erroneous registration of binary data in relation to an asynchronous binary asymmetric homogeneous single-photon communication channel without memory and with erasure.

References

1. Yiannopoulos K., Sagias N.C., Boucouvalas A.C. On the photon counting error probability and its application in optical wireless communications. *Physical Communication*, 2019, vol. 36, pp. 100756–100764. **DOI:** 10.1016/j.phycom.2019.100756

2. Hu S., Mi L., Zhou T., Chen W. 35.88 attenuation lengths and 3.32 bits/photon underwater optical wireless communication based on photon-counting receiver with 256-PPM. *Optics Express*, 2019, vol. 26, no. 17, pp. 21685–21699. **DOI:** 10.1364/OE.26.021685

3. Bourennane M., Karlsson A., Pena J.C., Mathés M. Single-photon counters in the telecom wavelength region of 1550 nm for quantum information processing. *Journal of Modern Optics*, 2001, vol. 48, no. 13, pp. 1983–1995. **DOI:** 10.1080/09500340110075131

4. Timofeev A.M. [The effect of single photon transmission time on the probability of erroneous registration of asynchronous data of quantum cryptographic communication channels]. *Vestnik TGTU* [Transactions TSTU], 2019, vol. 25, no. 1, pp. 36–46 (in Russian). **DOI:** 10.17277/vestnik.2019.01.pp.036-046

5. Scheglov A.Yu. *Analiz i proektirovanie zaschityi informatsionnyih sistem. Kontrol dostupa k kompyuternyim resursam: metodyi, modeli, tehnicheskie resheniya* [Analysis and design of information systems protection. Control of access to computer resources: methods, models, technical solutions]. St. Petersburg, Professional literature Publ., 2017, 416 p.

6. Vacca J.R. Managing Information Security, 2nd ed. Elsevier Inc., Waltham, 2014, 372 p. **DOI:** 10.1016/C2011-0-08782-3

7. Dmitriev S.A., Slepov N.N. *Volokonno-opticheskaya tehnika: sovremennoe sostoyanie i novyie perspektivyi* [Fiber optic technology: current state and new perspectives], 3rd ed. Moscow, Technosphere Publ., 2010, 608 p.

8. Cova S.D., Ghioni M. Single-photon counting detectors. *IEEE Photonics Journal*, 2011, vol. 3, no. 2, pp. 274–277. **DOI:** 10.1109/JPHOT.2011.2130518

9. Aull B. Geiger-mode avalanche photodiode arrays integrated to alldigital CMOS circuits. *Sensors*, 2016, vol. 16, pp. 495–508. **DOI:** 10.3390/s16040495

10. Jani P., Vamos L., Nemes T. Timing resolution (FWHM) of some photon counting detectors and electronic circuitry. *Meas. Sci. Technol*., 2007, vol. 18, no. 1, pp. 155–160. **DOI:** 10.1088/0957-0233/18/1/019

11. Zadeh I.E., Los J.W.N., Gourgues R.B.M., Steinmetz V., Bulgarini G., Dobrovolskiy S.M., Zwillerb V., Dorenbos S.N. Single-photon detectors combining high efficiency, high detection rates, and ultra-high timing resolution. *APL Photonics*, 2017, vol. 2, pp. 111301-1–111301-7. **DOI:** 10.1063/1.5000001

12. Privitera S., Tudisco S., Lanzano L., Musumeci F., Pluchino A., Scordino A., Campisi A., Cosentino L., Finocchiaro P., Condorelli G., Mazzillo M., Lombardo S., Sciacca E. Single photon avalanche diodes: towards the large bidimensional arrays. *Sensors*, 2008, vol. 8, pp. 4636–4655. **DOI:** 10.3390/s8084636

13. Campajola M., Capua F.D., Fiore D., Sarnelli E., Aloisio A. Proton induced dark count rate degradation in 150-nm CMOS single-photon avalanche diodes. *Nuclear Instruments and Methods in Physics Research. Section A: Accelerators, Spectrometers, Detectors and Associated Equipment*, 2019, vol. 947, pp. 162722–162728. **DOI:** 10.1016/j.nima.2019.162722

14. Stipčević M., Skenderović H., Gracin D. Characterization of a novel avalanche photodiode for single photon detection in VIS-NIR range. *Optics Express*, 2010, vol. 18, pp. 17448–17459. **DOI:** 10.1364/OE.18.017448

15. Nuriyev S., Ahmadov F., Sadygov Z., Akberov R., Ahmadov G., Abbasov I. Performance of a new generation of micropixel avalanche photodiodes with high pixel density and high photon detection efficiency. *Nuclear Instruments and Methods in Physics Research. Section A: Accelerators, Spectrometers, Detectors and Associated Equipment*, 2018, vol. 912, pp. 320–322. **DOI:** 10.1016/j.nima.2017.12.006

16. Stucki D., Ribordy G., Stefanov A., Zbinden H., Rarity J.G., Wall T. Photon counting for quantum key distribution with Peltier cooled InGaAs/InP APDs. *Journal of Modern Optics*, 2001, vol. 48, no. 13, pp. 1967–1981. **DOI:** 10.1080/09500340108240900

17. Castelletto S.A., Degiovanni I.P., Schettini V., Migdall A.L. Reduced deadtime and higher rate photon-counting detection using a multiplexed detector array. *Journal of Modern Optics*, 2007, vol. 54, pp. 337–352. **DOI:** 10.1080/09500340600779579

18. Prochazka I., Blazej J., Kodet J. Single photon detector package with subpicosecond limiting precision and stability. *Nuclear Instruments and Methods in Physics Research. Section A: Accelerators, Spectrometers, Detectors and Associated Equipment*, 2018, vol. 912, pp. 213–216. **DOI:** 10.1016/j.nima.2017.11.044

19. Kalachev A.A. [Components of long-distance quantum communication. Part 1]. *Fotonika* [Photonics], 2017, no. 1, pp. 88–98 (in Russian). **DOI:** 10.22184/1993-7296.2017.61.1.88.98

20. Kalachev A.A. [Components of long-distance quantum communication. Part 2]. *Fotonika* [Photonics], 2017, no. 2, pp. 80–88 (in Russian).
DOI: 10.22184/1993-7296.2017.62.2.80.88

21. Kilin S.Ya. *Kvantovaya kriptografiya: idei i praktika* [Quantum cryptography: ideas and practices]. Minsk, Belarus, Sci. Publ., 2007, 391 p.

22. Zhang J., Itzler M.A., Zbinden H., Pan J.-W. Advances in InGaAs/InP single-photon detector systems for quantum communication. *Light: Science & Applications*, 2015, vol. 4, pp. 1–13. **DOI:** 10.1038/lsa.2015.59

23. Hong Z., Yan Q., Li Z., Zhan T., Wang Y. Photon-counting underwater optical wireless communication for reliable video transmission using joint source-channel coding based on distributed compressive sensing. *Sensors*, 2019, vol. 19, no. 5, pp. 1042–1054.
DOI: 10.3390/s19051042

24. Gulakov I.R., Zenevich A.O. *Fotopriemniki kvantovyih sistem: monografiya* [Photodetectors of quantum systems: monograph]. Minsk, EI HSCC Publ., 2012, 276 p.

25. Timofeev A.M. [Information transfer rate of a single photon communication channel with a receiver module based on a photon counter with a dead time of a prolonged type]. *Trudy BGTU. Ser. 3, Fiziko-matematicheskie nauki i informatika* [Proceedings of BSTU. Iss. 3. Physics and mathematics. Informatics], 2019, no. 2, pp. 79–86 (in Russian).

26. Timofeev A.M. [Estimation of the photons counter lasting dead time influence on the probability of erroneous data registration of quantum-cryptographic communication channels]. *Vestnik svyazi* [Communication bulletin], 2018, no. 1, pp. 56–62 (in Russian).

27. Timofeev A.M. [Assessment of the Influence of Intensity of Optical Signal on the Probability of Erroneous Data Registration in a Single-Photon Communication Channel]. *Informatika* [Informatics], 2021, vol. 18, no. 2, pp. 72–82 (in Russian).
DOI: 10.37661/1816-0301-2021-18-2-72-82

28. Bikkenin R.R., Chesnokov M.N. *Teoriya elektricheskoy svyazi* [The theory of electrical communication]. Moscow, Publ. Cent “Academy”, 2010, 336 p.

29. Gulakov I.R., Kholondyrev S.V. *Metod scheta fotonov v optiko-fizicheskih izmereniyah* [Photon counting method in the optical and physical measurements]. Minsk, University Publ., 1989, 256 p.

Структуроскопия витков пружин после высокотемпературной механической обработки на основе измерения скорости рэлеевских волн

В.В. Муравьев[1,2], Л.В. Гущина[1]

[1]*Ижевский государственный технический университет имени М.Т. Калашникова, ул. Студенческая, 7, г. Ижевск 426069, Россия*

[2]*Удмуртский федеральный исследовательский центр Уральского отделения Российской академии наук, ул. имени Татьяны Барамзиной, 34, г. Ижевск 426067, Россия*

Поступила 01.10.2021
Принята к печати 17.05.2022

Для изготовления рессорных пружин подвижного состава (вагонов, локомотивов, автомобилей) применяют прутки из пружинных сталей. При высокотемпературной механической обработке при навивке пружин и их закалке возникает различие в скоростях охлаждения внутренней и наружной сторон витков пружины, что приводит к различию в структурном состоянии и сказывается на долговечности пружин. Цель работы – исследование влияния структурных изменений в наружной и внутренней поверхности витков пружин рессорной стали после операций навивки и высокотемпературной механической обработки на измеряемые характеристики рэлеевских акустических волн.

Исследованы скорости распространения рэлеевских волн в рессорно-пружинной стали 60С2А после операций навивки и высокотемпературной механической обработки. Для исследований использованы теневой метод и метод автоциркуляции с пьезоэлектрическими преобразователями ЦТС-19 частотой 5 МГц с конструкцией специального блока. Преобразователи обеспечивают ввод и приём рэлеевской волны по внутренней и наружной образующей поверхности пружины. Показано, что метод сравнения результатов измерения скорости рэлеевских волн на фиксированной базе по образующей витка на внутренней и внешней поверхностях пружины чувствителен к нарушениям в структуре материала и появлениям дефектов. Найдена однозначная связь структурных состояний на внешней и внутренней стороне пружины со скоростью рэлеевской волны.

В результате проведённых измерений сделан вывод о значимой чувствительности рэлеевских волн к структурному состоянию исследуемой стали. Обнаружен рост скорости волны на внутренней поверхности витка в зоне контакта с оправкой относительно внешней стороны витка, сигнализирующий о неполной закалке стали в этой зоне в процессе высокотемпературной механической обработки. Относительная разница скоростей в разных образцах пружин составляет приблизительно до 1 % (≈ 30 м/с), что является значительной величиной для оценки качества высокотемпературной механической обработки.

Ключевые слова: скорость рэлеевских волн, теневой метод и метод автоциркуляции, рессорно-пружинная сталь.

DOI: 10.21122/2220-9506-2022-13-2-147-154

Адрес для переписки:
Гущина Л.В.
Ижевский государственный технический университет имени М.Т. Калашникова,
ул. Студенческая, 7, г. Ижевск 426069, Россия
e-mail: pmkk@istu.ru

Address for correspondence:
Gushchina L.V.
Kalashnikov Izhevsk State Technical University,
Studencheskaya str., 7, Izhevsk 426069,
Udmurt Republic, Russia
e-mail: pmkk@istu.ru

Для цитирования:
В.В. Муравьев, Л.В. Гущина.
Структуроскопия витков пружин после высокотемпературной механической обработки на основе измерения скорости рэлеевских волн.
Приборы и методы измерений.
2022. – Т. 13, № 2. – С. 147–154.
DOI: 10.21122/2220-9506-2022-13-2-147-154

For citation:
V.V. Murav'ev, L.V. Gushchina.
[Structuroscopy of Coils after High-Temperature Mechanical Treatment on the Basis of Measurements of Rayleigh Waves Velocity].
Devices and Methods of Measurements.
2022, vol. 13, no. 2, pp. 147–154 (in Russian).
DOI: 10.21122/2220-9506-2022-13-2-147-154

Structuroscopy of Coils after High-Temperature Mechanical Treatment on the Basis of Measurements of Rayleigh Waves Velocity

V.V. Murav'ev[1,2], **L.V. Gushchina**[1]

[1]*Kalashnikov Izhevsk State Technical University, Studencheskaya str., 7, Izhevsk 426069, Russia*

[2]*Udmurt Federal Research Center, Ural Branch of the Russian Academy of Sciences, Tatiana Baramzinoy str., 34, Izhevsk 426067, Russia*

Received 01.10.2021
Accepted for publication 17.05.2022

Abstract

For the manufacture of spring springs of rolling stock (wagons, locomotives, cars), bars made of spring steels are used. With high-temperature machining, when winding springs and quenching them, there is a difference in the cooling rates of the inner and outer sides of the spring coils, which leads to a difference in the structural state and affects the durability of the springs. The aim of the work is to study the effect of structural changes in the outer and inner surfaces of spring steel coils after winding and high–temperature machining operations on the measured characteristics of Rayleigh acoustic waves.

The propagation velocities of Rayleigh waves in spring-spring steel 60C2A after winding and high-temperature machining operations are investigated. The shadow method and the autocirculation method with piezoelectric converters CTS-19 with a frequency of 5 MHz with a special block design were used for research. The converters provide input and reception of the Rayleigh wave along the inner and outer forming surface of the spring. It is shown that the method of comparing the results of measuring the velocity of Rayleigh waves on a fixed base by the coil generator on the inner and outer surfaces of the spring is sensitive to disturbances in the structure of the material and the appearance of defects. An unambiguous relationship of the structural states on the outer and inner sides of the spring with the velocity of the Rayleigh wave is found.

As a result of the measurements, a conclusion was made about the significant sensitivity of Rayleigh waves to the structural state of the steel under study. An increase in the wave velocity was detected on the inner surface of the coil in the contact zone with the mandrel relative to the outer side of the coil, signaling incomplete hardening of steel in this zone during high-temperature machining. The relative speed difference in different spring samples is approximately up to 1 % (≈ 30 m/s), which is a significant value for assessing the quality of high-temperature machining.

Keywords: Rayleigh wave velocity, through transmission method and auto-circulation method, spring steel.

DOI: 10.21122/2220-9506-2022-13-2-147-154

Адрес для переписки:
Гущина Л.В.
Ижевский государственный технический университет имени М.Т. Калашникова,
ул. Студенческая, 7, г. Ижевск 426069, Россия
e-mail: pmkk@istu.ru

Address for correspondence:
Gushchina L.V.
Kalashnikov Izhevsk State Technical University,
Studencheskaya str., 7, Izhevsk 426069,
Udmurt Republic, Russia
e-mail: pmkk@istu.ru

Для цитирования:
В.В. Муравьев, Л.В. Гущина.
Структуроскопия витков пружин после высокотемпературной механической обработки на основе измерения скорости рэлеевских волн.
Приборы и методы измерений.
2022. – Т. 13, № 2. – С. 147–154.
DOI: 10.21122/2220-9506-2022-13-2-147-154

For citation:
V.V. Murav'ev, L.V. Gushchina.
[Structuroscopy of Coils after High-Temperature Mechanical Treatment on the Basis of Measurements of Rayleigh Waves Velocity].
Devices and Methods of Measurements.
2022, vol. 13, no. 2, pp. 147–154 (in Russian).
DOI: 10.21122/2220-9506-2022-13-2-147-154

Введение

Рессорные элементы тележки грузовых и пассажирских вагонов в процессе эксплуатации подвержены воздействию нагрузок, отличающихся значениями, уровнем, характером и методом действия. Наиболее опасным явлением в рессорных пружинах является усталость металла, особенно существенно проявляющаяся в местах концентрации напряжений, в качестве которых могут быть структурные несовершенства [1–3]. Для изготовления рессорных пружин подвижного состава (вагонов, локомотивов, автомобилей) применяют прутки из пружинных сталей 60С2А, которые подвергаются таким воздействиям, как обработка металлов давлением, высокотемпературная механическая обработка (ВТМО), термическая обработка. В процессе ВТМО при навивке пружин и их закалке возникает различие в скоростях охлаждения внутренней и наружной сторон витков пружины, что приводит к различию в структурном состоянии и сказывается на долговечности пружин [4, 5].

Проблема поиска новых подходов к исследованию отклонений структурного состояния различных частей термически обрабатываемых металлоизделий и после различных внешних энергетических воздействий – одна из важнейших в металловедении [6–8]. Получаемые структурные состояния и физико-механические свойства материалов выгодно оценивать ультразвуковыми методами [9–14]. Основным информативным параметром при выполнении акустической структуроскопии является скорость распространения волн. Большинство методик акустической структуроскопии базируется на методах с использованием контактных пьезоэлектрических преобразователей, при этом предъявляются высокие требования к геометрическим размерам, плоскопараллельности поверхности ввода и отражающей поверхности, чистоте обработки поверхности, качеству контакта и др. Недостаточно высокая точность методик, а также необходимость использования эталонных образцов ограничивает их применение. Поэтому исследование возможности оценки структурного состояния материала на криволинейной поверхности пружин, основанное на измерении скорости рэлеевских акустических волн, является актуальной задачей.

Используемые подходы. Методика эксперимента

Различие структурных состояний на внутренней и внешней поверхностях витка пружины, возникающих при производстве пружин в процессе ВТМО, не выявляется штатными методами. Однако они существенно сокращают долговечность пружин. Из рисунка 1 видно, что в месте касания горячей заготовки пружины с оправкой, в связи с уменьшением скорости охлаждения при закалке ниже критической, возникает зона с недостаточным теплоотводом при взаимодействии с закалочной средой, которая не проникает в эту зону. Вследствие чего, после операции закалки не реализуется высокопрочная структура и образуется зона неполной закалки, характеризующаяся продуктами немартенситного распада с наличием зёрен феррита и перлита (рисунок 2*a*) в отличие от полной закалки с мартенситным превращением (рисунок 2*b*).

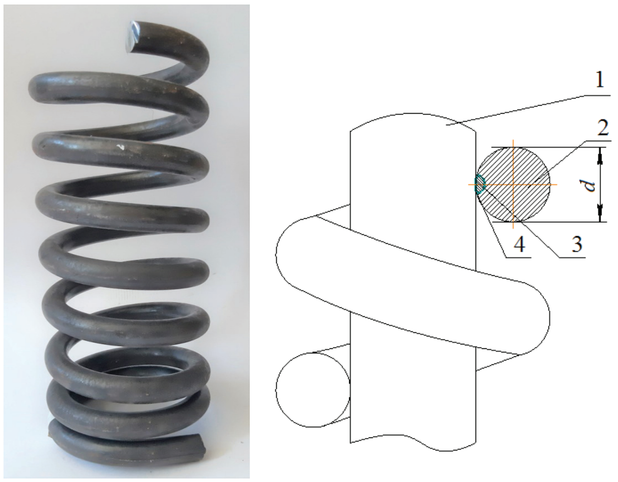

a *b*

Рисунок 1 – Внешний вид пружины (*a*) и навивка её на оправку при высокотемпературной механической обработке (*b*): 1 – оправка; 2 – сечение витка; 3 – зона с пониженной температурой; 4 – линии контакта – зона неполной закалки

Figure 1 – Spring appearance (*a*) and its winding on the mandrel at high temperature mechanical machining (*b*): 1 – mandrel; 2 – cross – section of the coil; 3 – zone with low temperature; 4 – contact lines – zone of incomplete hardening

Известно, что скорость распространения ультразвуковых волн в сплавах связана с их структурой [15]. Наиболее выгодным вариантом для разработки методики структуроскопии является использование волн Рэлея, распространяющихся на строго фиксированной базе. С целью исследования структурного состояния пружин тележки железнодорожного вагона были сконструированы 4 блока рэлеевских преобразователей для пружин разного диаметра (рисунок 3), соответственно по два блока для установки на наружной и внутренней поверхностях витка пружины. В конструкции преобразователей использовались пьезопластины ЦТС-19 частотой 5 МГц.

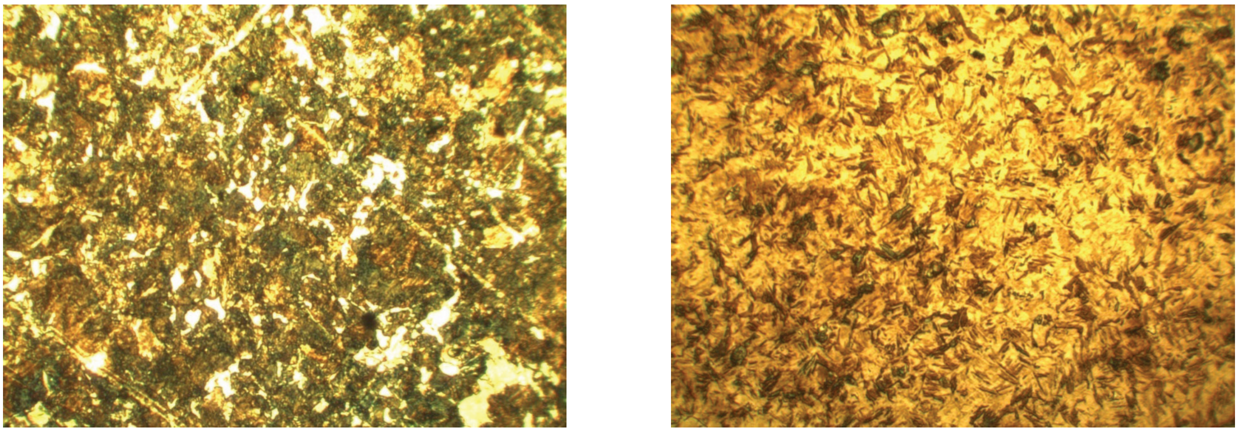

a *b*

Рисунок 2 – Микроструктура вблизи внутренней (*a*) и внешней (*b*) частей витка пружины при увеличении 1000

Figure 2 – Microstructure near the inner (*a*) and outer parts (*b*) part of the spring coil at 1000 magnification

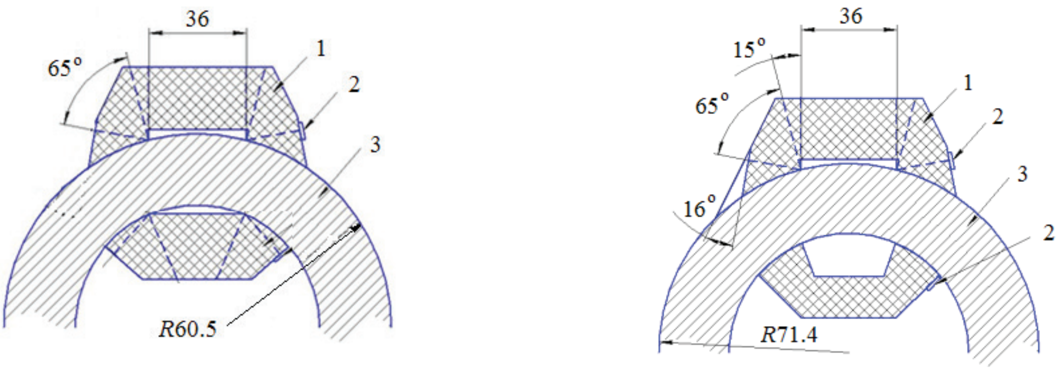

a *b*

Рисунок 3 – Рэлеевские преобразователи для контроля структурного состояния пружин радиусом 60,5 мм (*a*) и 71,4 мм (*b*): 1 – корпус преобразователя из оргстекла; 2 – пьезоэлемент; 3 – пружина

Figure 3 – Rayleigh transducers for the control of the structural state of springs with a radius of 60.5 mm (*a*) and of 71.4 mm (*b*): 1 – plexiglass transducer housing; 2 – piezoelectric element; 3 – spring

Преобразователи, показанные на рисунке 3, обеспечивают ввод рэлеевской волны по внутренней и наружной образующей поверхности пружины. Для точности контроля крайне важно, чтобы расстояние, пройденное рэлеевской волной на внешней стороне витка пружины и на внутренней, было одинаково. Поэтому расстояние между точками ввода и выхода рассчитали теоретически и проверили экспериментально, что составило для внешнего и внутреннего преобразователей 20 и 36 мм соответственно.

Для исследования образцов пружин были использованы структуроскоп ИСП-12 (ультразвуковой индикатор структурных превращений) и ультразвуковой дефектоскоп DIO 1000.

Схема контроля с помощью структуроскопа ИСП-12 представлена на рисунке 4.

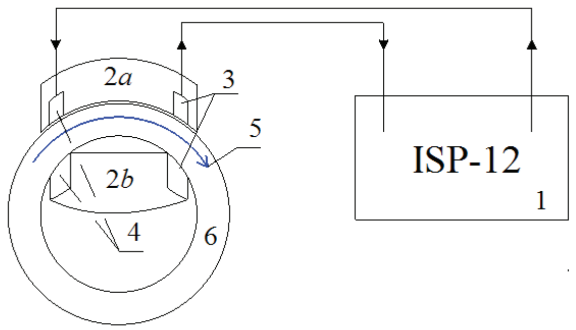

Рисунок 4 – Схема установки блока преобразователей на витке пружины: 1 – структуроскоп ИСП-12; 2*a* – преобразователь для внешней части витка пружины; 2*b* – преобразователь для внутренней части витка пружины; 3 и 4 – излучающие и приёмные пьезоэлементы; 5 – путь рэлеевской волны; 6 – виток пружины

Figure 4 – Plant layout of the transducers unit on the spring coil: 1 – structuroscopy ISP-12; 2*a* – transducer for the exterior part of spring; 2*b* – transducer for the internal part of spring; 3 and 4 – radiating and receiving piezoelectric elements; 5 – Rayleigh wave way; 6 – spring coil

В основе работы структуроскопа ИСП-12 лежит метод автоциркуляции импульсов, суть которого заключается в том, что генератор импульсов, возбуждающий пьезоэлектрический преобразователь, синхронизируется импульсами, прошедшими через анализируемую среду. Прошедший по образцу ультразвуковой импульс, принимается приёмным пьезопреобразователем и преобразуется в электрический сигнал, формирующий следующий вводимый в образец импульс. При этом частота следования импульсов зависит от времени пробега импульсом расстояния между пьезопреобразователями, следовательно (при неизменном расстоянии между пьезопреобразователями), от скорости распространения ультразвука в образце.

Измерения времени распространения рэлеевской волны с помощью дефектоскопа DIO 1000 проводились следующим образом: ультразвуковой импульс возбуждался и принимался непосредственно дефектоскопом, затем по регистрируемым импульсам рассчитывался интервал времени между излучением и приёмом волны, проходящей по дуге окружности пружины от излучающего к приёмному преобразователю (рисунок 5).

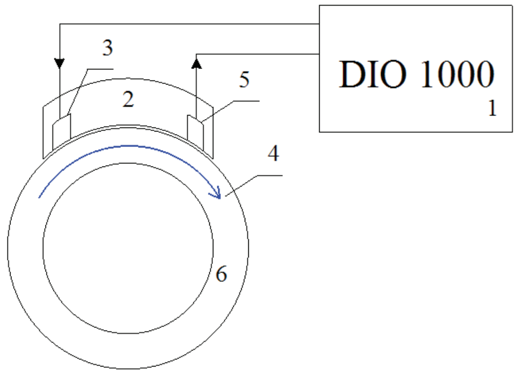

Рисунок 5 – Схема установки блока преобразователей на витке пружины: 1 – дефектоскоп DIO 1000; 2 – блок преобразователей; 3 и 5 – излучающие и приёмные пьезоэлементы; 4 – путь рэлеевской волны; 6 – виток пружины

Figure 5 – Plant layout of the transducers unit on the spring coil: 1 – flaw detector DIO 1000; 2 – transducers unit; 3 и 5 – radiating and receiving piezoelectric elements; 4 – Rayleigh wave way; 6 – spring coil

Результаты исследования

Исследования проводились на 4-х образцах-вырезках пружин внешним диаметром 143 мм и на 3-х – диаметром 121 мм, изготовленных по технологии ВТМО в разное время из разных партий прутков. Пружины изготовлены из стали марки 65С2Г, поверхность которых имеет шероховатость Rz40.

Химический анализ металла образцов пружины № 1 диаметром 121 мм, виток Ø 15 мм, № 2 диаметром 143 мм, виток Ø 20 мм и № 3 диаметром 121 мм, виток Ø 18 мм показал, что химические составы образцов соответствуют требованиям ГОСТ 14959-2016.

Отклонение по твёрдости на торце витка в разных точках по диаметру с шагом 1 мм от внутренней поверхности до наружной составило 1 HRC. Твёрдость измерялась на приборе ПМТ-3. Образец диаметром 143 мм: 56–57 HRC; образцы диаметром 121 мм: 46–47 HRC.

Результаты исследования относительного изменения частоты автоциркуляции для образцов пружин диаметром 143 и 121 мм структуроскопом ИСП-12 представлены в таблице. В образце № 1 пружины диаметром 143 мм относительное изменение частоты существенно меньше, чем на образцах № 2–4, что свидетельствует о менее значимых различиях в структуре на внутренней и внешней стороне витка. Для пружин диаметром 121 мм также наблюдаются различия по относительному изменению частоты в разных образцах. Следовательно, можно заключить, что операции ВТМО, проводимые в разное время и на разных партиях, могут отличаться по качеству структур на внутренней стороне витка.

Наблюдаемое различие относительного изменения частоты автоциркуляции от внутренней до внешней стороны пружины во всех 7 образцах свидетельствует о повышении скорости распространения рэлеевской волны на внутренней части пружины, что означает разницу структурных состояний внешней и внутренней частей пружины. Согласно [12, 13], увеличение скорости соответствует увеличению равновесности структурного состояния, в отличие от закалочных структур.

Регистрируемое дефектоскопом DIO 1000 время прохождения сигнала по фиксированному пути, показывает снижение времени по внутренней стороне пружины, что означает рост скорости волны относительно внешней стороны и сигнализирует о неполной закалке стали в процессе ВТМО либо о самоотпуске. Средняя погрешность измерения времени прохождения импульса составила 0,01 мкс. Максимальная погрешность составляет не более 0,03 мкс.

Погрешность измерений частоты автоциркуляции колеблется для разных образцов от 1 до 5 Гц. Основными факторами, влияющими на погрешность, являются различия в шероховатости поверхности и отклонения установки преобразователя по образующей вследствие кривизны пружины, а также различия в условиях ввода и приёма волн для внешнего и внутреннего преобразователя. Относительная погрешность измерений составила 0,01 %, что соответствует исследованиям, изложенным в [16].

На основе результатов измерений частоты автоциркуляции структуроскопом ИСП-12 рассчитана скорость рэлеевских волн. Значение частоты f_a представляет собой величину, обратную времени t_a прохождения ультразвуковой волны от излучающей пьезопластины до приёмной. Время t_a складывается из двух времён: времени задержки ультразвуковой волны в призме преобразователя t_p и времени распространения рэлеевской волны в образце пружины t_R:

$$f_a = \frac{1}{t_a};$$

$$t_a = 2t_p + t_R;$$

$$t_p = \frac{l_p}{C_p};$$

$$C_R = \frac{l_s f_a C_p}{C_p - 2l_p f_a}.$$

Таблица / Table

Относительные изменения частоты автоциркуляции ($\Delta f_a/f_a$) и скорости ($\Delta C_R/C_R$) в исследованных образцах с использованием ИСП-12 и относительные изменения времени прохождения сигнала ($\Delta t/t$) и скорости ($\Delta C_R/C_R$), зарегистрированных дефектоскопом DIO 1000

Relative changes in the frequency of autocirculation ($\Delta f_a/f_a$) and velocity ($\Delta C_R/C_R$) in the studied samples using ISP-12 and relative changes in the signal transit time ($\Delta t/t$) and velocity ($\Delta C_R/C_R$) recorded by the DIO 1000 flaw detector

№	D, mm	ISP-12		DIO 1000	
		$\Delta f_a/f_a$	$\Delta C_R/C_R$	$\Delta t/t$	$\Delta C_R/C_R$
1	143	0.0032	0.0055	0.0018	0.0041
2		0.0041	0.0092	0.0030	0.0066
3		0.0043	0.0095	0.0033	0.0049
4		0.0038	0.0089	0.0030	0.0074
5	121	0.0046	0.0103	0.0033	0.0090
6		0.0044	0.0096	0.0025	0.0090

Скорость продольной волны в призме преобразователя, изготовленного из оргстекла, C_p = 2670 м/с. Расстояние, проходимое волной в призме l_p = 0,02 м. Расстояние, проходимое волной в образце пружины, равное базе преобразователя, l_s = 0,036 м. Относительное изменение скорости рэлеевских волн по результатам измерения частоты автоциркуляции структуроскопом ИСП-12 по внутренней и внешней стороне пружин отражены в таблице, также в таблице представлены относительные изменения скорости рэлеевских волн, рассчитанных по результатам измерений времени прохождения импульса с помощью DIO 1000.

Из результатов видно, что наблюдается уменьшение скорости рэлеевской волны в наружной части витка пружины относительно внутренней. По результатам исследований можно отметить, что метод измерения скорости ультразвука чувствителен к нарушениям в структуре материала и появлениям дефектов.

Заключение

Показано, что метод сравнения результатов измерения скорости рэлеевских волн на фиксированной базе по образующей витка на внутренней и внешней поверхностях пружины чувствителен к нарушениям в структуре материала и появлениям дефектов. Различие скорости рэлеевских волн свидетельствует о различии структурного состояния металла.

Обнаружен рост скорости волны на внутренней поверхности витка в зоне контакта с оправкой относительно внешней стороны витка, сигнализирующий о неполной закалке стали 65С2Г в этой зоне в процессе высокотемпературной механической обработки. Относительная разница скоростей в разных образцах пружин составляет до 1 % (≈ 30 м/с), что является значительной величиной для оценки качества высокотемпературной механической обработки.

Благодарности

Исследование выполнено за счёт гранта РФФИ Бел-а (проект № 20-58-0015) с использованием УНУ «Информационно-измерительный комплекс для исследования акустических свойств материалов и изделий».

Acknowledgments

The research was carried out at the expense of the RFBR Bel-a grant (project no. 20-58-0015) using the UNU "Information measurement system for the research of acoustic properties of materials and products".

Список использованных источников

1. *Орлова А.М.* Подходы к оценке напряженно-деформированного состояния пружин рессорного подвешивания грузовых вагонов / А.М. Орлова [и др.] // Известия Петербургского университета путей сообщения. – 2020. – Т. 17, № 2. – С. 221–232.
DOI: 10.20295/1815-588X-2020-2-221-232

2. *Сунь Х.* Анализ остаточных напряжений в винтовых цилиндрических пружинах при высокой температуре / Х. Сунь, В.Л. Данилов // Наука и образование: научное издание МГТУ им. Н.Э. Баумана. – 2015. – № 6. – С. 384–396.
DOI: 10.7463/0615.0778617

3. *Del Llano-Vizcaya L., Rubio-Gonzales C., Mesmacqueb G., Banderas-Hernándeza A.* Stress relief effect on fatigue and relaxation of compression springs // Materials and Design, 2007, vol. 28, no. 4, pp. 1130–1134.
DOI: 10.1016/j.matdes.2006.01.033

4. *Ulrike Karr, Yusuke Sandaiji, Ryota Tanegashima, Shogo Murakami, Bernd Schönbauer, Michael Fitzka, Herwig Mayer.* Inclusion initiated fracture in spring steel under axial and torsion very high cycle fatigue loading at different load ratios // International Journal of Fatigue, 2020, vol. 134, p. 105525.
DOI: 10.1016/j.ijfatigue.2020.105525

5. *Лавриненко Ю.А.* Исследование напряженно-деформированного состояния при навивке пружин под воздействием комбинированного нагружения / Ю.А. Лавриненко // Заготовительные производства в машиностроении. – 2017. – Т. 15. – № 9. – С. 399–404.

6. *Околович Г.А.* Термическая обработка пружин железнодорожного транспорта / Г.А. Околович, Д.В. Кураков, Т.Г. Шарикова, С.А. Чекалина // Ползуновский альманах. – 2015. – № 2. – С. 141–145.

7. *Титов А.В.* Влияние режимов термической обработки на микроструктуру пружин ответственного назначения из стали 60с2а и титанового сплава ВТ16 / А.В. Титов // Металлообработка. – 2015. – № 5 (89). – С. 43–49.

8. *Орлова А.М.* Анализ методик расчета горизонтальной жесткости пружин рессорного подвешивания грузовых вагонов / А.М. Орлова [и др.] // Известия Петербургского университета путей сообщения. – 2019. – Т. 16. – № 2. – С. 191–201.
DOI: 10.20295/1815-588X-2019-2-191-201

9. *Григорьев В.М.* Анализ разрушений пружин пассажирского вагона / В.М. Григорьев, В.М. Макиенко, П.В. Соколов // Транспорт Азиатско-Тихоокеанского региона. – 2015. – № 1 (2–3). – С. 94–97.

10. *Марков А.М.* Пружины рессорного комплекта тележек грузовых вагонов / А.М. Марков [и др.] // Актуальные проблемы в машиностроении. – 2016. – № 3. – С. 194–198.

11. *Злобин Д.В.* Особенности построения аппаратуры электромагнитно-акустической дефектоскопии прeuткового проката с использованием стержневых волн / Д.В. Злобин, О.В. Муравьёва // Вестник Ижевского государственного технического университета. – 2012. – № 4. – С. 99–104.

12. *Муравьева О.В.* Влияние глубины залегания дефекта на параметры многократно-теневого

электромагнитно-акустического метода контроля прутков / О.В. Муравьева, М.Ю. Соков // Вестник ИжГТУ им. М.Т. Калашникова. – 2016. – Т. 19. – № 3. – С. 46–50.

13. *Петров К.В.* Влияние конструктивных особенностей проходного электромагнитно-акустического преобразователя на результаты контроля цилиндрических объектов / К.В. Петров, М.Ю. Соков, О.В. Муравьева // Вестник ИжГТУ им. М.Т. Калашникова. – 2018. – Т. 21. – № 2. – С. 135–146.
DOI: 10.22213/2413-1172-2018-2-135-146

14. *Баев А.Р.* Ультразвуковой метод анализа поверхностного упрочнения металлических изделий / А.Р. Баев, А.Л. Майоров, М.А. Тищенко // Литье и металлургия. – 2010. – № 4. – С. 267–271.

15. *Волкова Л.В.* Использование многократного зеркально-теневого метода при ультразвуковом контроле пера подошвы рельса / Л.В. Волкова, А.В. Платунов // Вестник ИжГТУ им. М.Т. Калашникова. – 2019. – Т. 22. – № 4. – С. 38–45.
DOI: 10.22213/2413-1172-2019-4-38-45

16. *Муравьев В.В.* Скорость звука и структура сталей и сплавов / В.В. Муравьев, Л.Б. Зуев, К.Л. Комаров // Новосибирск: Наука, 1996. – 184 с.

References

1. Orlova A.M., Rudakova E.A., Shevchenko D.V., Gusev A.V., Shalpegin G.S. [Approaches to assessing the stress-strain state of freight car spring suspension coils]. *Izvestiya peterburgskogo universiteta putej soobshcheniya*, 2020, vol. 17, no. 2, pp. 221–232 (in Russian).
DOI: 10.20295/1815-588X-2020-2-221-232

2. Sun' H., Danilov V.L. [Analysis of residual stres-ses in helical cylindrical springs at high temperature]. *Nauka i obrazovanie: nauchnoe izdanie MGTU im. N.E. Baumana* [Science and Education of Bauman MSTU], 2015, no. 6, pp. 384–396 (in Russian).
DOI: 10.7463/0615.0778617

3. Del Llano-Vizcaya L., Rubio-Gonzales C., Mesmacqueb G., Banderas-Hernándeza A. Stress relief effect on fatigue and relaxation of compression springs. *Materials and Design*, 2007, vol. 28, no. 4, pp. 1130–1134.
DOI: 10.1016/j.matdes.2006.01.033

4. Ulrike Karr, Yusuke Sandaiji, Ryota Tanegashima, Shogo Murakami, Bernd Schönbauer, Michael Fitzka, Herwig Mayer. Inclusion initiated fracture in spring steel under axial and torsion very high cycle fatigue loading at different load ratios. *International Journal of Fatigue*, 2020, vol. 134, p. 105525.
DOI: 10.1016/j.ijfatigue.2020.105525

5. Lavrinenko YU.A. [Study of strain-stress state during springs coiling by combination loading]. *Zagotovitel'nye proizvodstva v mashinostroenii*, 2017, vol. 15, no. 9, pp. 399–404 (in Russian).

6. Okolovich G.A., Kurakov D.V., Sharikova T.G., Chekalina S.A. [Heat treatment of springs of railway transport]. *Polzunovskij al'manah*, 2015, no. 2, pp. 141–145 (in Russian).

7. Titov A.V. [The effect of heat treatment on the microstructure of springs for critical applications SA of steel and titanium alloy VT16]. *Metalloobrabotka*, 2015, no. 5(89), pp. 43–49 (in Russian).

8. Orlova A.M., Rudakova E.A., Shevchenko D.V., Gusev A.V., Popovich C.I., Savushkin R.A. [Analysis of design procedures for horizontal spring stiffness of bogie suspension of freight cars]. *Izvestiya peterburgskogo universiteta putej soobshcheniya*, 2019, vol. 16, no. 2, pp. 191–201 (in Russian).
DOI: 10.20295/1815-588X-2019-2-191-201

9. Grigor'ev V.M., Makienko V.M., Sokolov P.V. [Analysis of the springs destruction of the passenger carriage]. *Transport Aziatsko-Tihookeanskogo regiona*, 2015, no. 1(2–3), pp. 94–97 (in Russian).

10. Markov A.M., Gabets A.V., Gabets D.A., Gavrikov D.V. [Coil spring group for freight-car truck]. *Aktual'nye problemy v mashinostroenii* [Actual problems in machine building], 2016, no. 3, pp. 194–198 (in Russian).

11. Zlobin D.V., Murav'eva O.V. [Development features of electromagnetic acoustic defectoscopy equipment for bar iron using rod waves]. *Vestnik IzhGTU imeni M.T. Kalashnikova*, 2012, no. 4, pp. 99–104 (in Russian).

12. Murav'eva O.V., Sokov M.YU. [Influence of the defect depth on the parameters of electromagnetic-acoustic multiple-shadow method of the rod testing]. *Vestnik IzhGTU imeni M.T. Kalashnikova*, 2016, vol. 19, no. 3, pp. 46–50 (in Russian).

13. Petrov K.V., Sokov M.YU., Murav'eva O.V. [The effect of electromagnetic acoustic transducer design features on results of cylinder object testing]. *Vestnik IzhGTU imeni M.T. Kalashnikova*, 2018, vol. 21, no. 2, pp. 135–146 (in Russian).
DOI: 10.22213/2413-1172-2018-2-135-146

14. Baev A.R., Majorov A.L., Tishchenko M.A. Ultrasonic methods of analysis of the metal articles surface hardening. *Foundry production and metallurgy*, 2010, no. 4, pp. 267–271 (in Russian).

15. Volkova L.V., Platunov A.V. [Rail base point inspection using the mirror through transmission testing technique on multiple reflections]. *Vestnik IzhGTU imeni M.T. Kalashnikova*, 2019, vol. 22, no. 4, pp. 38–45 (in Russian). **DOI:** 10.22213/2413-1172-2019-4-38-45

16. Murav'ev V.V., Zuev L.B., Komarov K.L. [Sound Speed and Structure of Steels and Alloys]. Novosibirsk, Nauka Publ., 1996, 184 p.

ПРАВИЛА ОФОРМЛЕНИЯ СТАТЕЙ

Статьи, направленные в редакцию журнала, должны удовлетворять требованиям «Инструкции о порядке оформления квалификационной научной работы (диссертации)…», утвержденной Постановлением ВАК РБ от 28.02.2014 г. № 3

1. Материал статьи должен соответствовать профилю журнала и излагаться предельно ясно.

2. Статья представляется на русском или английском языке и публикуется на языке представления.

3. Поступившие в редакцию статьи проходят двойное полуслепое рецензирование. Основные критерии целесообразности опубликования – актуальность тематики, информативность, научная новизна.

4. Статья представляется в распечатанном и в электронном виде в формате текстового редактора Word for Windows, набор – сплошным текстом (без деления на колонки). Объём статьи не должен превышать 14 страниц, включая текст (шрифт Times New Roman, размер 12 п., интервал 1,5), таблицы, графический материал, всю необходимую информацию на английском языке.

5. На первой странице статьи указываются: название статьи, фамилии авторов (фамилия автора, с которым следует вести переписку, отмечается звёздочкой и указывается его адрес электронной почты), названия и почтовые адреса организаций (улица, номер дома, индекс, город, страна), в которых работают авторы, на русском и английском языках. Статья включает: аннотацию (в пределах 200–250 слов); ключевые слова (не более 5); введение, в котором делается краткий обзор сделанного в мире и конкретно формулируется цель работы; основную часть; заключение, в котором в сжатом виде сформулированы основные полученные результаты с указанием их новизны, преимуществ и возможностей применения; список использованных источников. Аннотация, ключевые слова, список использованных источников представляются на русском и английском языках.

6. Аннотация должна быть информативной (содержать «выжимку» из всех разделов статьи – введения с указанием цели работы, методики, основной части и заключения).

7. Графический материал должен быть контрастным и чётким. Необходимо придерживаться единообразия техники исполнения однотипных иллюстраций. Рисунок должен располагаться после абзаца, содержащего ссылку на него. Не допускается размещение рисунков в конце подраздела и статьи. Изобразительный материал вставляется в текст статьи, а также даётся в виде отдельных файлов **(формат tif, jpg, разрешение не менее 300 dpi)**. Текст на рисунках набирается основной гарнитурой; размер кегля соизмерим с размером рисунка (желательно 8 пунктов). Все рисунки нумеруются и сопровождаются подрисуночными подписями. Фрагменты рисунка обозначаются строчными курсивными латинскими буквами – «*a*», «*b*» и т. д. Надписи на рисунках и подписи к рисункам даются на русском и английском языках. Все сокращения и обозначения должны быть расшифрованы в подрисуночной подписи. Рисунки желательно предоставлять в цвете. На рисунках должны быть указаны оси с обозначением приводимых величин и масштабов. На графиках не нужно давать координатную сетку, если это не осциллограмма. Во всех случаях на рисунках должен быть приведён масштаб.

8. У графиков, имеющих числовые значения по осям, рамки должны быть открыты, а засечки направлены внутрь рамки. На рисунках, представляющих собой графики зависимостей, не следует делать размерную сетку, следует дать лишь засечки на осях, причем все засечки должны быть оцифрованы. Если оси на рисунках оцифрованы, то они завершаются на позиции очередной засечки, где засечка не ставится, а вместо числовых значений даются обозначения переменной и единица измерения. Если оси не оцифровываются, то они завершаются стрелками, рядом с которыми даются обозначения переменных без единиц измерения.

9. Полутоновые фотографии приборов или их частей представляются при публикации в тех случаях, когда они несут существенную информацию, которую нельзя выразить иным способом. Фотографии должны быть высококачественными, контрастными, с хорошо различимыми деталями.

10. Иллюстрации (графики, диаграммы, схемы, чертежи), рисованные средствами MS Office, должны быть контрастными и чёткими. Недопустимо нанесение средствами MS Word каких-либо элементов поверх вставленного в файл рукописи рисунка (стрелки, подписи) ввиду большого риска их потери на этапах редактирования и вёрстки. Иллюстрации должны иметь размеры, соответствующие их информативности: 8–8,5 см (на одну колонку), 17–17,5 см (на две колонки) или 23 см (во весь лист). Поэтому желательно изображать отдельные элементы и надписи на рисунке так, чтобы при уменьшении масштаба рисунка до одного из указанных размеров буквы и цифры приобрели высоту 2–2,5 мм, элементы схем 3–5 мм, отдельные точки 1 мм, а линии должны быть при этом разнесены на расстояние не менее 0,5–1 мм.

11. Надписи и обозначения на иллюстрациях следует располагать так, чтобы они не соприкасались ни с какими её частями. На задний план иллюстрации желательно не добавлять серый (цветной) фон или сетки.

12. Таблицы не должны дублировать графики. Каждая таблица имеет заголовок. На все таблицы

и рисунки следует давать ссылки в тексте. Таблицы не должны содержать вертикальные линии, делящие таблицу на столбцы. Название и содержание таблиц представляется на русском и английском языках.

13. Обозначения и сокращения, принятые в статье, расшифровываются непосредственно в тексте.

14. Размерность всех величин, принятых в статье, должна соответствовать Международной системе единиц измерений (СИ).

15. Набор формул должен проводиться в редакторе MathType целиком. Набор формул из составных элементов не допускается, номера формул – по правому краю. Нумеруются лишь формулы, на которые есть ссылки в тексте.

16. Необходимо использовать следующие установки редактора формул. Размеры: полный – 10 пт, подстрочный – 9 пт, под-подстрочный – 7 пт, символ – 14,5 пт, подсимвол – 12,5 пт. Стили: текст, функция, число, кириллица – шрифт «Times New Roman», вектор-матрица – шрифт «Times New Roman», жирный; греческий малый, греческй большой, символ – шрифт «Symbol», прямой; переменная – шрифт «Times New Roman», курсив.

17. Отдельные строчные буквы и специальные символы набираются в тексте гарнитурой Symbol **без использования редактора формул**. При наборе формул и буквенных обозначений необходимо учитывать следующие правила: **русский алфавит не используется**; греческие буквы, математические символы (grad, div, ln, min, max и др.), единицы измерения (Вт, Дж, В, кг и др.), кириллические буквы, сокращения от русских слов ($q_{\text{ср}}$); обозначения химических элементов и соединений (в т. ч. в индексе) набираются **прямо**; латинские буквы – переменные и символы физических величин (в т. ч. в индексе) набираются **курсивом**; векторы – жирным шрифтом (стрелки вверху не ставятся).

18. Начертание обозначений в формулах и в основном тексте должно быть полностью идентично. В расшифровке формул, которая начинается словом «где», символы и их порядок должны соответствовать символам и их порядку следования в формулах.

19. Список использованных источников составляется в порядке упоминания ссылок по тексту, должен содержать полные библиографические данные и приводится в конце статьи. Не рекомендуется давать ссылки на материалы конференций, статьи из электронных журналов без идентификатора **DOI**, учебные пособия, интернет-ресурсы. Ссылки на неопубликованные работы не допускаются. Желательно, чтобы количество ссылок было не менее 10; самоцитирование – не более 20 %.

20. Авторы на отдельной странице предоставляют о себе следующие сведения: фамилия, имя, отчество, ученая степень и звание, место работы и занимаемая должность, адрес электронной связи.

21. Статьи, излагающие результаты исследований, выполненных в учреждениях, должны иметь соответствующее разрешение на опубликование в открытой печати.

22. При необходимости в конце основного текста указываются наименование фонда, оказавшего финансовую поддержку, или уровень и наименование программы, в рамках которой выполнена работа, на русском и английском языках.

23. Авторы несут ответственность за направление в редакцию статей, ранее уже опубликованных или принятых к печати другими изданиями.

24. Статьи, не соответствующие перечисленным требованиям, к рассмотрению не принимаются и возвращаются авторам. Датой поступления считается день получения редакцией первоначального варианта текста.

25. Редакция предоставляет возможность первоочередного опубликования статей лицам, осуществляющим послевузовское обучение (аспирантура, докторантура, соискательство), в год завершения обучения; не взимает плату с авторов за опубликование научных статей; оставляет за собой право производить редакторские правки, не искажающие основное содержание статьи.

AUTHOR GUIDELINES

1. Article materials should correspond to the journal profile and be clearly written.
2. An article should be submitted in Russian or English and will be published in its original language.
3. Articles received by the Editorial Board will be reviewed by 2 specialists. The main criteria of acceptance are theme actuality, information value, and scientific novelty.
4. All materials should be submitted in two hard copies together with electronic file in the Word for Windows format (97/2000/2003). The paper should not exceed 14 pages of the typewritten text (Times New Roman, 12 points, 1.5-space).
5. The article should contain UDC number, Title (printed in capitals), Authors' names (the corresponding author name should be marked with asterisk), full Address of organization(s) in which the author(s) work, Abstract (200–250 words), Keywords (not more than 5 words), Introduction, the Text of the paper with tables, diagrams and figures (if there are any), Conclusion with clearly stated inferences, List of References, List of Symbols and Abbreviations (if it is necessary). Title, Authors' names and affiliation(s), Abstract, Keywords should be presented both in English and Russian languages.
6. The abstract should be informative (contain "squeeze" from all sections of the article – the introduction stating the purpose of the work, methods, main part and conclusion).
7. Figures should be black-and-white, represented in graphical formats tif, attached with Excel or MS Graph and added with captions. All symbols in figures should be descripted.
8. Tables should be placed directly in the article body. Diagrams and tables should not contain the same information. Each table should have the title. All tables, diagrams and figures should be referenced in the text.
9. Symbols and abbreviations which are used in articles should be deciphered directly in the text and also (if necessary) taken out on a separate page.
10. Dimensions of all quantities used in the article should correspond to International System of Units.
11. Formulas should be taped in MathType.
12. List of References is to be placed at the end of the article with full bibliographic information. Order of references should correspond to the order of their occurrence in the text. It is not recommended to refer to conference proceedings, papers from electronic journals without **DOI** number, textbooks, internet resources. References on unpublished works are prohibited. It is recommended to refer to not less than 10 references, self-citations – not more than 20 %.
13. The following information about every co-author should be presented: family name, first name, patronymic (or second) name (if there are any), scientific degree and title, organization and position, full address with the postal code for correspondence, office or mobile phone numbers, fax, e-mail.
14. Articles containing investigation results obtained in organizations should have a corresponding permission for publication.
15. Names of Foundations or Programs financially granted the research may be acknowledged in the end of the text.
16. Authors are responsible for submitting articles previously published or accepted by other publisher.
17. Articles not meeting the requirements of the Editorial Board would not be accepted and may be returned to the authors. The date of receipt is considered to be the day when the Editorial Board receives the author's original paper.
18. Authors conducting postgraduate (graduate studies, doctoral studies) have a priority in publishing their articles out of queue in the year of completion. Authors do not pay for publishing scientific articles. The Editorial Board can shorten and/or change the text if it does not strain the meaning of the article.

Индексы:
74835; 748352